Department of Physics and Astronomy

University of Heidelberg

Master thesis

in Physics

submitted by

Elsa Wilken

born in Hamburg

2018

Retrieval Advances of BrO/SO$_2$

Molar Ratios from NOVAC

This Master thesis has been carried out by Elsa Wilken

at the

Institute for Environmental Physics, University of Heidelberg,

Germany

under the supervision of

Prof. Ulrich Platt,

Dr. Nicole Bobrowski,

Florian Dinger

Optimierte Bestimmung des molaren BrO/SO$_2$ Verhältnisses aus NO-VAC Daten

Die Messung der absoluten Menge und von Konzentrationsverhältnissen vulkanischer Gas Emissionen geben Einsicht in magmatische Prozesse. Das Network for Observation of Volcanic and Atmospheric Change (NOVAC) besteht aus einem System von automatisierten UV-Spektrometern, welche die Gas Emissionen der Vulkane aufzeichnen. Die Emission von BrO und SO$_2$ kann mithilfe von Differenzieller optischer Absorptionsspektroskopie (DOAS) aus den aufgenommen Spekren bestimmt werden wobei die optische Absorption in der Fahne mit einem Reference Spectrum verglichen wird. Dies setzt voraus, dass das Reference Spectrum frei von Vulkanische Gasen ist. Typischerweise wird das Reference Spectrum für einen Scan bei einem Elevationswinkel aufgenommen welcher welcher so gewählt wird dass das Instrument nicht in die Fahne schaut. Es hat sich jedoch gezeigt, dass auch diese Spektren noch durch Vulkanische Emissionen verunreinigt sein können. Als alternative Referenzspektren könnten 1) ein theoretisches Solar Atlas Spektrum oder 2) ein nicht verunreinigtes Referenz Spektrum des selben Messgeräts dienen. Option 1) hat den Nachteil einer verringerten Messgenauigkeit, da Instrumenteneffekte hier modelliert werden müssen und ist daher nur für das typischerweise in hoher Konzentration vorkommende SO$_2$ anwendbar. Option 2) setzt voraus, dass das Referenzspektrum unter ähnlichen Wetter- und Strahlungsbedingungen aufgenommen wurde. Wir verwenden die erste Methode um (SO$_2$) Kontaminierung zu identifizieren und greifen für die Bestimmung der Gas Konzentration auf die zweite Methode zurück um eine hohe Qualität der Messung sicher zu stellen. Im Folgenden stellen wir unsere Methode für NOVAC Daten von den Vulkanen Tungurahua und Nevado Del Ruiz vor.

Retrieval advances of BrO/SO$_2$ molar ratios from NOVAC

Measurements of magnitude and composition of volcanic gas emissions allow insights in magmatic processes. Within the Network for Observation of Volcanic and Atmospheric Change(NOVAC) automatically scanning UV-spectrometers are monitoring gas emission at volcanoes. The emissions of BrO and SO$_2$ can be retrieved from the recorded spectra by applying Differential Optical Absorption Spectroscopy(DOAS) and comparing the optical absorption of the volcanic plume to the background. Therefore, the background spectrum must not be affected by volcanic influence. Classically, the background spectrum is taken from the same scan but from an elevation angle which has been identified to be outside of the volcanic plume. However, experience shows those background spectra can still be contaminated by volcanic gases. Alternatively reference spectra can be derived from 1) a theoretical solar atlas spectrum or 2) a volcanic-gas-free reference spectrum recorded by the same instrument. 1) comes with a drawback of reduced precision, as the instrumental effects have to be modeled and added to the retrieval. For 2), the alternative reference spectrum should be recorded at similar conditions with respect to meteorology and radiation. We use the first option to check for contamination and the second to evaluate the spectra to maintain a god fit quality. We present our approach and its results when applied on NOVAC data from Tungurahua and Nevado Del Ruiz.

Contents

1 Introduction

Volcanic activities on Earth have always shaped the Earth surface and influenced atmospheric processes. Volcanism is a geological phenomena which is related to the raise of magma from the Earth's interior to the Earth's surface. Volcanic activity is linked to tectonic active regions, thus hotspots mainly are at the margins of the continental plates. significantly less volcanic activities occurs at the the interior of continental or oceanic shelves (Schmincke, 2000).

Volcanoes are often particularly recognized by their dramatic consequences of a major volcanic eruption. But volcanoes influence our lives in more than this way. Volcanic gases can effect the weather by emitting aerosols or on larger time-scales even the climate (Schmidt and Robock, 2015). Examples are the Laki eruption in Iceland (1783-1784) followed by a very hot summer and a cold winter in central Europa (Thordarson and Self, 2003) and the Tambora eruption, Indonesia in 1815 which caused the "year without summer" in 1816.

Volcanic gases can alter the radiative balance of the Earth due to scatter and absorption of solar radiation (Schmidt et al., 2015). A decrease of stratospheric ozone (O_3) has been observed after the eruption of El Chickon in 1982 and the eruption of Mount Pinatubo 1991. The depletion comes from volcanic aerosols which serve to transform anthropogenic chlorine/bromine into more reactive forms (Solomon et al., 1998).

The gas composition of the volcano plume change with activity and can be a indicator for the processes inside the Earth .

The change of the gas composition with volcanic activity is a result of the specific pressure dependency of the solubility of each dissolved gases within the magma. Therefore the relatively concentration of a gas change with its origin source depth due to pressure dependency on the depth below the crater vent. Therefore the ratio of two gases can be used to draw conclusions on the origin source depth of the gases. This work particularly deals with the ratio of BrO and SO_2. The advantage of using the ratio of these two gases is the possibility of getting continues data by using the NOVAC spectral data.

The BrO to SO_2 ratio changes due to pressure differences with depth, thus the BrO/SO_2 ratio changes with its origin source depth. It is possible to conclude from the BrO/SO_2 ratio to the degassing source depth and therefore the ratio is a proxy for volcanic processes. A change in BrO/SO_2 prior to eruption was observed at Etna and Nevado del Ruiz.

The Network for Observation of Volcanic and Atmospheric Change (NOVAC) is a network to record volcanic emissions. The aim of NOVAC is mainly to provide

new parameters for risk assessment and volcanological research, both locally and on a regional and global scale. NOVAC is a Network of spectrographic instruments located next to about 30 volcanoes in Asia, America, Africa and Europe. At each of these volcanoes are two to four spectrograph's installed, recording back-scattered solar radiation spectra at different viewing angles.

NOVAC is a network which produces a large amount of data and thus provides the chance to evaluate long time periods which is a unique opportunity to study volcanic trace gases.

The instruments and the maintenance need to be cheap, thus the instruments need to have a rather simple construction. Therefore it was decided not to implement temperature stabilization even at the expense of the quality of the data.

The data recorded by NOVAC are evaluated using Differential Optical Absorption Spectroscopy (DOAS) Platt and Stutz (2008). DOAS utilises the wavelength dependency of the absorption of light and is based on the Beer-Lambert law. The gas concentration is retrieved from the characteristic difference in absorption structures between the plume and a reference region. Thus it is fundamental to have a reference which is free of the gases of interest, to assure that the retrieved concentration is correct.

The reference region, is usually treated as free of volcanic trace gases. If the reference region is for any reason contaminated by volcanic trace gases, the reference spectrum has to be replaced by a volcanic-gas-free reference. Alternative spectra could be for example a theoretical solar atlas spectrum or a volcanic-gas-free reference spectrum recorded in the temporal proximity (eg. a day before) by the same instrument. The first option comes with the drawback of reduced precision, as the instrumental effects have to be modelled and added to the retrieval. The reduction in precision is acceptable for the SO_2 retrieval, but not suitable for a BrO retrieval because then most data would be below the detection limit. The advantage of the first option is, that the absolute column density is calculated, since, the theoretical solar atlas spectrum is absolutely gas free. For the second option, the alternative reference spectrum should have been recorded at similar conditions with respect to meteorology, radiation,intensity and in temporal proximity due to instrumental changes with time and ambient conditions. We combined both options in order to achieve both, enhanced accuracy but still maximum possible precision of the SO_2 and BrO retrievals. We present an algorithm which finds the optimal reference spectrum automatically. As first step, a possible SO_2 contamination of the standard reference is checked by a comparison with the theoretical solar atlas. If a contamination is detected, as second step, the algorithm picks a volcanic-gas-free reference (beforehand automatically checked for contamination) from another scan.

To gain a better understanding volcanism it is elementary to improve the measurement techniques. The aim of this thesis is to improve the retrieval of the BrO/SO2 ratio by using data from Tungurahua in Ecuador and Nevado del Ruiz a volcano located in Colombia, provided by NOVAC.

Part I

Theoretical background

2 Volcanism and volcanic chemistry

2.1 Volcanism

The high thermal energy in the deep interior of the earth is mostly well separated from the earth's surface by the earth's crust. A volcano is a geological structure that allows magma to reach the earth's surface. Such a phenomenon can occur in various ways. In the following paragraphs the different types of volcanoes are described.

Mid-ocean ridge volcanism The mid-ocean ridge volcanism can be traced back to tectonic processes of oceanic plates. The spreading of two plates, that are pulled apart, leads to a thinning of the oceanic earth crust. This way solid material from the upper mantel (lower than 100 km) can ascend to depths of approximately 50 km. As the pressure at this depth is much lower, the mantle material starts to melt to basaltic magma that fills the gap between the two plates.

Continental rift zone volcanism Similar to mid-ocean ridge volcanism continental rift zone volcanism are located at two continental plates that are pulled apart.

Hot-spot volcanoes Hot-spot volcanoes occur on continental or oceanic plates. This type of volcanoes arises from a hot spot at the coremantle boundary inside earth that leads to a plume in the mantle where solid material can rise. This material melts to basaltic magma at a depth of 100-150 km. Through a futher rise also other types of magma (e.g. rhyolitic, more-viscous magma) can arise.

Subduction zone volcanoes Subduction zone volcanoes occur if an oceanic plate converges under another plate (oceanic or continental). This way the descending plate penetrate into the lower mantle. At a depth of 80-150 km the water of this plate evaporates and rises and causes the mantle material above to melt. The resulting water-rich magma mainly consists of andesite. Subduction zone volcanoes are known for their violent eruptions caused by the low viscosity magma.
In this thesis data from two subduction zone volcanoes, Tungurahua and Nevado del Ruiz, are evaluated. Both located in South America.

Table 2.1: Volcanic gas constituents at the emission vent and global estimated source strength. Adapted from Textor et al. (2004).

Species	H_2O	CO_2	SO_2	H_2S	COS	SC_2	HCl	HBr	HF
% / vol	50 - 90	1 - 40	1 - 25	1 - 10	10^{-4} - 10^{-2}	10^{-4} - 10^{-2}	1 - 10	?	< 10^{-3}
Tg / year	?	75	1.5 - 50	1 - 2.8	0.005 - 0.1	0.007 - 0.096	0.4 - 11	0.0078 - 0.1	0.06 - 6

2.2 Volcanic degassing

2.2.1 Volcanic plume chemistry

Volcanoes emits gases and aerosols particles, which are rising and forming the volcanic plume. The temperature where the gases and aerosols are emitted is approximately 500°C (Gerlach, 2004). Due to the high temperatures the gas raises, cools down and mix up with ambient air. This process leads to many chemical reactions. The large amount of aerosols catalyses heterogeneous reactions.

The most abundant volatile species released during a volcanic eruption are water vapour (H_2O; relative amount of the plume: 50%-90%) and carbon dioxide (CO_2; relative amount of the plume: 1%-40%) (Platt and Bobrowski, 2015). A typically volcanic plume consists of many different gases alongside H_2O and CO_2. Sulfur dioxide (SO_2) contributes with 1%-25% to the plume, hydrogen sulfide (H_2S) with 1%-10% and hydrogen chloride with (HCl) 1%-10%. Furthermore there are trace gases for example carbon disulfide (CS_2), carbon sulfide (COS) carbon monoxide (CO) hydrogen fluoride (HF), hydrogen bromide (HBr) and many other species (Platt and Bobrowski, 2015).

The volcanic gases are listed in table 2.1.

In the following the chemical reactions of the plume constituents BrO and SO_2 will be discussed. The main focus of this thesis lays on the evaluation of those two gases.

2.2.2 Sulphur species

Sulphur species are the third most abundant gases in volcanic plumes. Hereby SO_2 contributes with about 25% and H_2S with 1 to 10%. Only H_2O and CO_2 have a larger share on the volcanic gases in the plume table 2.1.

The SO_2 amount inside he plume can easily reach 1ppm (Oppenheimer et al., 2003). Whereas, in contrast, the typical atmospheric concentration is about 1ppb and thus negligble compared to the concentration in a young volcanic gas plume. When H_2S escapes from the volcano vent, it enters the oxidizing conditions in the atmosphere. H_2S goes through a series of reactions, leading to the SO_2 formation (Seinfeld and

Pandis, 2016)

SO_2 is removed from the atmosphere by dry or wet deposition. At homogeneous reactions the lifetime is from 1-3 weeks (Robock, 2000). Heterogeneous reactions that take place on particles or liquid phases lead to much faster depletions. But this has not yet been observed in volcanic plume measurements.

Further discussions of the stability of SO_2 in the atmosphere can be found at Lübcke (2014).

However, SO_2 can be considered as stable several hours after the release of the volcanic vent.

The long lifetime alongside with the negligible amount of SO_2 in the atmospheric background makes SO_2 a good tracer of the volcanic plume. Therefore relative to other trace gases SO_2 may be used to examine their evolution independent of the plume dispersion.

One attempt to use SO_2 to examine other trace gases is made by Bobrowski et al. (2007). They found a higher BrO/SO_2 ratio at the edges of volcano plumes (Mt. Etna on Sicily, Italy, in August–October 2004 and May 2005 and Villarica in Chile in November 2004) and concluded that the BrO amount is higher at the edges due to the insufficient mixing with ozone rich air inside of the plume (see fig. 2.1).

In this thesis it is assumed that SO_2 is stable on time-scales occurring with ground based remote sensing measuring of about 20 minutes.

2.2.3 Bromine oxide

The amount of bromine in volcanic plumes is rather low compared to SO_2. The first time bromine monoxid (BrO) was observed at a volcano was 2013 at the soufriere hills by Bobrowski et al. (2003). Since then many others were able to detect BrO using ground based remote sensing measurement techniques (DOAS: see section 4.1) for example: Bobrowski and Platt (2007), Bobrowski et al. (2007),Vogel (2011) and Lübcke et al. (2014)

The main bromine formation which is released from the volcano is HBr. BrO is formed due to mixing with the ozone rich atmosphere at ambient temperatures (Bobrowski et al., 2007).

Due to the raising of hot air in the volcano vent , ambient air is pulled into the vent. There temperatures of 600°C to 1200°C prevent the formation of BrO. Only Br is formed. BrO occur after further cooling and mixing while rising. When the temperature cooles down to ambient conditions the so called "Bromine Explosion" causes a non linear formation of BrO. The "Bromine Explosion" is illustrated in
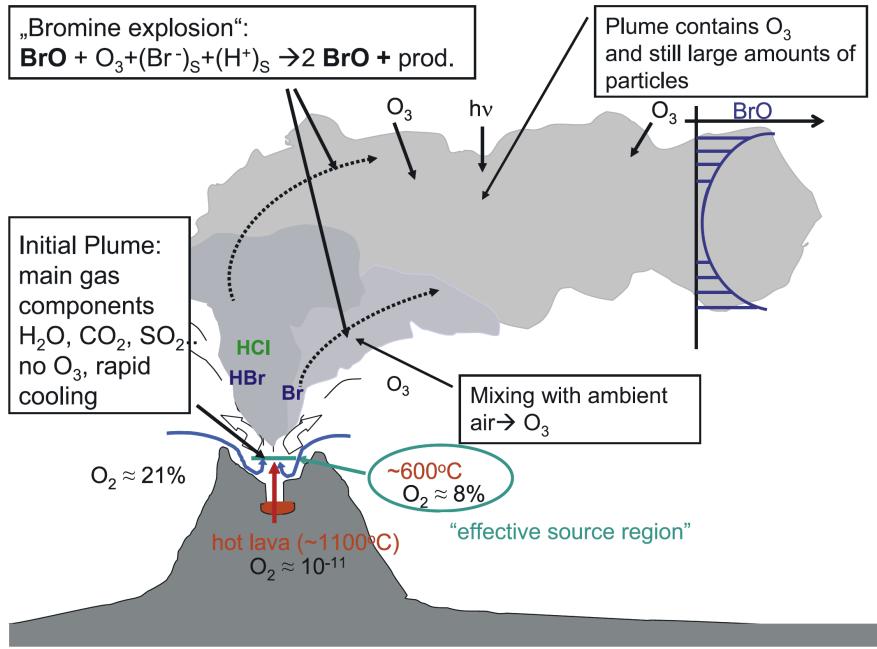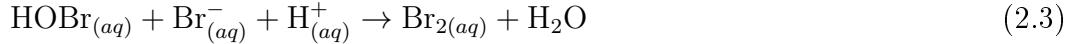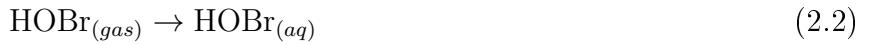
Figure 2.1: schematic sketch of a bromine Explosion. Release of HBr at the volcanic vent. Mixing with ambient air in the effective source region leads to Br formation. This resulting bromine species react to BrO with ozone from the plume. Adapted from Bobrowski et al. (2007)

fig. 2.2 and can be described with the following reaction cycle:

$$\text{HBr}_{gas} \rightarrow \text{Br}^-_{aq} + \text{H}^+_{aq} \tag{2.1}$$

$$\text{HOBr}_{(gas)} \rightarrow \text{HOBr}_{(aq)} \tag{2.2}$$

$$\text{HOBr}_{(aq)} + \text{Br}^-_{(aq)} + \text{H}^+_{(aq)} \rightarrow \text{Br}_{2(aq)} + \text{H}_2\text{O} \tag{2.3}$$

$$\text{Br}_{2,aq} \rightarrow \text{Br}_{2,gas} \tag{2.4}$$

$$\text{Br}_2 + h\nu \rightarrow 2\text{Br} \tag{2.5}$$

$$\text{Br} + \text{O}_3 \rightarrow \text{BrO} + \text{O}_2 \tag{2.6}$$

$$\text{BrO} + \text{HO}_2 \rightarrow \text{HOBr} + \text{O}_2 \tag{2.7}$$

$$\text{BrO} + \text{BrO} \rightarrow 2\text{Br} + \text{O}_2 \tag{2.8}$$

$$\text{BrO} + \text{BrO} \rightarrow \text{Br}_2 + \text{O}_2 \tag{2.9}$$

The gaseous HBr emitted by the volcano is split heterogeneously int H^+ and Br^- (eq. (2.1)). Inside of an aerosol it forms with HOBr Br_2 and H_2O (eq. (2.3)). Br_2 evaporates to the gaseous phase and splits photolytic into 2Br. Including an ozon molecule (O_3) the two Br react to 2BrO. The last step o the circle visualized in fig. 2.2 with blue lines is the reaction of a BrO with H_2O to an HOBrO molecule condensing into the liquid phase and thuse closing the circle. The non linear explosion occurs due the formation of two BrO particles from one Hbr from the volcano.
The BrO formation is slightly diminished due to self reaction of BrO molecules
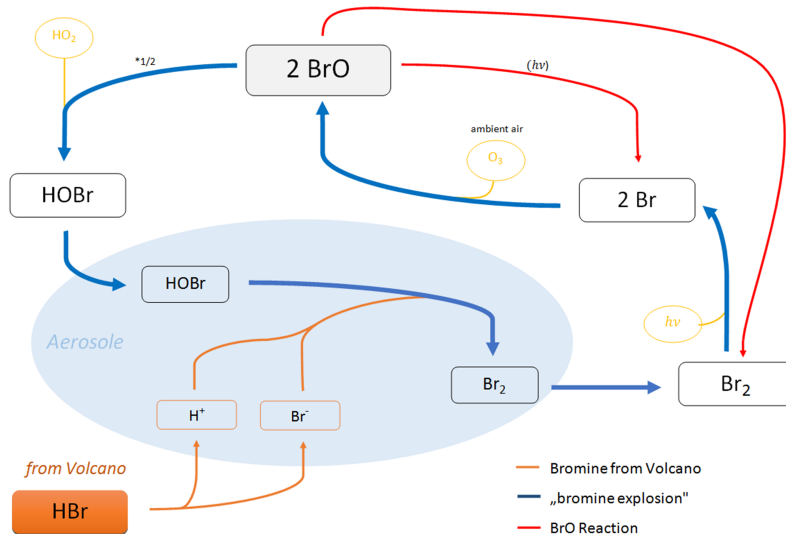
Figure 2.2: Bromine reactions inside of a volcanic vent. The release of Hbr at the volcaninc vent is drawn in orange. Inside of aerosols heterogeneous dissociation with HOBr forms Br_2. Then Br_2 splits photolytically into single Br radicals. BrO results through a reaction with O_3upon mixing with ambient air. Reactions with H_2O forms HOBr creating an autocatalytic cycle. The reaction cycle along the blue lines are called bromine explosion. From Warnach (2015).

marked with the red lines in fig. 2.2. The 2BrO react with themselves and form Br_2 or may split photolyticaly into 2Br.
The BrO concentration reaches a maximum approximately five to ten minutes after emission and then remains constant for the next 25 minutes (Lübcke et al., 2014).

2.3 Using the BrO/SO$_2$ ratio to study volcanic activity

Volcanic degassing is influenced by many factors, which can be exploit to study volcanic activity by using the gas composition of the volcano plume. Therefore remote sensing should be an additional tool for forecasting of volcanic activity next to classical monitoring techniques like seismographic and deformation measurements. Inside of volcanoes volatiles are in solution in magmatic melt. The Henry law shown in eq. (2.10) describes the necessary conditions for gas formation:

$$P = K_H \cdot c \tag{2.10}$$

Here P is the partial pressure at equilibrium of the solute, c is the concentration and K_H is the Henry constant which is anti proportional to the solubility α ($\alpha = \frac{1}{K_H}$). If the partial pressure of the gas solute (in this case a magmatic gas constituent) exceeds the pressure of the surrounding solvent, a formation of gaseous bubbles occur.
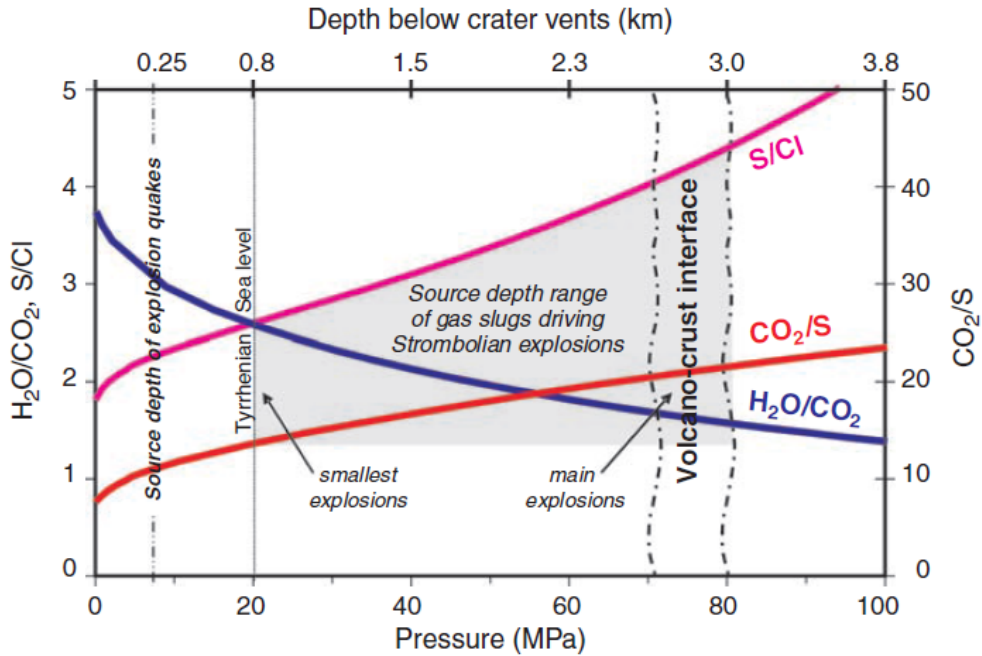
Figure 2.3: Dependence of the ratios of different volcanic trace gases on depth. Data originate from Stromboli volcano. From Lübcke (2014) reproduced from Burton et al. (2007)

Otherwise, if the partial pressure of the gas in the solution is below the surrounding pressure the formation of gas bubbles stops.

The solubility α depends on the temperature, the chemical composition and on the solvent (here magma). Whereas the partial pressure of the constituent depends on the surrounding pressure. The pressure below the volcanic vent increases with depth. This leads to a correlation between the partial pressure of the constituents and the depth. The result is, that the gas starts exsolving at a certain depth depending on the partial pressure of the constituent. Thus, the gas bubble formation increases with rising magma. But at a certain depth the percentage of solved gas is different for each volcanic gas. The result is, that the composition of the gases changes with depth. So gas ratios contain information about its originating source depth.

Prior to volcanic eruptions the magma starts raising. Because the gas is mostly less dense than the magma, it raises faster and could therefore be an indicator for its origin source depth and thus an indicator for the volcanic activity.

Figure 2.3 shows the empirical measured ratios of H_2O/CO_2, S/CL, CO_2/S as a function of the pressure respectively on the depth. Noguchi and Kamiya (1963) found a decrease of Cl/S prior to eruptive periods Pennisi and Le Cloarec (1998) observed a lower CL/S ratio during eruptive periods compared to non eruptive periods at Mt. Etna. Burton et al. (2007) found CO_2/SO_2 and SO_2/hCl ratios 3-5 times higher during explosions compared to quiet degassing episodes. The authors compared
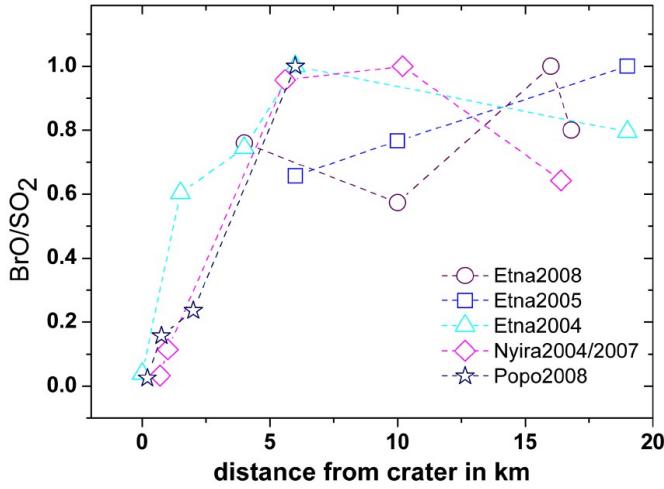
Figure 2.4: BrO/SO_2 ratio as a function of the distance from the volcanic vent with a constant wind speed of 10 m/s. From Lübcke (2014).

these data to gas formation simulations for different degassing source depth, they concluded that these eruptions were driven by gas slugs from deeper levels where the ratios were higher while quiet degassing originates from from shallow magma. Especially halogen-sulfur ratios are interesting as possible tracer for the volcanic activity because the ambient air concentrations are negligible. BrO/SO_2 curves equivalent as in fig. 2.3 are yet not available due to lack of bromine solubility curve but the following observations are made: Changes of BrO/SO_2 are found by Bobrowski and Giuffrida (2006): multiple eruptions between 2006 and 2009 highest ratios 2-3 month before the eruptions the ratio then decreased and was lowest during eruptive phase. Therefore it could be concluded that bromine exsolves earlier, at lower depth than sulphur. Lübcke et al. (2014) found decrease of BrO 5 month prior to the eruption 2012 at Nevado del Ruiz which also can be attributed to a earlier exsolution of bromine during rising magma. Despite the lack of the solubility curve of BrO until now, the BrO/SO_2 has a great potential for investigations of the volcanic activity. The first reason is, that both gases can be measured with remote sensing by DOAS instruments. For examples ground based measurements by Bobrowski et al. (2007), Lübcke (2014) or satellite based measurement by Hörmann et al. (2013) or Beirle et al. (2014). The advantage of remote sensing techniques is the possibility of measuring during eruptions which is with in situ measurements not always possible. Secondly due to the NOVAC network (See chapter 3) continues measurements are possible.

Another reason for the research on BrO/SO_2 ratios at volcanoes is that the ratio is almost constant from 5 to at least 30 minutes after release (Bobrowski et al., 2007);(Lübcke, 2014). Furthermore fig. 2.4 shows a almost constant ratio from 5 to
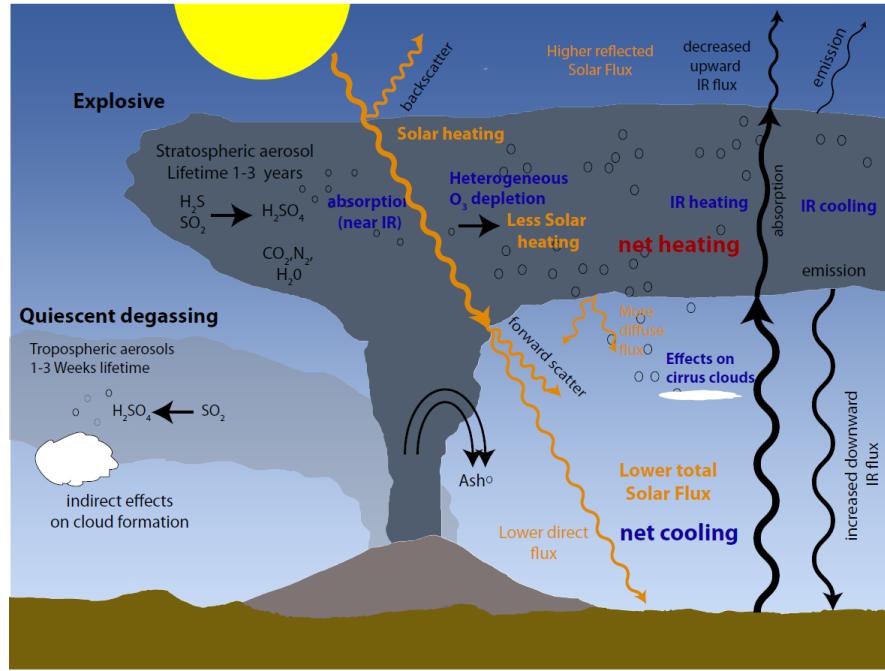
Figure 2.5: Influence of volcanic eruptions and quiet degassing on earth climate. Redrawn on the basis of Robock (2000)

20 km off the volcano. This ensures that the data measured from different positions or at different conditions are comparable.

Volcanic gases and their impact on the climate

Volcanoes emit various gases (see table 2.1) in the atmosphere. This can occur due to volcanic eruptions or due quiet degassing. Gas emitted by quiet degassing remains in the troposphere while eruptions can inject volcanic gases up to the stratosphere (Robock, 2000). The larger lifetime in the stratosphere and a larger sensitivity of the stratospheric chemistry to volcanic gases leads to an higher impact on the earth climate of these gases. Volcanic gases have a large influence on the earth climate especially CO_2 and SO_2 or more specific its oxidation product sulfur acid.
The relevance of CO_2 for the climate is a subject of many discussions about the climate change. Compared to other atmospheric CO_2 sources, the share of volcanic CO_2 is rather low.

Even though the SO_2 emissions during eruptive episodes are up to one order higher than during quite degassing episodes, Halmer et al. (2002) estimates that quiescent degassing contributes 40% of the accumulated SO_2 between 1972 to 2000.
Halmer et al. (2002) estimated the mean annual SO_2 emitted from volcanoes from

16

1972 to 200 as 7.5 to $10.5 TgSyr^{-1}$, while the anthropogenic SO_2 amount for 2000 is estimated as 55 $TgSyr^{-1}$ (IPCC, 2013). Despite the less SO_2 occurring from volcanoes the impact may be higher as the impact of the anthropogenic SO_2. Graf et al. (1997) supposed that the volcanic SO_2 has a higher impact on the climate because its reaches up to the stratosphere while the anthropogenic SO_2 is mostly located in planetary boundary layer. In the lower troposphere sulphuric acid has a lifetime of about a week whereas the lifetime in the stratosphere is about a year (IPCC, 2013). Sulphuric acid in the atmosphere increases the earth albedo due to direct backscattering radiation. Additional the condensation on sulphuric acid particles leads to finer droplets and thus to more stable and more white clouds. This increases the albedo as well (Twomey, 1974). Volcanic particles can be surfaces for heterogeneous reaction. The result is a depletion of stratospheric ozone, and thus a more high energetic solar flux on the earth surface. Large particles may backscatter IR radiation from the earth surface and the lower atmosphere, leading to a small reduction of the net cooling of the lower troposphere. In the upper troposphere or stratosphere absorption of IR or UV radiation results in a net heating in the stratosphere and a cooling at the earth surface. Figure 2.5 shows the above described effects and their localization in the atmosphere. The dominating radiative effect of volcanic gases is a cooling of the earth atmosphere due to more backscattered radiation, more diffusive scattering(Robock, 2000). IPCC (2013) records a volcanic radiative forcing of $-0.11 W/m^2$ between 2008 and 2011. For comparison the radiative of CO_2 is estimated as $1.68 W/m^2$.

# 3 Network for Observation of Volcanic and Atmospheric Change
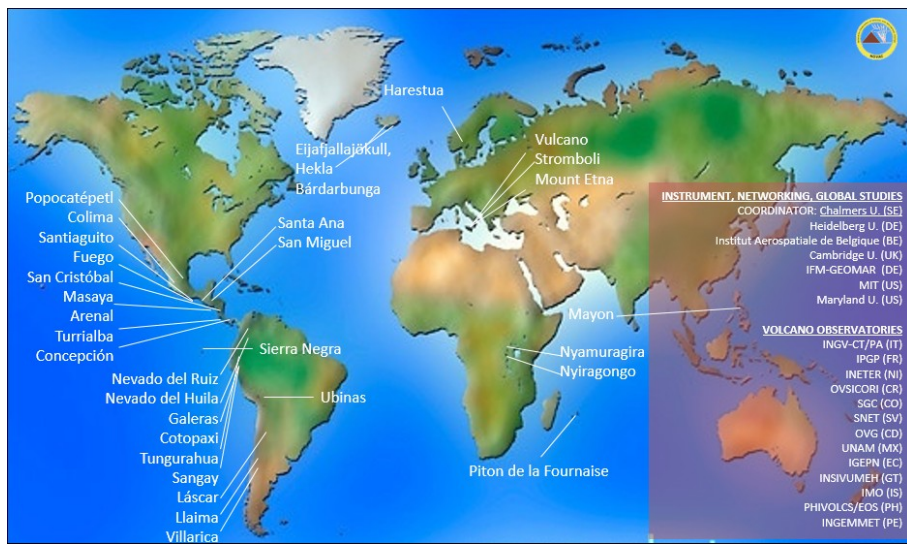
Figure 3.1: Global map of the volcanoes monitored by NOVAC. Used with friendly permission of Santiago Arellano.

The Network for Observation of Volcanic and Atmospheric Change (NOVAC) is a network of instruments monitoring volcanoes over the whole world. NOVAC was installed to add a monitoring parameter for volcanic activity by installing automatised instruments measuring SO_2 emissions during daytime.
NOVAC was originally an European funded research project from 2005 until 2010. The aim of NOVAC is to establish a global network of stations for the quantitative measurement of volcanic gas emissions in particular SO_2. At the beginning, NOVAC encompassed observatories of 15 volcanoes in Africa, America and Europe, including some of the most active and strongest degassing volcanoes in the world. Although the EU-funding has stopped, the network has been constantly growing since it was founded. In 2018 more than 100 instruments are installed at over 40 volcanoes in more than 13 countries. Figure 3.1 shows a map, with all volcanoes of the Network for Observation of Volcanic and Atmospheric Change.

The great advantage of the data monitored in NOVAC is the fact that NOVAC provides continues gas emission data over many years. This ensures statistically meaningful results for the data evaluation.
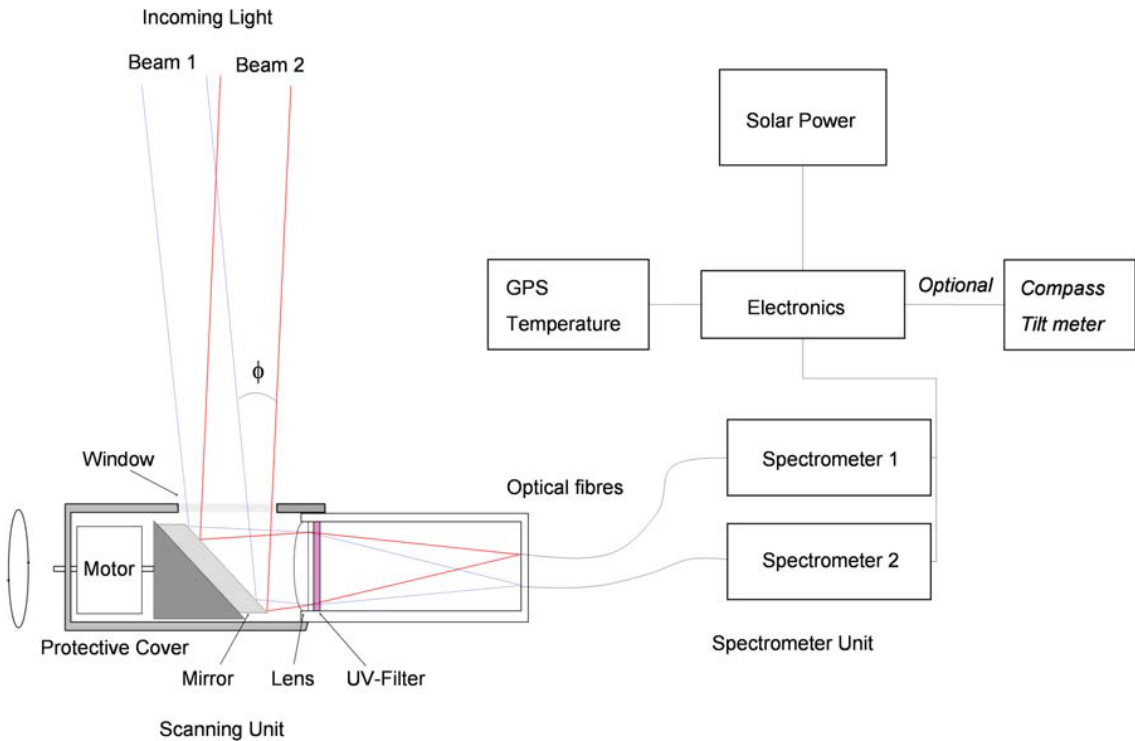
Figure 3.2: schematic sketch of a NOVAC instrument. From Galle et al. (2010)

The instruments used in NOVAC are scanning UV-spectrometer named Mini Doas instruments.

The Mini DOAS instrument represents a major breakthrough in volcanic gas monitoring as it is capable of real-time semi-continuous unattended measurement of the total emission fluxes of SO_2 and BrO from a volcano. Semi-continues in this case means that the measurement is only possible during daytime.

  The basic Mini DOAS system consists of a pointing telescope fiber-coupled to a spectrograph. Ultraviolet light from the sun, scattered from aerosols and molecules in the atmosphere, is collected by means of a telescope with a quartz lens defining a field-of-view of 12 mrad (NOVAC-website).

The spectrometers measure in the UV region in a wavelength range of 280 to 420 nm. In this range the differential structures of SO_2 and BrO structures are dominant.

The lack of temperature stabilization at the instruments used by NOVAC comes with a reduced precision of the data, but the huge amount of data produced by NOVAC compensates for this limitation.

3.1 Measurement routine

The instruments are set up five to ten km downwind of the volcano. To cover most of the occurring wind directions two to five instruments are installed at each volcano. Ideally, the measurement plane is orthogonal to the plume, to get the best
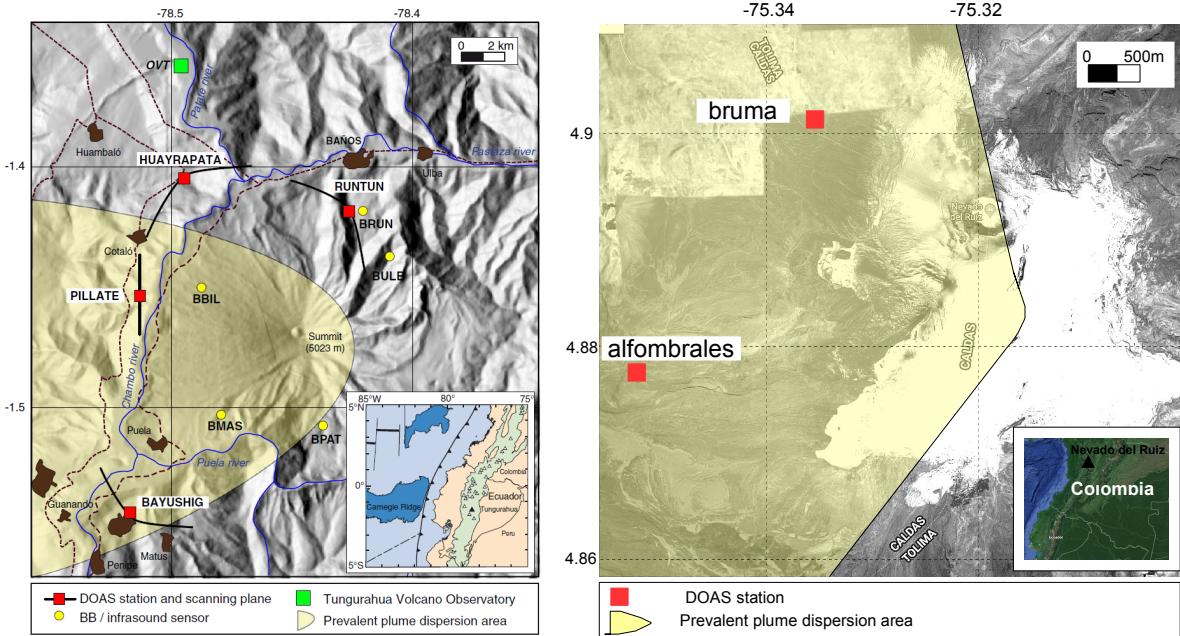
Figure 3.3: Topographig Map of the Tungurahua Volcano (left, from Hidalgo et al. (2015)) and Nevado del Ruiz volcano (right). The predominant plume direction is shaded in yellow. The NOVAC stations are shown as red squares, the corresponding scanning geometry is sketched with black lines. The prevalent plume dispersion is taken from the wind rose shown in nevado-del-ruiz colombia: Windrose the topographic map is taken from google maps.

measurement results. In reality, the measurement plane might be rotated.

For the calculations of gas data from the DOAS retrieval a spectrum of the plume (plume spectrum) and a scan without any volcanic trace gases (reference spectrum) is needed. This is done without any knowledge of the plume location by scanning the whole sky. The measurement routine starts with a spectrum in zenith direction: the pre-reference. The exposure time of the pre-reference will be used for the whole scan. Afterwards, the dark current spectrum is recorded for the correction of the dark and offset.
Then the telescope turns automatically to the side, recording spectra at the elevation angle from -90° to 90° with steps of 3.6°.
The instruments records 53 spectra per scan, the pre-reference, the dark current spectrum and 51 spectra at different elevation angles. One whole measurement cycle from horizon to horizon takes 6 to 15 minutes depending on the current illumination conditions.

Instrument	D2J2140	I2J8546	I2J8548
compass	90.0	30.0	360.0
latitude	-1.453584	-1.543492	-1.404719
longitude	-78.513047	-78.517179	-78.494777
altitude	2609.980	2782.352	2911.253
volcano	Tungurahua	Tungurahua	Tungurahua
site	pillate	bayushig	huayrapata
observatory	igepn	igepn	igepn
serial	D2J2140	I2J8546	I2J8548
spectrometer	S2000	S2000	S2000
instrumenttype	gothenburg	gothenburg	gothenburg
version	2.1	2.1	2.1

Table 3.1: Technical data of the instruments installed at the Tungurahua volcano.

Tungurahua

Tungurahua is a steep-sided andesitic-dacitic subduction zone volcano located in the Ecuadorian Andes (Lat: 1.467°S; Long: 78.442°W). 2014 Tungurahua was one of the most active volcanoes in southern America, since then the activity is decreasing. Tungurahua is 5023m high and is one of the defining volcanoes of the eastern volcanic rows in Ecuador (Hall et al., 1999).
The modern volcano was formed by a sequentially construction of three major edifices on a basement of metamorphic rocks. It has a total diameter of 12 km. Tungurahua I was roughly located at the same place as today and was build up in the mid-Pleistocene, mainly by andesitic and dacitic lava flows as well as interbedded tephra. Tungurahua II was formed in the past 14,000 years as a result of the collapse of the initial edifice.
3000 years ago the Tungurahua II edifice collapse. The collapse of Tungurahua II produced a large debris-avalanche deposit and a horseshoe-shaped caldera which is open to the west side. Tungurahua III the current glacier caped stratovolcano was constructed in this caldera (Program).
The current ongoing long term eruption started in October 1999. The eruptive ohase was preceded by hydrothermal tremors between 1994 and 1997 (Samaniego et al., 2003).
From September 1998 to July 1999 an increase of seismic activity like volcano tectonic earthquakes indicated the raising of magma. This eruptive phase was characterized by alternating periods of high and low volcanic activity.

At Tungurahua three instruments described in table 3.1, with data recorded in the time span from July in 2008 to August in 2009, are used in this thesis. Table 3.1 shows the exact position, of the instruments, the altitude, and other specifications.

Instrument	D2J2200	D2J2201
compass	115.0	59.0
tilt	0.0	0.0
latitude	4.900917	4.876183
longitude	-75.335134	-75.353408
altitude	4866.500	4494.259
volcano	Nevado del Ruiz	Nevado del Ruiz
site	bruma	alfombrales
observatory	ingeominas	ingeominas
serial	D2J2200	D2J2201
spectrometer	S2000	S2000
instrumenttype	gothenburg	gothenburg
version	2.2	2.2
softwareversion	1.82	1.82
compiledate	Feb 19 2009	Feb 19 2009

Table 3.2: Technical data of the instruments installed at the Nevado del Ruiz volcano.

Nevado del Ruiz

Nevado del Ruiz is a glacier-covered, subduction zone volcano which is located in the Central Cordillera of Colombia, 140 km west of Bogota (Lat: 4.892°N; Long: 75.324°W). Nevado De Ruiz has a hight of 5389 m and covers an area of more than 200 km^2. Three major edifices has been constructed since the beginning of the Pleistocene, consisting of andesitic and dacitic lavas and pyrolastics (Program).

The current cone is build within the caldera of older edifice and consists of a cluster of lava domes. The crater on the summit with the name Arenas crater, has diameter of 1 km and a depth of 240 m. The last big eruption was in 1985. This was South America's deadliest eruption.

In this thesis the data of two NOVAC instruments (see table 3.2) in the time from the end of 2009 to the end of 2011 are used.

4 Remote sensing of volcanic gases

In this thesis we are interested in the volcanic trace gases SO_2 and BrO, both measured with the Differential Optical Absorption Spectroscopy (DOAS) a remote sensing technique proposed by Platt et al. (1980)

Beer-Lambert Law

The Beer-Lambert law describes the attenuation of light when travelling through a material.
This section will give an overview about the reasons for decreasing light intensity when going through a medium.
The Beer-Lambert law describes the attenuation of light when travelling through a material.
Atoms and molecules exists in several energy states, depending on the different electron configuration. Moreover molecules have additionally rotation and vibration states, also enclose to the energy states. If a photon energy matches the energy gap between two possible energy states, this includes, that the lower energy state is occupied and the selection rules are fulfilled the molecule could absorb the photon, remaining in a higher energy state.
The additional energy could be loosed by collision with another molecule or by emission. But the direction of the emitted photon is mostly not the same direction of the absorbed photon, thus the intensity I_0 of the light before passing the medium is higher than the intensity I after travelling the distance L through the medium. This can be described as:

$$I\left(L, \lambda\right) = I_0\left(\lambda\right) \cdot exp\left(-\int_0^L \sigma\left(\lambda, p(l), T(l)\right) \cdot c\left(l\right) dl\right) \tag{4.1}$$

where λ is the wavelength,$c\left(l\right)$ is the location-dependent concentration of the trace gas of interest. $\sigma\left(\lambda, p, T\right)$ is the absorption cross section, $\sigma\left(\lambda, p, T\right)$ is unique for each molecule and depends on pressure p and on the temperature T.
An important quantity used in many optical remote sensing techniques is the optical density τ. The optical density is a measure for the weakening of radiation when going through a material. At a volcano the variation of temperature and pressure in different viewing angles is negligible, thus, $\sigma\left(\lambda, p(l), T(l)\right)$ is independent of l required to consider it within the integral. Then τ can be calculated using the
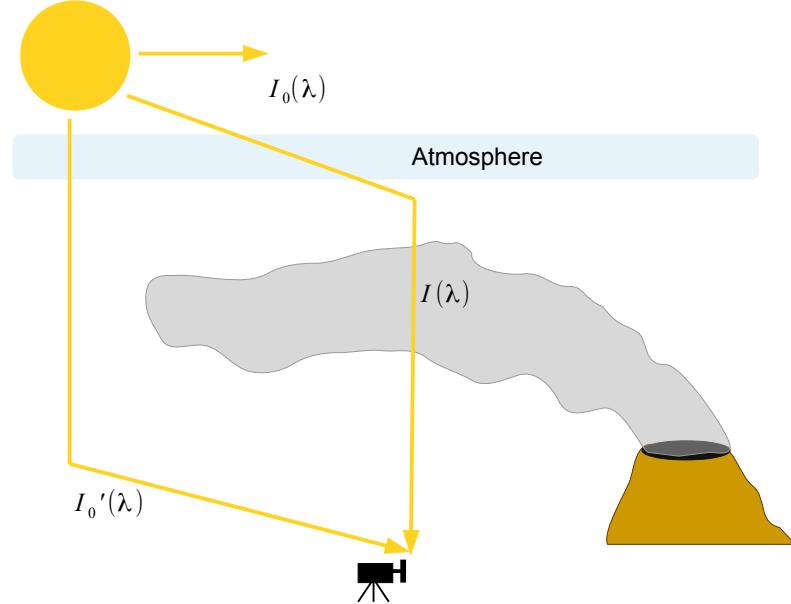
Figure 4.1: Schematic sketch of the DOAS measurement of volcanic plume constituents. The column density of the plume constituent of interest is retrieved by comparing the spectrum $I(\lambda)$ which is measured through the plume with the spectrum $I_0'(\lambda)$ measured outside of the plume.

Beer-Lambert law:

$$\tau = ln\left(\frac{I_0(\lambda)}{I(\lambda)}\right) = \sigma \cdot S \tag{4.2}$$

With S is the column density. S can be calculated as:

$$S = \int_0^L c(l)\, dl \tag{4.3}$$

The column density is the concentration of the trace gas when integrating along the light path, the dimension of S is therefore the number of molecules divided by an area: $\frac{molec}{cm^2}$.

When measuring in atmosphere, the situations gets more complex, because one need to deal with several absorbers and scattering processes have to be taken into account. Scattering processes in the atmosphere can be roughly grouped in Rayleigh scattering, scattering at very small particles and Mie scattering, scattering at larger particles (radius$\approx \lambda$). The effects on the spectrum caused by scattering need to be considered in the calculations. One possibility is to treat scattering effects as pseudo absorbers with the respective extinction coefficients for Rayleigh (ϵ_R) and Mie (ϵ_M) scattering.

$$\tau = \int_0^L \sum_j \sigma_j(\lambda, p, T) \cdot c_j(l) + \epsilon_R(\lambda, l) + \epsilon_M(\lambda, l)\, dl \tag{4.4}$$

The first term of eq. (4.4): multiple absorbers j are considered, the corresponding concentration depends on the position l of the light path. The last two terms describe the extinction due to Rayleigh and Mie scattering in the atmosphere.

Inelastic scattering (for example the Ring effect) and effects due to turbulences in the atmosphere are neglected in eq. (4.4).

4.1 Differential Optical Absorption Spectroscopy (DOAS)
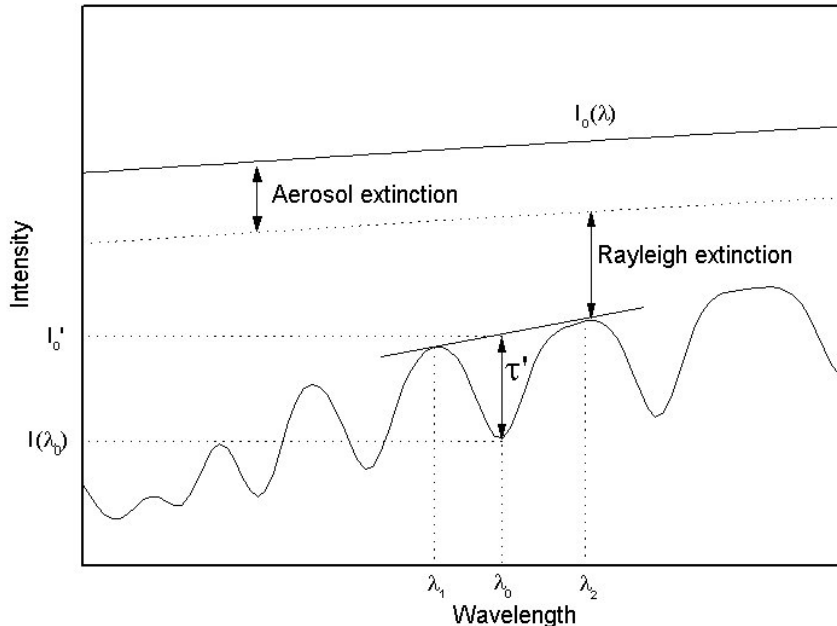
Figure 4.2: Basic idea of the DOAS principle: Light attenuate due to broad band and narrow band effects. The broad band extinction is caused by aerosols and Raylight scattering $\left(I_0 \rightarrow I^{'}\right)$. The measured intensity I is formed by narrow band effects due to differential absorption structures by trace gases with the optical density $\tau^{'}$. Adapted from Kern (2009)

Differential Optical Absorption Spectroscopy (DOAS) was invented in the late 1970s by Perner and Platt (1979). This section will give an overview about the DOAS technique. More detailed information ca be found in the work of Platt and Stutz (2008)

DOAS uses the fact that the broad bands effect do not need to be quantified to determine the column density. Therefore it is not necessary to apply eq. (4.4) to real measurements.

Differential Optical Absorption Spectroscopy uses the fact, that absorption can be

divided into broad-band parts and narrow-band parts. Broad band parts are effects that only changes weakly with the wavelength, i.e. scattering and instruments effects have a broad-band structure. The narrow band part includes effects that strongly depends on the wavelength. Within the DOAS-Method only narrow-band absorption features of molecules are used to obtain their column densities. The absorption cross section of trace gases j have broad-band ($\sigma_b(\lambda)$) and narrow band ($\sigma'(\lambda)$) features, only the narrow-band structures are used in DOAS.

$$\sigma(\lambda) = \sigma_b(\lambda) + \sigma'(\lambda) \tag{4.5}$$

With this considerations the Beer-Lambert law eq. (4.4) can be rewritten dividing the exponential part into a narrow-band part and a broad-band part:

$$I(\lambda, L) = \overbrace{I_0(\lambda) \cdot exp\left(-\int_0^L \sum_j \sigma_{b,j}(\lambda, p, T) \cdot c_j(l) + \epsilon_R(\lambda, l) + \epsilon_M(\lambda, l)\, dl\right)}^{=I_0'(\lambda)} \cdot$$

$$exp\left(-\int_0^L \sum_j \sigma_j'(\lambda, p, T) \cdot c_j(l)\, dl\right) \tag{4.6}$$

The so defined $I_0'(\lambda)$ differs from $I_0(\lambda)$ only by broad band effects. In this context the dependency of the absorption cross section on the temperature and the pressure can be neglected. With $I_0'(\lambda)$ a differential optical density τ' can be defined:

$$\tau' = ln\left(\frac{I_0'(\lambda)}{I(\lambda)}\right) = \int_0^L \sum_j \sigma_j'(\lambda) \cdot c_j(l)\, dl = \sum_j \sigma_j'(\lambda) \cdot S_j \tag{4.7}$$

The optical density can now be calculated by using the difference of the column density S_M in the measurement spectrum to the column density S_R of a reference spectrum. From eq. (4.6) it is known:

$$I_{M,R} = I_0' \cdot exp\left(-S_{P,R} \cdot \sigma(\lambda)\right)^* \tag{4.8}$$

In general the obtained column density S_M is called differential slant column density: "dSCD". If the reference spectrum does not contain the trace gas of interest (is not contaminated with trace gases) that means $S_R = 0$, S_M is called the slant column density (SCD). With eq. (4.8) the optical density can be derived by:

$$\tau(\lambda) = -ln\left(\frac{I_M}{I_R}\right) = \sigma(\lambda) \cdot (S_M - S_R) \tag{4.9}$$

4.1.1 Technical implementation of the DOAS approach

The theory explained above only describes the ideally situation. In real measurements more problems occur due to instrument limitations inelastic scattering causing

the Ring effect and due to impacts of external parameters like temperature.
In the following a short overview about these problems and their consequences for our retrieval is given. Further information can be found in Lübcke (2014).

Optical and spectral resolution of the spectrometer

The resolution of the spectrometer is finite, thus, the detector receives a spectrum $I^*(\lambda)$ which can be retrieved with a convolution of the incident spectrum $I(\lambda)$ with the instrument function H(λ):

$$I^*(\lambda) = I(\lambda) * H(\lambda) = \int I(\lambda - \lambda') \cdot H(\lambda - \lambda') \, d\lambda' \tag{4.10}$$

For the evaluation all σ_j of the trace gases of interest need to have the same spectral resolution as the instrument used for recording the spectra. In this work I will use high resolution cross sections and convolute them with the instrument function H:

$$\sigma*(\lambda) = \sigma(\lambda) * H(\lambda) \tag{4.11}$$

The instrument function H can be approximated by using a the spectral lines of an mercury lamp because the width of those lines is only a few pm, they could be treated as delta peaks when comparing it to the resolution of the spectrometers.

Effects of the detector

The detector only has discrete pixels, therefore a wavelength interval is mapped to a pixel i.

$$I'(i) = \int_{\lambda(i)}^{\lambda(i+1)} I^*(\lambda' d) \, d\lambda' \tag{4.12}$$

For the retrieval the relationship between the detector channels and the wavelength of the spectrum need to be known. The wavelength to pixel mapping (WPM) for a detector with q channels can be calculated as:

$$\lambda(i) = \sum_{k=0}^{q-1} \gamma_k \cdot i^k \tag{4.13}$$

Hereby, is γ_0 a shift of the spectrum and γ_1 is a squeeze (respectively stretch) of the spectrum. The wavelength to pixel mapping can be discovered by using a mercury lamp again and compare pixel-position with the well known wavelength of the individual HG-lines of the mercury lamp.
The wavelength to pixel mapping depends on the instrument temperature as well as on the ambient pressure (Lübcke et al., 2014).

Ring effect

As mentioned above inelastic scattering causes the Ring effect (named after Grainger and Ring, 1962). The Ring effect is observable through a filling of the Fraunehofer lines in spectra of scattered solar radiation, (e.g. if the sunlight travels through the earth atmosphere). When compared to direct sunlight measurements (e.g. outside of the earth atmosphere). (Bussemer (1993),Solomon et al. (1987)) identified rotational Raman scattering mainly of O_2 and N_2 in the atmosphere as the origin of the Ring effect. Solomon et al. (1987) suggested to treat the Ring effect as a pseudo-absorber.

4.2 Evaluation routine

The fitting routine used for this thesis is based on the DOASIS software (Kraus, 2006). The equations of the DOAS retrieval of this work are slightly different from Equation (4.7) and therefore described in the following. Equation (4.4) can be rewritten as:

$$
\begin{aligned}
ln\left(I\left(\lambda, L\right)\right) = & ln\left(I_0\right) + P\left(\lambda\right) - \int_0^L \sum_j \sigma_j\left(\lambda, p, T\right) \cdot c_j\left(l\right) dl \\
= & ln\left(I_0\right) + P\left(\lambda\right) - \sum_j \sigma_j\left(\lambda, p, T\right) \cdot S_j
\end{aligned}
\tag{4.14}
$$

The polynomial $P\left(\lambda\right)$ accounts for all broad-band effects which approximates the scattering effects of the atmosphere as well as broad band absorptions.

The task of the DOAS retrieval is to find a model function $F\left(\lambda\right)$ that minimizes χ^2:

$$
\chi^2 = \sum_{i=\lambda_1}^{\lambda_2} \left(ln(I(i)) - F(i)\right)^2
\tag{4.15}
$$

While $F\left(\lambda\right)$ can be expressed on the basis of Equation (4.14):

$$
F\left(\lambda\right) = ln\left(I_0\right) + P\left(\lambda\right) - \sum_j \sigma_j\left(\lambda\right) \cdot S_j
\tag{4.16}
$$

The DOAS fitting routine uses a combination of a standard least-squares fit and a Levenberg-Marquard algorithm to minimize χ^2

Prior to the DOAS fitting. the spectra need to be calibrated, this done by using a wavelength to pixel mapping function (WMP) developed by Lehmann (2011). The WMP uses a solar atlas spectrum that is concolced with the Hg line of the single instruments, hereby am initial calibration based on the Hg lines is given as a first parameter. The calibration is done by fitting the Fraunhofer lines of the recorded spectrum on the convolved Solar Atlas spectrum. The Rayleigh scattering

is considered by adding a Ring spectrum as well as a wavelength dependent Ring spectrum (proportional to λ^4) (Wagner et al., 2009). Mie scattering and broadband absorption structures were accounted due to adding a third order polynomial to the retrieval well as an offset polynomial to correct for stray-light influence (Lübcke et al., 2014).

The SO_2 evaluation is performed for a wavelength range between 314.8 nm and 328 nm. Including a SO_2 absorption cross section recorded at a temperature of 298K (Vandaele et al., 2009) and a O_3 absorption cross section recorded at 221K (Burrows et al., 1999).

The BrO evaluation is performed for a wavelength range between 330.6 nm and 352.7 nm (found by Vogel (2011)). The sum in Equation (4.16) includes for the BrO evaluation the following absorption cross sections: BrO at 298K (Fleischmann et al., 2004), the SO_2 and O_3 absorption cross sections described above, O_4 (Hermans et al., 2003), NO_2 at 298K (Vandaele et al., 1998) and CH_2O at 298K (Meller and Moortgat, 2000).

The choice of the wavelength range as well as the considered trace gases used in the fits is based on studies on the optimal evaluation wavelength range in a combination of real measurement data and theoretical studies

The choice of the wavelength range as well as the considered tracfor BrO and SO_2, made by Vogel (2011).

The spectra of the trace gases were convoluted by using the 334.15 nm line of a mercury lamp.

A further effect influencing the evaluation is the I_0 effect, in order to account for the I0-effect (Platt and Stutz, 2008) an iterative approach was used. Further informations can be found at (Wagner et al., 2002), Lübcke et al. (2014),Vogel (2011)). To further correct for small inaccuracies of the WMP, the FRS and both Ring spectra as one set, and all trace gases absorption cross sections as another set, are allowed to be shifted, and first order squeezed against the measurement spectrum.

NOVAC provides spectral data for roughly 50 different elevation angles. For the DOAS evaluation a reference and a measurement spectrum is needed. Obtaining the complete amount of volcanic gases is only possible in the case of the availability of references which is free of the volcanic gases of interest (this will be discussed more detailed in Section 4.4). The column density of BrO and SO_2 of the measurement spectrum relatively to the reference spectrum can be calculated Equation (4.15) and 4.16.

4.3 Conventional evaluation routine

In the following I describe the technical implementation of the DOAS approach using the data of NOVAC instruments:

The first step is to correct each spectrum of the scan for dark current and offset
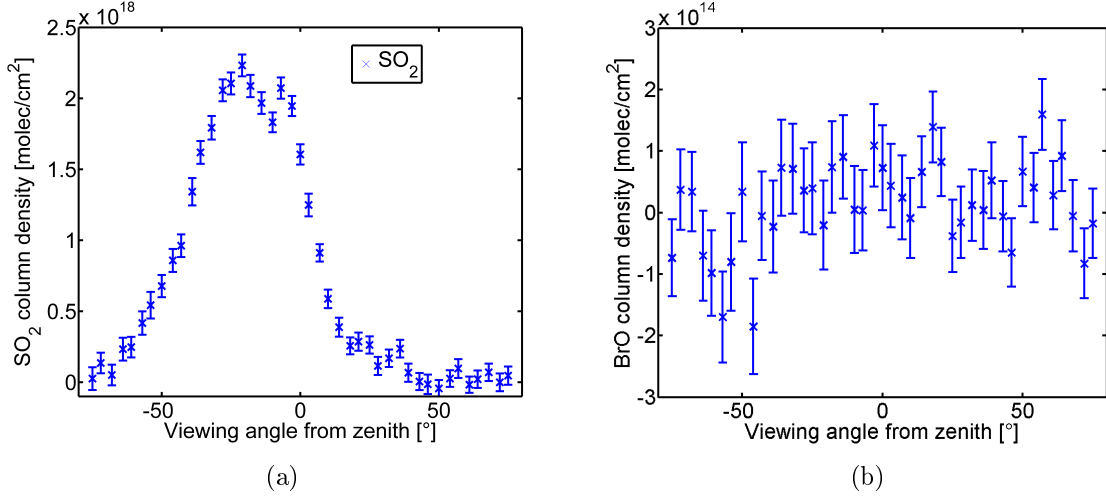
Figure 4.3: (a) SO$_2$ SCD as a function of the elevation angle with error bars computed by the DOASIS fitting routin. (b) BrO SCD as a function of the elevation angle with fit error bars computed by the DOASIS fitting routine. Taken from Warnach (2015)

using the dark spectrum. The next task is to locate the spectra in and outside of the volcanic plume. First a "pre-reference" (the spectrum recorded at an elevation angle of 0°) is used to perform the evaluation of the scan spectra recorded at every elevation angle. For every spectrum of the scan the SO$_2$ differential slant column density (dSCD) with respect to the pre-reference is calculated using Equation (4.16) by the DOASIS fit routine.

The result is SO$_2$ dSCDs as a function of the elevation angle. This way the elevation angle corresponding to the maximum and the minimum of the SO$_2$ column density can be determined. The location of the SO$_2$ maximum defines the location of the plume. The assumption is that the minimum of the SO$_2$ curve corresponds to a region outside of the plume which is true in most cases. The background SO$_2$ amount in the Earth's atmosphere around Tungurahua is usually negligible (see Section 2.2.2).

We use a gauss fit of the SO$_2$-elevation-angle-curve to define the plume region. The sum over all plume spectra is taken, which are in the elevation angle interval of the gauss peak plus minus one sigma, to increase the photon statistic and to reduce the residuum. If the gauss curve is too wide, what this means in specific is that more then 10 spectra are added within the gauss evaluation, The running mean is calculated and the 10 spectra with the highest SO$_2$ amount are used for the retrieval. As reference the sum of the 10 spectra with the lowest SO$_2$ amount is used.

The absolute slant column densities (SCDs) of BrO and SO$_2$ can now be calculated with the previously defined reference and plume spectrum. In Figure 4.3 (a) an example SO$_2$ SCD as a function of the elevation angle is shown. The SO$_2$ curve has a maximum at the position of the plume at an elevation angle of approximately

30
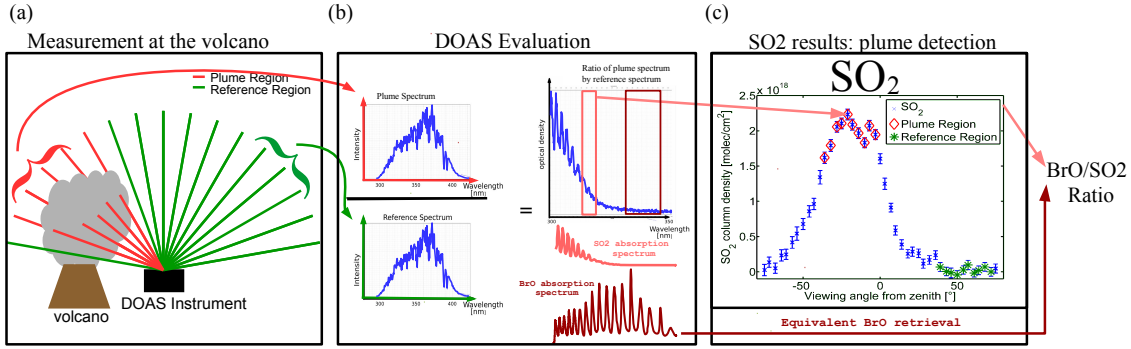
Figure 4.4: NOVAC evaluation: (a) Measurement at the volcano (b) Evaluation of the spectral data with the DOAS routine using the absorption cross sections of BrO and SO$_2$. (c) Finding the location of the plume and reference(taken from Warnach (2015)). With the so found plume and reference spectra, the BrO/SO$_2$ can be calculated.

$-30°$ to $0°$ and a reference region at an elevation angle of $40°$ to $70°$. Figure 4.3 (b) illustrates that extrema of the BrO curve are not as distinct as it is the case for the SO$_2$ curve.

Since the BrO column density is much lower than the SO$_2$ column density, and just lies slightly above the detection limit, the plume is hard to detect using the BrO column density as it is shown in fig. 4.3 (b). Therefore BrO is only in the plume location determined by using SO$_2$ evaluated.

To avoid a distortion of the data as a consequence of relatively bad scans, only scans with a χ^2 (BrO fit) below 10^{-3} (≈ 95 % of all suitable scans) are considered. In a further step multiple reference and plume spectra of successive measurements are added to further increase the fit quality. Figure 4.4 visualizes the different steps described above in the retrieval of the BrO/SO$_2$ ratios.

Figure 4.5 (b) shows the routine of adding multiple spectra of consecutive measuring times. In the following the spectra resulting from the multi adding technique will be referred to as "Multi Add Spectra". The algorithm for co-adding is visualized in Figure 4.5 (b) was invented by Vogel (2011) and Lübcke et al. (2014). At Tungurahua periods with significant degassing have a mean temporal resolution of 19 and up to 45 "Multi Add Spectra" per day (resulting from three instruments)

The mean standard deviation of BrO SCD is about $2.6 \cdot 10^{13} \frac{molec}{cm^2}$. Hereby the standard deviation is estimated as 2 times the DOAS fit error of the multi-scan BrO fit Stutz and Platt (1996)

The SO2 detection limit is in the order of $6 \cdot 10^{16} \frac{molec}{cm^2}$.

Taking the BrO/SO$_2$ molar ratios if the column densities are close to zero yields unpredictable and unrealistic results. Thus, spectra measured in a thin volcano plume need to be excluded. This could be achieved by setting a BrO or/and an SO$_2$ threshold. A reasonable BrO threshold needs to be at least in the order of the
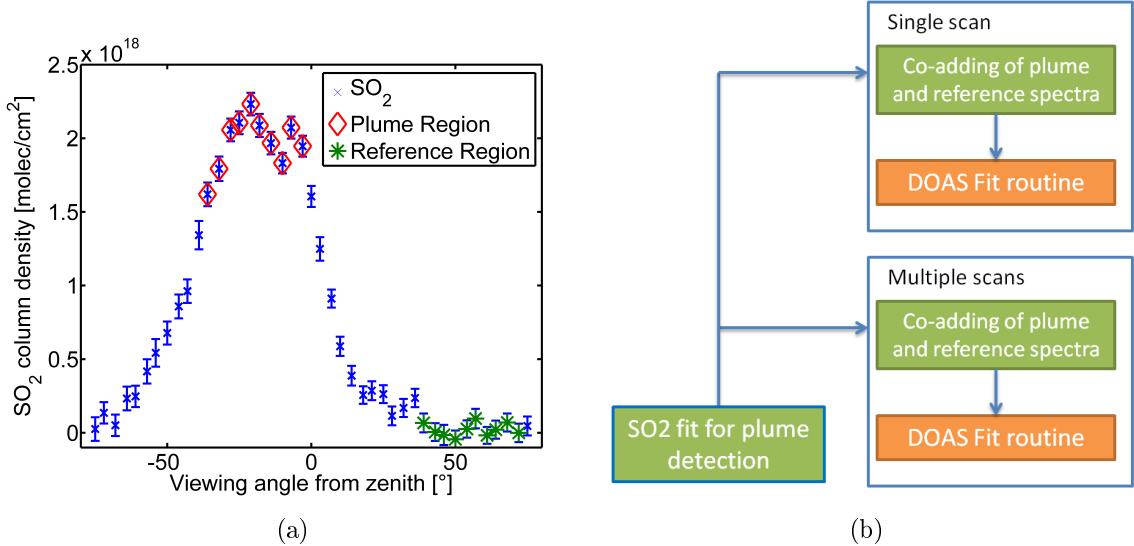
Figure 4.5: (a) SO$_2$ SCD as a function of the elevation angle. The co-added plume region is marked with red diamonds, and the co added reference region with green stars. From Warnach (2015). (b) Flow chart of the BrO and SO$_2$ evaluation. From Lübcke (2014).

DOAS fit error. The BrO detection limit can be enhanced by an daily averaging, then one get an detection limit of: $\text{BrO}_{DT} = \frac{2.6 \cdot 10^{13}}{n} \cdot \frac{molec}{cm^2}$ (n: number of Multi Add Scans per day, the minimum amount is four): However most BrO SCDs are below the detection limit. Rejecting all BrO SCDs below the detection limit leads to an drastical decreases of data points since only the high BrO SCDs will be maintained and thus to systematic elevated BrO/SO$_2$ ratios (Lübcke et al., 2014).

The other possibility is to set an SO$_2$ threshold to ensure only measuring in strong degassing periods. In this thesis an SO$_2$ threshold (plume limit) of $7 \cdot 10^{17} \frac{molec}{cm^2}$ is used for the selection of spectra for the evaluation of the BrO/SO$_2$ ratio.

Within the data above a SO$_2$ plume limit of $7 \cdot 10^{17} \frac{molec}{cm^2}$ the maximum detection limit of the BrO/SO$_2$ ratio is estimated as $(BrO/SO2)_{DT} = \frac{\text{BrO}_{DT}}{SO2_{thres}} = \frac{4}{\sqrt{n}} \cdot 10^{-5} \leq 1 \cdot 10^{-5}$. A plume limit of $7 \cdot 10^{17} \frac{molec}{cm^2}$ is a high threshold for the column density. However, this approach assures that only strongly significant gas amounts are accounted (Lübcke et al., 2014). Choosing the SO$_2$ threshold in this way is a compromise getween a low BrO/SO$_2$ detection limit and a sufficient amount of data.

Increasing a plume limit leads to a decrease of usable data. The amount of usable daily means as a function of the plume limit is shown in Figure 4.6. A plume limit of $7 \cdot 10^{17} \frac{molec}{cm^2}$ leads to a ratio of usable data of approximately 10%.
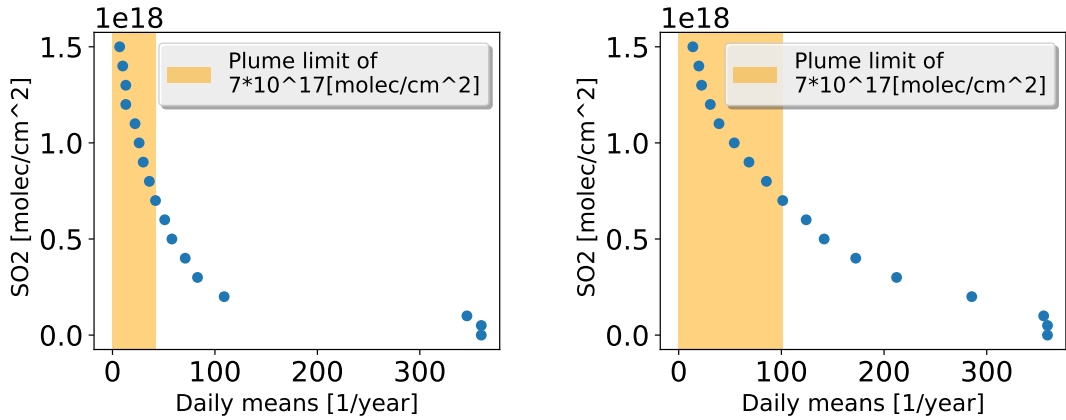
Figure 4.6: The ceSO2 SCD as a function of the decrease of the amount of daily means amount above the plume limit. The SO_2 SCDs below the actual plume limit of $7 \cdot 10^{17} \frac{molec}{cm^2}$ are marked with a yellow shade. Left: Data of three instruments at Tungurahua. Right: data of two instruments at Nevado del Ruiz.

4.4 Retrieval of absolute slant column densities

At the volcano the atmospheric background levels in SO2 are negligible, thus one can interpret the dSCDs as SCDS. However, this is not the case if any volcanic trace gases are contaminating the reference spectrum. The conventional evaluation is based on the assumption, that the reference is free of volcanic gases. This assumption was checked by using a volcanic gas free a high resolution solar atlas spectrum (see below) to evaluate the reference (Lübcke (2014); Salerno et al. (2009)). In some reference spectra an amount of SO_2 different from zero is found. Thus one can conclude, that there are some references which contain a non-negligible amount of volcanic trace gases. In rare (ca. 10% of the data) scenarios, the volcanic plume covers the whole scan region. This could happen if for example the volcanic plume of the day before extends over the hole scan area as a consequence of windless conditions. In consequence, the reference is contaminated with volcanic trace gases. Thus, the gas amount is underestimated by the conventional NOVAC-evaluation: In Figure 4.7 an example from April 2011 (Tungurahua) where the reference region is contaminated by volcanic trace gases is shown. The blue SO_2 curve shows the calculations with the NOVAC-evaluation, but since there is still SO_2 in the reference region, the assumption, that the SO_2 amount could be set to zero in the reference region is wrong. The red curve shows the SO_2 curve, retrieved with a solar atlas spectrum as reference, which lies significantly above the NOVAC -curve.

If the reference region for any reason is contaminated by volcanic trace gases, there
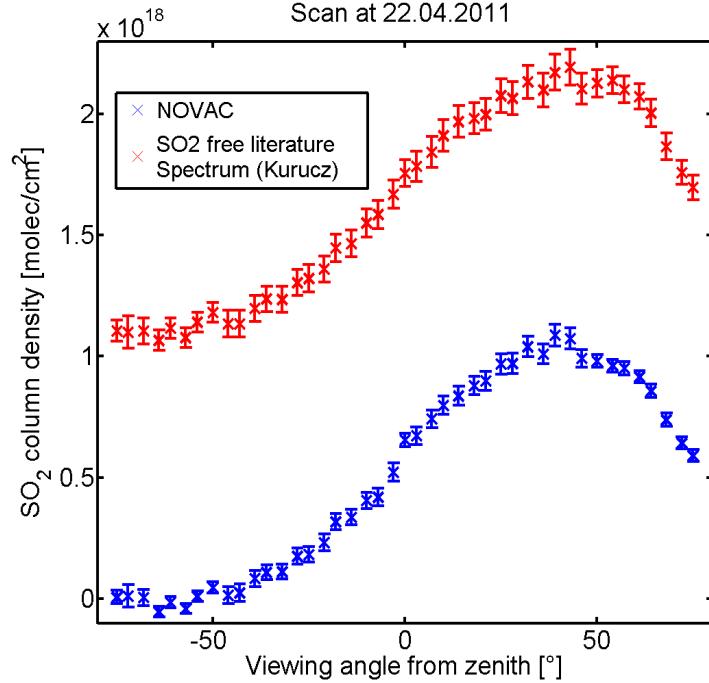
Figure 4.7: Scan with a contaminated reference spectrum from April 2011. From Warnach (2015)

are two possibilities: excluding the contaminated data from the evaluation or the reference spectrum has to be replaced by a volcanic-gas-free reference. Alternative spectra are a theoretical solar atlas spectrum or a volcanic-gas-free reference spectrum recorded by the same instrument at another time.

A further possibility is to assume, that contamination only occurs for SO2, but not for BrO due to the smaller lifetimes of BrO, thus it is possible to use the Solar atlas spectrum for the SO_2 evaluation, but the reference, recorded by the NOVAC-instrument at the same time for the BrO retrieval. Hereby the assumption, that BrO is not contaminated need to be proved.

In the following I will discuss the two alternative reference spectra.

Evaluation using a Solar Atlas spectrum

An alternative for choosing the region with the lowest column density as reference region is to use a theoretical high resolution solar atlas spectrum as reference (Chance and Kurucz, 2010). The use of a theoretical solar atlas spectrum as a reference which is completely volcanic-trace-gases-free was first proposed by Salerno et al. (2009) and evolved by (Lübcke et al., 2014). The advantage of using a solar atlas spectrum as reference is, that it is sure that it is not affected by past or current volcanic gas emissions. Thus, it allows for a retrieval of the absolute trace gas SCDs

in the volcanic gas plume. The disadvantage is, that using a solar atlas spectrum comes along with a drawback of precision: The spectral resolution of the theoretical solar atlas spectrum is much higher than of the NOVAC instruments. Therefore the instrument functions would need to be perfectly modeled and added to the retrieval. This is not straight forward, because the instrumental line-shape varies over the wavelength region and is also mathmatically often not perfectly described by a simple approach like Gauss, lorents,..etc.

The reduction of precision is acceptable for the SO_2 retrieval but not suitable for a BrO retrieval because then most data would be below the detection limit.

Possible contaminations can be checked by a theoretical solar atlas spectrum to evaluate the SO_2 amount in the reference.

Evaluation using a spectrum of the same instrument

An alternative reference spectrum could be a volcanic-gas-free reference spectrum recorded by the same instrument at a different time. When using such a reference several problems occur:

As described in chapter 3 the instruments used in NOVAC do not include features like temperature stabilization. Due to that the measurements are not independent of external parameters. So it is necessary to choose a reference recorded at similar conditions with respect to meteorology and radiation as well as in the temporal proximity due to instrumental changes with time and ambient conditions. Ideally the external conditions should be equal to the conditions at the time when the plume was recorded.

When performing the evaluation with the Solar Atlas Spectrum as reference, finding the instrument function occur to be a central challenge. If the instrument function for the solar atlas spectrum is found the functions is typically used for a few years This could lead to higher errors due to an gradual worse matching instrument function. Using the reference of the same instrument but recorded at another day, leads also to problems caused by different instrument functions, but compared to the calculated instrument function used for the evaluation with the solar atlas spectrum those differences in the instrument function could be smaller.

In this work I combine both options in order to achieve both, enhanced accuracy but still maximum possible precision of the SO_2 and BrO retrievals. So I use the solar atlas spectrum to check for contamination and a reference spectrum recorded in temporal proximity by the same instrument as reference.

The probability of contamination changes with the daytime as can be seen in fig. 4.8. In the Morning the probability of contamination is much lower than at noon. Thus one can conclude that the conditions at the day favors the occurrence of contamination more than the conditions at night. The decrease of contamination at the evening can be a result of less data, and is therefore not significant.

If contamination occurs it is possible to choose a new reference from a list of
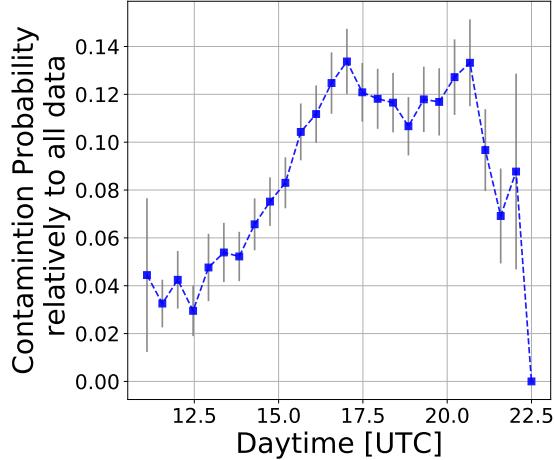
Figure 4.8: The possibility of contamination relatively to all not contaminated data recorded at the same time as a function of the day time. The probability is calculated by dividing the amount of contaminated scans recorded at a specific daytime by the amount of not contaminated data recorded at the same daytime. The square root of the data amount is taken as the error, the visualized error is than calculated by using error propagation. The local time can be calculated from the daytime as UTC-5h. The data are taken from the Nevado del Ruiz volcano.

gas free alternative references. In theory, for ideal instruments all references should lead to the same results for the gas retrievals. But instruments are imperfect (see Chapter 4) thus the reference need to be chosen carefully in order to ensure reliable results.

4.4.1 Contamination of the plume

As discussed above it might occur, that the reference is contaminated for example by the plume of the day before. If that happens, the gas amount is underestimated by using a contaminated reference. But another possibility is, that the plume itself is also contaminated. This might be the case if the volcanic gas of the volcano is not taken away by the wind, but accumulates at the instrument. If this is the case, using an other reference would lead to an overestimation of the column density of gases. With the data retrieved by the NOVAC instruments it is very difficult to discover whether the plume is contaminated or not.

Plume contamination could occur in a scenario described by fig. 4.9. This might be the case if the volcanic gas of the volcano is not taken away by the wind, but accumulates in the vicinity of the volcano and thus is seen by the instrument. In such a scenario, using an contamination free reference recorded at another time would
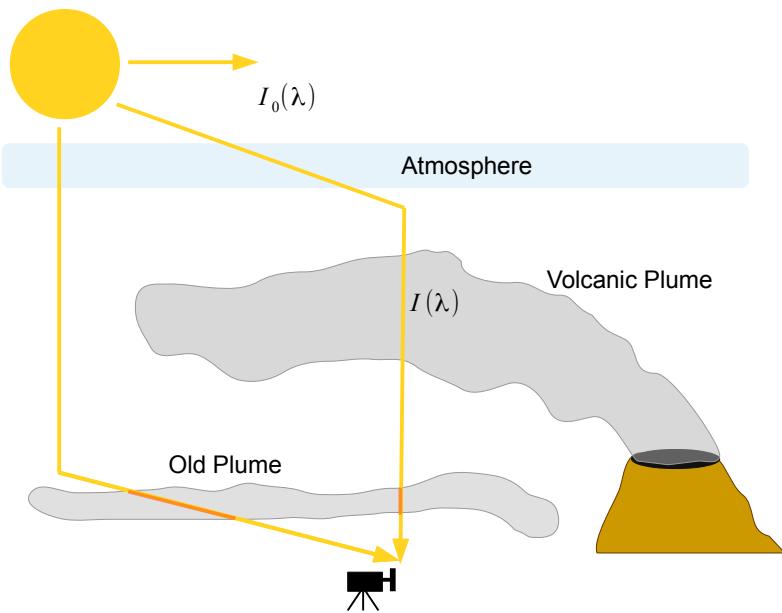
Figure 4.9: Visualization of the contamination of the plume. Due to a lack of wind the old plume sinks down an accumulates above the instrument. The light path trough the old plume is longer when recording the reference spectra (orange).
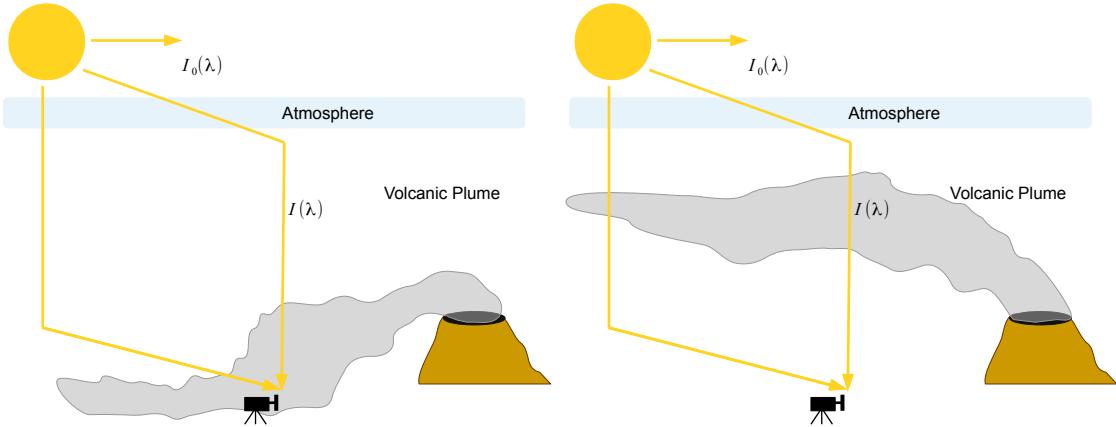
Figure 4.10: Visualization of possible scenarios for contamination. Left: the plume sinks in a way that the instrument is within the plume, therefore, all elavation angles will contain volcanic trace gases, while the plume is not additionally contaminated. Right: the plume covers the hole sky, thus all elvation angles "see" volcanic trace gases.
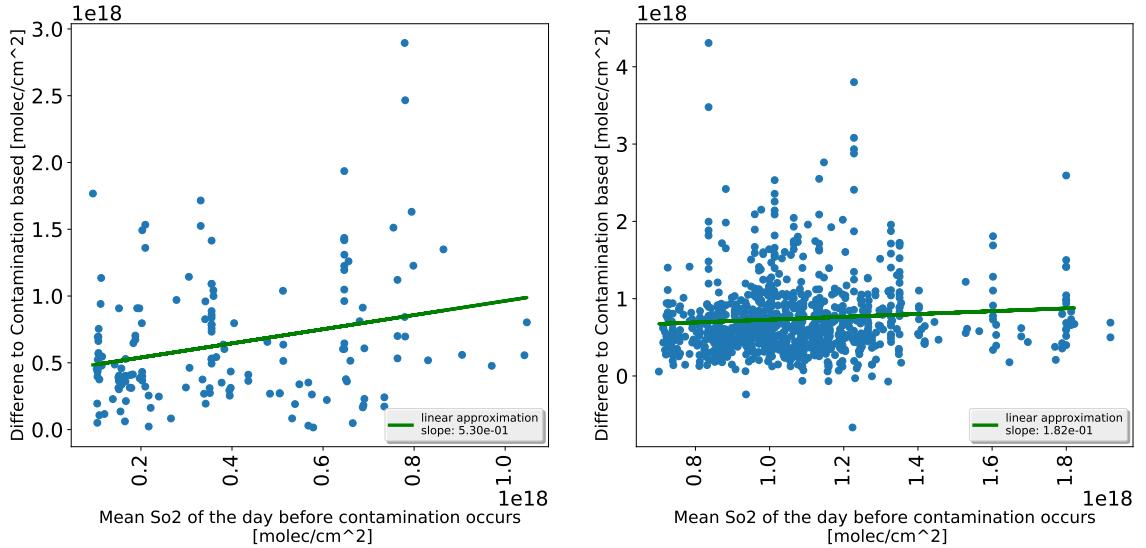
Figure 4.11: The strength of contamination as function of the mean SO_2 column density (daily mean) of the day before. The strength of contamination is defined as the difference in SO_2 SCD when evaluation with an alternative reference, or neglect the contamination. Left: data from Tungurahua. Right: data from Nevado Del Ruiz.

lead to an overestimation of the gas column densities in the plume.

This is one possible occurrence of contamination. As it can be seen gas of the old plume affects the measurement of the reference and the plume. However, for this example the influence on the measurement of the reference is much larger since the light path trough the old plume (coloured orange in fig. 4.9) is longer for the reference than for the measurement of the volcanic plume. Thus, the gas amount is underestimated by not using a gas free reference, but might be overestimate a gas free reference spectrum is used. The real gas amount might be between the measured amount with and without using a reference measured at another time.

With the data retrieved by the NOVAC instruments it is very difficult or even impossible to discover whether the plume is contaminated or not.

If the contamination is a result of strong emissions of the day before, a dependency of the strength of contamination on the emission of the day before could appear. The mean SO_2 SCDs of a day (daily mean) could be used as a proxy for the total emission. The strength of contamination can be calculated as the difference between the evaluation for SO_2 with a contaminated reference recorded at the same time as the plume spectrum was recorded and using a gas free reference. Such a plot is shown for Tungurahua and Nevado del Ruiz in fig. 4.11. Even though both plots

show a slight increase of contamination strength with the mean amount of SO_2 of the day before, the increase is not significant. Another possible proxy for the SO_2 emission would be the maximum SO_2 SCD of the day before contamination occures. However, taking the maximum does not lead to more significant relation between the emission and the strength of contamination.

Thus the SO_2 emission is if it influences the possibility of contamination not the only significant factor. To further examine the reasons for contamination the wind conditions should be studied in particular.

However this thesis is build on the assumption, that the plume is free of additional contamination. In the following I discuss how to automatically determine an optimal reference from another scan.

Part II

Empirics

5 BrO evaluation and its limitations

This chapter discusses the evaluation of the BrO SCD , calculated from the spectra recorded by the spectroscopic instruments of NOVAC. The BrO SCD error hereby taken as a measure for the quality of the BrO retrieval.
Figure 5.1 shows the BrO "Multi Add"[*] retrieval error distribution, which is centered around $1.1 \cdot 10^{+13}$ to $1.4 \cdot 10^{+13} \frac{molec}{cm^2}$.

The evaluation of the data from NOVAC are separated in the evaluation of SO_2 and the evaluation of BrO. While the retrieval of SO_2 is relatively easy due to the high amount of SO_2 in the plume (magnitude of SO_2 at Tungurahua $\approx 1 \cdot 10^{18}$), the BrO evaluation is much more challenging due to not distinct BrO curves as a result of the lower BrO magnitudes (as can be seen in Figure 4.3). The magnitude of BrO SCD is around $\approx 1 \cdot 10^{14} \frac{molec}{cm^2}$.
 This results in a larger uncertainty of the BrO SCD. Most of the BrO data (98.3% of the data) are below the detection limit of $BrO_{err}/BrO_{value}{<}1/4$. Hereby is BrO_{err} the BrO fit error, and BrO_{value} the BrO SCD. In comparison SCDs of SO_2 in almost all cases (99.5% of the data) are above the detection limit.
Choosing a different reference spectrum than the reference measured at the same time as the plume in 99% of all possible cases results in an increasing of the absolute error. It is expected that the evaluation with an alternative spectrum results in general in a higher BrO error than when evaluated with the same time spectrum. However, for a contaminated same-time-reference the relative error might decrease due to the underestimation of the gas amount.
Due to the large uncertainty of BrO relative to SO_2 the optimization of the BrO error is of particular importance. Therefore, the reference is chosen with respect to the BrO error to maximize the quality of the BrO/SO_2 ratio.

The amount of gas free alternative references is around 1500 per year. To make an optimal choice, it is necessary to examine the conditions which influence the BrO retrieval.
Every spectrum is recorded under particular/unique ambient conditions. These measuring conditions generally are not equal for different scans. In this study, I show that references for which the surrounding conditions e.g temperature or cloudiness are similar with the surrounding conditions of the plume measuring lead to a smaller error.

---

[*]More information about the multiadd-retrieval and the fit settings can be found in Section 4.3
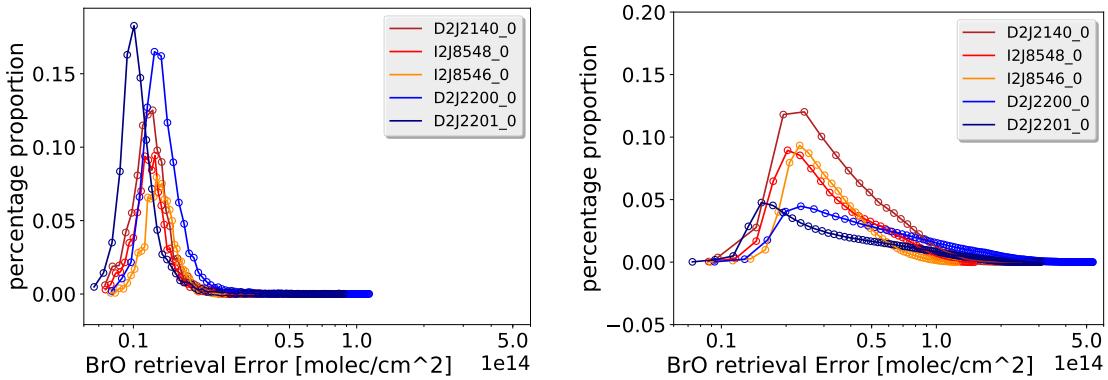
Figure 5.1: Histogram of BrO error, shown for all instruments considered in this thesis. Left: The BrO distribution for the "same time retrieval".Right: The BrO error distribution for the evaluation with a reference from another time, where the temporal difference between plume and reference is not longer that two weeks. The instruments of Nevado del Ruiz are coloured blue, while the the instruments of Tungurahua are coloured in yellow to red. The peaks for the single instrument are located at: D2J2140_0 : $1.2 \cdot 10^{13} \frac{molec}{cm^2}$; I2J8548_0 : $1.3 \cdot 10^{13} \frac{molec}{cm^2}$; I2J8546_0 : $1.4 \cdot 10^{13} \frac{molec}{cm^2}$; D2J2200_0: $1.4 \cdot 10^{13} \frac{molec}{cm^2}$; D2J2201_0: $1.1 \cdot 10^{13} \frac{molec}{cm^2}$

Data used for the analysis

I evaluate a fixed plume spectrum using more than 1000 recorded multi add reference spectra in order to find the optimal reference spectrum. This evaluation is performed for more than 1000 multi add plume spectra in order to obtain a high statistical significance. Thus 1000 recorded multi add spectra result in 1000^2 possible plume reference pairs and the corresponding differences in the external parameter and their associated BrO error.

5.1 Influence of ambient conditions on the measurement

The measurement and evaluation of the spectra monitored with NOVAC depends on the ambient conditions like temperature or cloudiness (Lübcke, 2014).
Thus, the ambient conditions need to be taken into account for choosing a new reference.
The analysis of these external parameters are performed for spectra recorded at Tungurahua and Nevado del Ruiz. At Tungurahua three instruments (I2J8548_0 ; D2J2140_0 ; I2J8546_0) with data recorded in the time span from July in 2008 to August in 2009 are used. Nevado del Ruiz contributes with two instruments (D2J2200_0; D2J2201_0) in the time from the end of 2009 to the end of 2011.

The ambient conditions that are considered in this thesis are:

Temporal difference	Temporal difference between measuring the plume and the reference.
Daytime	Time of the day, and thus a measure of solar altitude.
Temperature	The temperature of the instrument while recording the spectra.
Colour index	Ratio of two intensities at different wavelength as a measure for the cloudiness of the sky.
Exposure time	Length of time the sensor of the NOVAC instrument is exposed to light.
Elevation angle	Orientation of the instrument relative to the zenith, which corresponds to an elevation angle of zero degree.

5.1.1 Statistical assessment scale

The external parameters described above are analysed one by one in the following sections. Hereby I will proceed as follows: A first step is to define a maximal temporal difference to prevent too large computational time.

The BrO measurement error as a function of the difference in the specific external parameter between the reference spectrum and the plume spectrum is shown for each of the individual instruments at Tungurahua and Nevado del Ruiz. To quantify the dependence between the BrO retrieval error and the external parameter, the data are fitted with a first order polynomial for each of the individual instruments at Tungurahua and Nevado del Ruiz. Hereby only the absolute differences were used. For every external parameter the fitting parameters slope and intercept are calculated.

Moreover, the correlation(See site 44) between the BrO fit error and the absolute difference in the specific external parameter is calculated. If the BrO retrieval increases with increasing differences in surrounding condition between the plume spectra and the reference spectra, the difference, where the BrO retrieval error $Mean(\Delta EP_2)^*$ is twice as high as for no difference is also calculated.

Differences in external parameters can lead to large uncertainties in the retrieval, thus I analyse the amount of data possible references, if only data with differences smaller than $Mean(\Delta EP_2)$ in the specific external parameter are used. The advantage of restricting the accepted difference between the plume and the reference spectrum is a better control of the choice of the best reference. The disadvantage is

---

*EP: placeholder for any external parameter

that the amount of possible references decreases. Thus, it could occur that a reference is dismissed, which has a large difference in one parameter but is very similar in the remaining parameters.

The Mean, the corresponding standard deviation as well as the minimum and the maximum amount of references are calculated for each instrument.

The Correlation coefficient $\rho_{X,Y}$ used in this thesis refer to the pearson product-moment correlation coefficients. It is a measure of linear correlation between two variables X and Y. The pearson correaltion coefficients range from -1 to +1. Where +1 is total positive linear correlation, -1 describes a total negative linear correlation, and a correlation of 0 refers to no linear correlation. The formula for the correlation coefficient is:

$$\rho_{X,Y} = \frac{cov\,(X,Y)}{\sigma_X \sigma_Y}$$

were: cov is the covariance
σ_X is the standard deviation of X
σ_Y is the standard deviation of Y
Here the correlation is computed using the python[*] library Numpy (version 1.5.6)

5.1.2 Temporal difference

Variation in the ambient conditions cause a temporal variation if the instrument response function/cause an instrumental drift. This could a result of the same changes which lead to the wavelength shift over time observed by Warnach (2015). Warnach (2015) suggests that the drift is caused by a hysteresis effect. Figure 5.2 shows the wavelength shift as a function of the time for six NOVAC instruments located at Tungurahua in the time between 2008 to 2014. Figure 5.2 shows a rather steep drift in this time interval. Warnach (2015) observed a decrease of the shift after initial negative drift after the first two years at Pillate station. Thus an rather step drift at new installed instruments can be observed. Therefore, it is observed that the temporal difference becomes less important after an initial adaptation on the surroundings after the installation of the instruments.

When using reference and plume spectra of the same time, these effects are cut out since the shift is equal for the plume and reference spectrum.

To examine the effect of the temporal difference on the retrieved BrO error, for all reference-plume pairs the corresponding BrO error is calculated. Due to the large amount of reference plume pairs within one year, it takes more than a month (Hardware details: Intel(R) Core(TM) i5-4570 CPU @ 3.20Ghz 64 Bit operating system, amount of 4 kernels) to evaluate the corresponding BrO error for every possible reference-plume pair of one instrument. I did this for the D2J2140_0 instrument installed at Tungurahua:

With the data from the D2J2140_0 instrument the dependence between the BrO
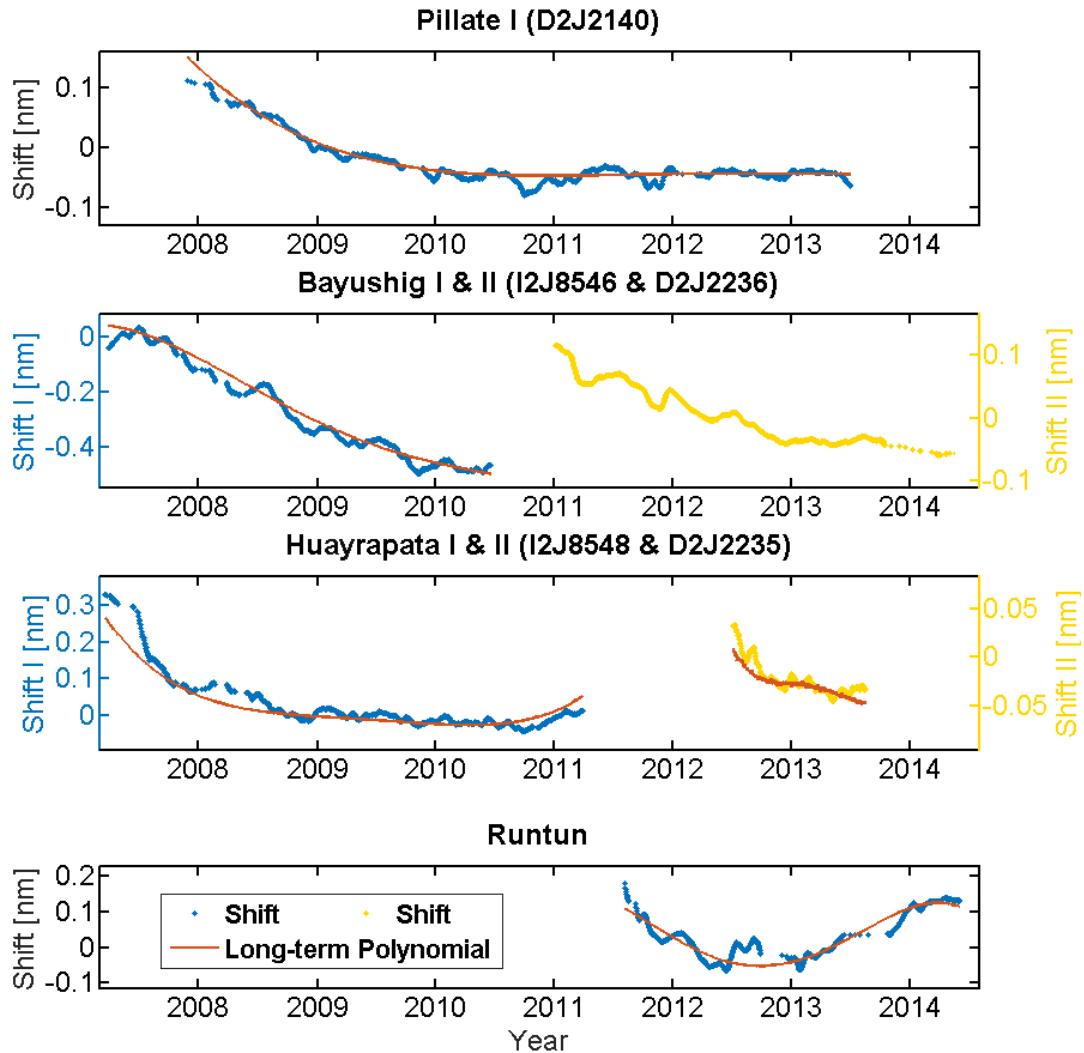
Figure 5.2: Wavelength shift over the time. The shift is shown for six NOVAC- instruments from Tungurahua. The red and yellow dots show the running mean over 20 days. Red line indicates a temperature independent long term polynomial. Source: Warnach (2015)
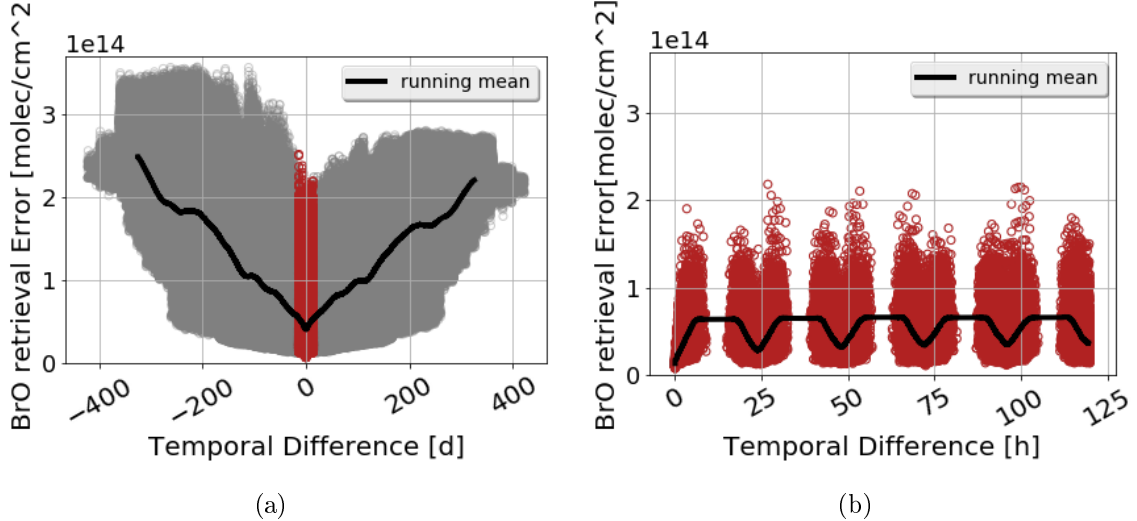
Figure 5.3: The BrO error as a function of the temporal difference shown for the Pillate instrument from Tungurahua (2008-2009). The running mean is plotted with a black line. (a) Temporal differences up to 400 days. (b) Absolute temporal differences up to $\pm$ 120h. The periodical BrO error evolution indicates the impact of the daytime.

retrieval error and the temporal difference between measuring the plume spectrum and the reference spectrum.

For an increasing temporal different between reference and plume measurement time the fit quality decreases on the average (On short timescales the influence of the temperature, daytime or other external parameter could be counteractive to the impact of the temporal distance). Thus a large temporal difference results in an increase of the BrO error of more than 600% (see fig. 5.3 (a)). BrO errors of such magnitudes are too large for our purposes. Therefore, it is useful to set a maximal temporal difference, to prevent too large BrO error and to reduce the calculation time. In fig. 5.3 (a) it can be seen that the evolution of the BrO error with the temporal difference is symmetric around zero. Thus it is not necessary to distinguish between positive or negative temporal differences.

To evaluate the maximal time difference, for which the results are still reliable for every plume, where the "same time reference" is contaminated, the alternative reference is chosen, which leads to the minimal BrO error.

In fig. 5.4 a histogram with the probability of picking the best reference as a function of the time difference is plotted. The mean of the Gaussian fitted on the data is slightly above zero. However the variance is calculated as approximately 14 days, thus a mean of 0.9 is statistical irrelevant. To simplify the evaluation, and for a better traceability the absolute maximal temporal difference between the recording time of the reference and the plume spectrum should be equal for references recorded before and after the plume. For the retrieval all time differences are al-
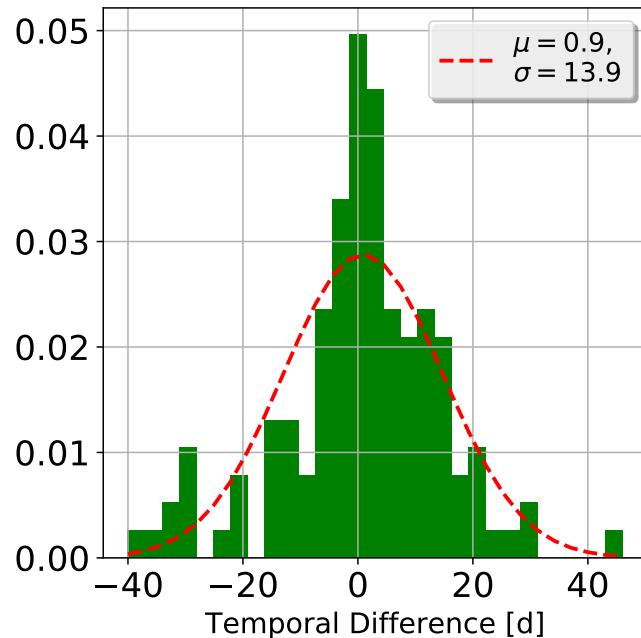
Figure 5.4: Histogram showing the frequency of getting the best reference as function of the temporal difference between plume and reference measuring. The temporal difference is negative if the reference spectrum was recorded after the plume spectrum. A Gaussian-like distribution is retrieved. The red dotted line visualizes a Gaussian fit for the shown histogram. The mean μ of the gaussian curve is: $\mu = 0.9$, the variance σ is: $\sigma = 13.9$. The width of the green bars is three days.

lowed within one sigma area. Thus, the maximal time difference is about two weeks.

Table 5.1: Amount of possible references when restricting the time span between plume and reference to two weeks. Here in the "Mean" and "Std" row for each instrument the average restriction is shown with the corresponding standard deviation. The "Min" and "Max" rows show the extend of restriction in the extreme cases.

Instrument	D2J2140_0	I2J8546_0	I2J8548_0	D2J2200_0	D2J2201_0
Mean	84.6	163.7	217.1	284.0	225.6
Std	35.8	29.9	64.8	69.5	41.2
Min	8	113	97	64	63
Max	169	214	399	433	297

By restricting the temporal difference to $\pm$ 14 days, the amount of possible gas free references decreases to an average of 195 alternative references per contaminated plume (see table 5.1). Hereby in the data considered in this thesis every plume has potential alternative reference spectra and the minimum amount of references is 8. However in general a plume without alternative references could occur.

If a continuous evaluation is required, this means the spectra are evaluated directly after the recording, the number of suitable gas free references halves since only references recorded before the plume are available.

For the following analysis of the remaining external parameters all absolute temporal differences are below 14 days.

Figure 5.3 (b) shows the evolution of the BrO error for a maximal absolute temporal difference of 120 hours. It is only possible to record data during daytime. This causes the lack of data in the night time. A periodic decrease of the BrO error can be seen. This is a result of a decrease of the BrO error when the ambient conditions coincidence. In this case the daytime coincidence causes the BrO error decrease. This effect is analysed in detail in the following.

5.1.3 Daytime

Here I discuss the dependence of the BrO retrieval error based on the bulk effect of a difference in daytime. During the day a lot of external parameters like temperature, solar zenith angle etc. change. In particular, the solar zenith angle could have an impact on the fit quality since the light path of the sun is much longer in the morning or evening compared to the noon. Therefore, the scattering effects and the light intensity are different for both spectra.

In fig. 5.6 the BrO error is plotted against the daytime difference between the plume spectrum and the reference spectrum.
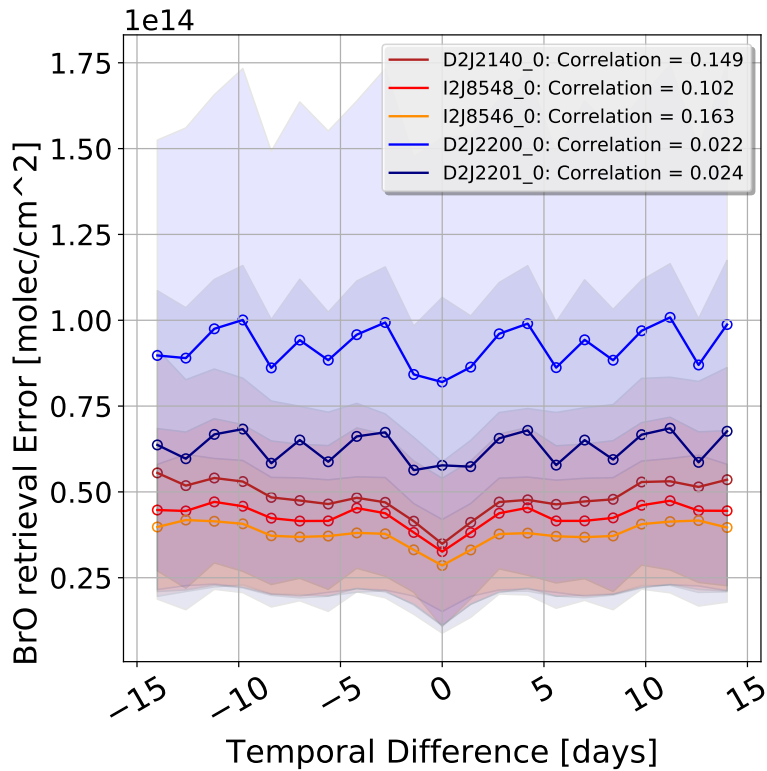
Figure 5.5: The BrO measurement error as a function of the temporal difference in days between the reference and the plume is shown for each of the individual instruments at Tungurahua and Nevado del Ruiz. The instruments at Nevado del Ruiz are coloured in blue, while the instruments at Tungurahua are coloured in red colour tones. To evaluate the plume spectra all reference spectra with a temporal distance of no longer than two weeks are used. An increase of the BrO error with the absolute difference in temperature is observable. This is quantified by a correlation between the BrO retrieval error and the absolute temporal difference. The plots reveal a symmetry around the axis with zero temperature difference.
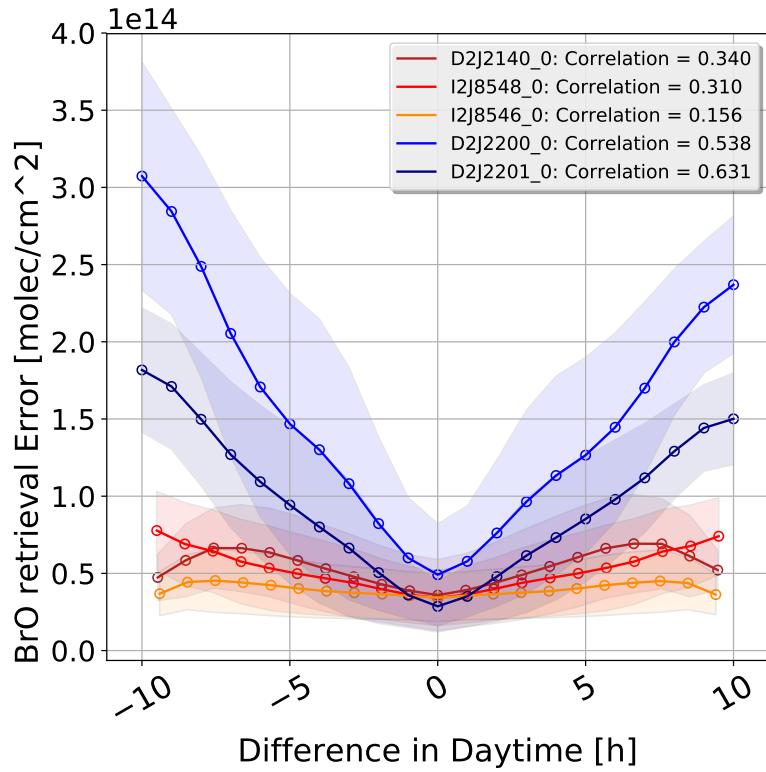
Figure 5.6: The BrO measurement error as a function of the difference of daytime between the reference and the plume is shown for each of the individual instruments at Tungurahua and Nevado del Ruiz. To evaluate the plume spectra all reference spectra with a temporal distance of no longer than two weeks are used. An increase of the BrO error with the absolute difference in daytime is observable. This is quantified by a correlation between the BrO retrieval error and the absolute difference in daytime. The plots reveal a symmetry around axis with zero daytime difference.

Because of the observed symmetry around zero the absolute daytime difference is used for the fit. The computed fitting parameters slope and intercept for each instrument are shown in tab. 5.2.

As it can be seen in tab. 5.2, the intercepts, which defines the main BrO retrieval error for a daytime difference of zero, vary at Tungurahua between $3.3 \cdot 10^{13} \frac{molec}{cm^2}$ and $3.4 \cdot 10^{13} \frac{molec}{cm^2}$. The variation at Nevado del Ruiz ranges from $2.2 \cdot 10^{13} \frac{molec}{cm^2}$ to $4.0 \cdot 10^{13} \frac{molec}{cm^2}$.

The correlation coefficient between daytime und BrO fit error ranges from 0.156 for the instrument I2J8546_0 to 0.631 for D2J2201_0 and exhibits a large variation between the instruments. This lead to the conclusion, that the dependence of the fit quality on the daytime depends largely on the location of the instrument.

The ΔDT_2, the daytime difference for which the BrO retrieval error doubles compared to a daytime difference of zero is rather high for the instruments installed at Tungurahua (6.8h to 24.2h) and rather low for the instruments installed at Nevado del Ruiz (11.62h to 1.9h).

Table 5.2: The BrO measurement error as a function of the difference of daytime in hours between the reference and the plume is fitted with a first order polynomial for each of the individual instruments at Tungurahua and Nevado del Ruiz. This table shows the fitting parameters slope and intercept. Moreover, the correlation between the BrO error and the absolute daytime difference is shown. In the ΔDT_2 row the daytime difference for which the error doubles compared to a daytime difference of zero is shown.

Instrument	D2J2140_0	I2J8546_0	I2J8548_0	D2J2200_0	D2J2201_0
Slope	$5.07 \cdot 10^{12}$	$1.40 \cdot 10^{12}$	$3.77 \cdot 10^{12}$	$2.04 \cdot 10^{13}$	$1.38 \cdot 10^{13}$
Correlation	0.340	0.156	0.310	0.538	0.631
Intercept	$3.43 \cdot 10^{13}$	$3.39 \cdot 10^{13}$	$3.28 \cdot 10^{13}$	$4.01 \cdot 10^{13}$	$2.24 \cdot 10^{13}$
ΔDT_2	6.8	24.2	8.7	1.9	1.62

The mean $Mean(\Delta DT_2)$ is calculated without taking the instrument I2J8546_0 into account due to the low correlation of 0.156. Using the I2J8546_0 instrument as well would lead to an $Mean(\Delta DT_2)$ of 8.6h, thus, the restriction would not have any influence, since the maximal time difference is limited to the time where the sun is shining.

Excluding references with daytime differences above 4.75h restricts the amount of potential references to 85.1% for D2J2140_0 to 96.8% for D2J2200_0. In extreme cases a restriction down to 51.3% of the entire set of references can occur (see table 5.3).
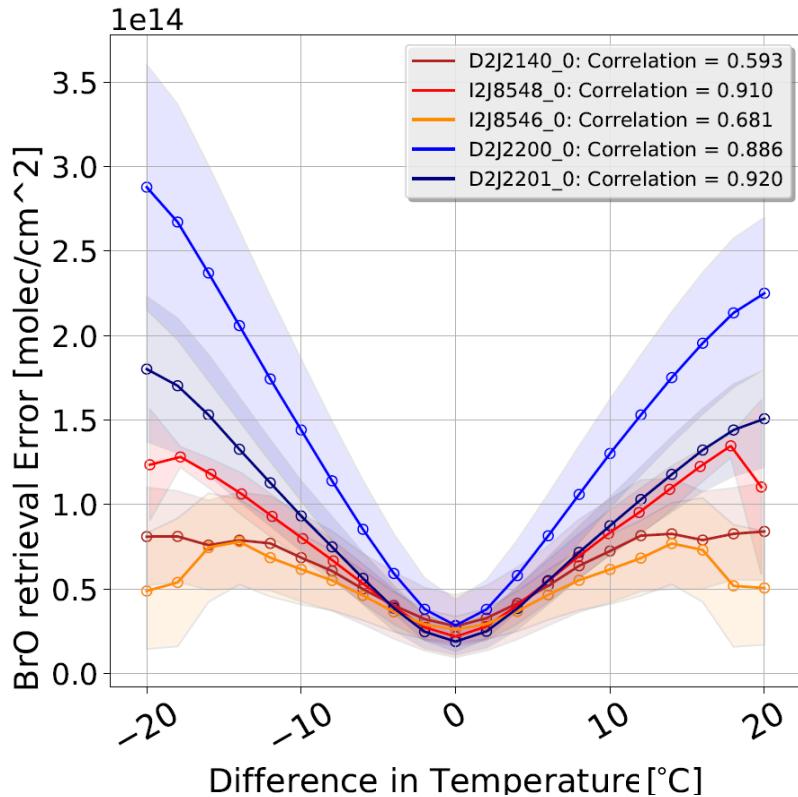
Figure 5.7: The BrO measurement error as a function of the difference of temperature between the reference and the plume is shown for each of the individual instruments at Tungurahua and Nevado del Ruiz. To evaluate the plume spectra all reference spectra with a temporal distance of no longer than two weeks are used. An increase of the BrO error with the absolute difference in temperature is observable. This is quantified by a correlation between the BrO retrieval error and the absolute difference in temperature. The plots reveal a symmetry around the axis with zero temperature difference.

Table 5.3: This table shows the absolute amount and the percentage corresponding to initial number of references without any restrictions of ambient conditions (see tab. 5.1) of remaining references if restricting the daytime difference to the mean ΔDT_2 over all instruments except I2J8546_0 due to the large uncertainty ($Mean(\Delta DT_2) = 4.75h$). Here in the "Mean" and "Std" row for each instrument the average restriction is shown with the corresponding standard deviation. The "Min" and "Max" rows show the extend of restriction in the extreme cases (minimum and maximum amount of available references / restriction ratio).

Instrument	D2J2140_0	I2J8546_0	I2J8548_0	D2J2200_0	D2J2201_0
Mean	72.0 ($\hat{=}85.1\%$)	147.4 ($\hat{=}90.0\%$)	198.4 ($\hat{=}91.4\%$)	275.0 ($\hat{=}96.8\%$)	205.8 ($\hat{=}91.2\%$)
Std	31.87 ($\hat{=}89.0\%$)	32.0 ($\hat{=}107.0\%$)	71.0 ($\hat{=}109.5\%$)	70.8 ($\hat{=}101.8\%$)	50.1 ($\hat{=}121.6\%$)
Min	6 ($\hat{=}75.0\%$)	58 ($\hat{=}51.3\%$)	91 ($\hat{=}93.8\%$)	54 ($\hat{=}84.4\%$)	45 ($\hat{=}71.4\%$)
Max	160 ($\hat{=}94.7\%$)	214 ($\hat{=}100\%$)	399 ($\hat{=}100\%$)	433 ($\hat{=}100\%$)	297 ($\hat{=}100\%$)

5.1.4 Temperature

In this section I discuss the particular effect of a difference in temperature, which has been shown to be the most important influence. The instrument design of the NOVAC instruments compromises between accuracy and robustness as explained in chapter 3. In particular, there are no internal thermal stabilizations installed as an attempt to reduce the instruments power consumption and increase the robustness. This can influence the recorded spectra.

The ambient temperature however has an influence on the optical adjustment of the NOVAC instrument and thus on the instrument line function and calibration of the spectrometer. The calibration for the wavelength to pixel mapping (WPM) is commonly determined by a mercury lamp or by the comparison with a highly resolved solar atlas Chance and Kurucz (2010). As the WPM depends on the optical alignment of the spectrometer, which itself depends on the temperature, it is not constant. Changes in the spectrometers temperature can cause changes in the instrument line function and shifts in the WPM (Pinardi et al., 2007). Moreover, Warnach (2015) show that, short term shifts are related to the instrument temperature (see fig. 5.8).

The above discussed temperature dependence of the instrument line function causes a reduction of the fit quality with increasing instrument temperature difference between plume and reference (see fig. 5.7). Thus, the BrO error also increases with the temperature difference. Compared to the other external parameters the temperature difference has the largest impact on the BrO error.
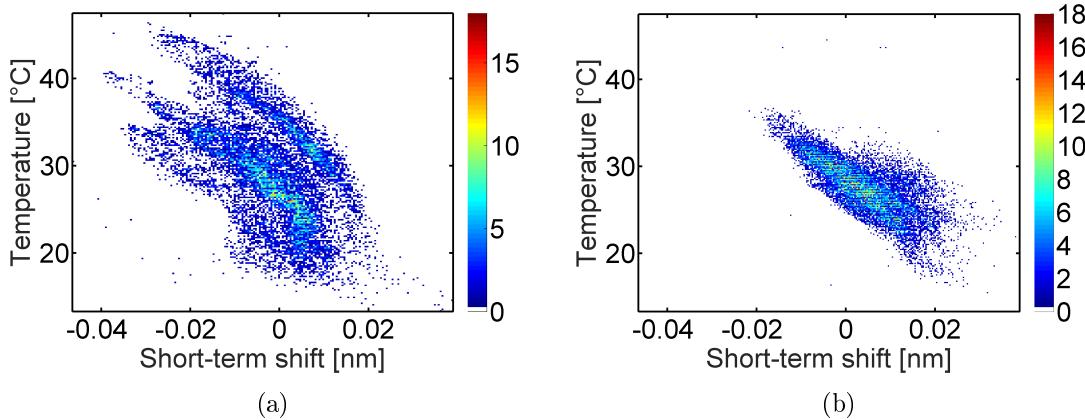
Figure 5.8: Short term wavelength as a function of the instrument temperature for Pillate 1. The coloring of the scatter points indicate the temporal evolvement. (a) initial period prior to January 2010 (b) after 2010. Source: Warnach (2015).

The plots reveal a symmetry around axis with zero temperature difference (see fig. 5.7), thus using only the absolute temperature difference for the fit is reasonable. The intercepts for the BrO fit error at Tungurahua vary from $1.6 \cdot 10^{13} \frac{molec}{cm^2}$ to $2.58 \cdot 10^{13} \frac{molec}{cm^2}$ (see tab. 5.4). The intercepts at Nevado del Ruiz are lower and ranges from $9.07 \cdot 10^{12} \frac{molec}{cm^2}$ to $1.38 \cdot 10^{13} \frac{molec}{cm^2}$. The ΔT_2 from the data of Tungurahua (2.5 K to 6.3K) are significantly higher as at Nevado del Ruiz (1.1 K). The mean ΔT_2 is 3.3K. Accordingly, the temperature has a stronger influence at the Nevado del Ruiz volcano.

The correlation between the BrO error and the absolute temperature difference has a high significance. The correlation coefficients ranges from 0.593 for the instrument D2J2140_0 to 0.92 for D2J2201_0 and exhibits a large variation between the instruments.

The computed fitting parameters slope and intercept for each instrument are shown in tab. 5.4.

If restricting the temperature difference to the mean ΔT_2 over all instruments ($Mean(\Delta T_2) = 3.3$) the amount of possible references decrease as shown in tab. 5.5. Excluding references with temperature differences above $Mean(\Delta T_2) = 3.3$ restricts the amount of potential references to 46.8% for the $D2J2140\_0$ instrument to 82.3% for the $D2J2200\_0$ instrument.

5.1.5 Colour index

Clouds have a strong influence on the atmospheric radiative transfer and thus affect the interpretation and analysis of DOAS (Wagner et al., 2014). Clouds can be identified by several measurement quantities which they influence. As Mie scattering is
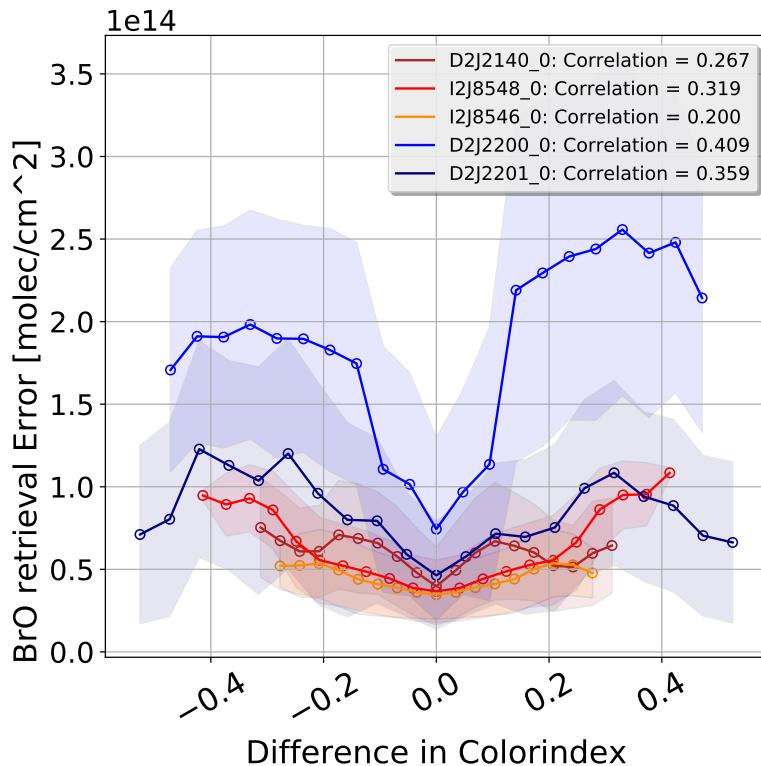
Figure 5.9: The BrO measurement error as a function of the difference of colour index between the reference and the plume is shown for each of the individual instruments at Tungurahua and Nevado del Ruiz. To evaluate the plume spectra all reference spectra with a temporal distance of no longer than two weeks are used. An increase of the BrO error with the absolute difference in colour index is observable. This is quantified by a correlation between the BrO retrieval error and the absolute difference in colour index. The plots reveal a symmetry around axis with zero colour index difference.

Table 5.4: The BrO measurement error as a function of the difference of temperature between the reference and the plume is fitted with a first order polynomial for each of the individual instruments at Tungurahua and Nevado del Ruiz. This table shows the fitting parameters slope and intercept. Moreover, the correlation between the BrO error and the absolute temperature difference is shown. For the temperature difference this correlation with an average of 0.797 is the highest compared to the other external parameters. In the ΔT_2 row the temperature difference for which the error doubles compared to a temperature difference of zero is shown. This is already the case for a difference of $3.3°C$

Instrument	D2J2140_0	I2J8546_0	I2J8548_0	D2J2200_0	D2J2201_0
Slope	$4.10 \cdot 10^{12}$	$3.93 \cdot 10^{12}$	$6.50 \cdot 10^{12}$	$1.24 \cdot 10^{13}$	$8.17 \cdot 10^{12}$
Correlation	0.593	0.681	0.910	0.886	0.920
Intercept	$2.58 \cdot 10^{13}$	$2.23 \cdot 10^{13}$	$1.60 \cdot 10^{13}$	$1.38 \cdot 10^{13}$	$9.07 \cdot 10^{12}$
ΔT_2	6.3	5.7	2.5	1.1	1.1

dominant in clouds the wavelength dependency of the light that is scattered is different than the Rayleigh sky. Different wavelengths are scattered similarly strong and thus clouds can be easily identified by their white color. Therefore, the cloudiness of the sky can be quantified in a scalar measure defined by the ratio of the measured intensity at two wavelengths, the so-called colour index (CI). Wagner et al. (2014) showed that for a zenith-looking instrument the measured radiation intensity is enhanced by clouds. Thus, clouds can cause large errors for the retrieved gas column density and the corresponding uncertainties. Cloud effects are especially severe if the cloudiness for the recorded plume and reference spectra strongly defer. Also for broken clouds the described effect can be observed as measurements at some elevation angles might be influenced by clouds while others are not. In this work I use the Colour Index between the intensities at 320nm and 360 nm. These two wavelengths are as far apart as the filter used for stray-light prevention in the spectrometers allows. On the other hand, the lower wavelength avoids the deep UV range where SO_2 and O_3 absorption plays a dominant role. The Mie scattering in the clouds is responsible for the higher amount of radiation from larger wavelengths. This results in a decrease of the CI which was observed for NOVAC instruments by Lübcke (2014).

I evaluated the CI at the zenith. To increase the stability of the fit I add 10 the intensities from 10 consecutive spectra. Using always the zenith to evaluate the colour index makes the colour index more comparable, but if broken clouds occur, the CI of the reference and the plume could differ from the calculated CI of the zenith. This could be a reason for the large deviations of the mean BrO error as function of the colour index (see fig. 5.9)

In fig. 5.9 the BrO error is plotted against the colour index difference between the plume and the reference spectrum. The plot is done similar as the plots for the

Table 5.5: This table shows the absolute amount and the ratio (to table 5.1) of remaining references if restricting the temperature difference to the mean ΔT_2 over all instruments ($Mean(\Delta T_2) = 3.3°C$). Here in the "Mean" and "Std" row for each instrument the average restriction is shown with the corresponding standard deviation. The "Min" and "Max" rows show the extend of restriction in the extreme cases (minimum and maximum amount of available references / restriction ratio).

Instrument	D2J2140_0	I2J8546_0	I2J8548_0	D2J2200_0	D2J2201_0
Mean	39.6 ($\hat{=}46.8\%$)	119.3 ($\hat{=}72.9\%$)	158.2 ($\hat{=}72.9\%$)	233.6 ($\hat{=}82.3\%$)	151.6 ($\hat{=}67.2\%$)
Std	24.7 ($\hat{=}68.9\%$)	50.4 ($\hat{=}168.6\%$)	76.0 ($\hat{=}117.2\%$)	84.5 ($\hat{=}121.6\%$)	72.6 ($\hat{=}176.2\%$)
Min	1 ($\hat{=}12.5\%$)	8 ($\hat{=}7.1\%$)	12 ($\hat{=}12.4\%$)	3 ($\hat{=}4.7\%$)	6 ($\hat{=}9.5\%$)
Max	130 ($\hat{=}76.9\%$)	213 ($\hat{=}99.5\%$)	386 ($\hat{=}96.7\%$)	414 ($\hat{=}95.6\%$)	296 ($\hat{=}99.7\%$)

temperature. The plots mostly reveal a symmetry around the zero colour index difference-axis. Thus, the absolute colour index can be used for the fitting which is done equivalently to the analysis of the temperature and the daytime. The computed fitting parameters slope and intercept for each instrument are shown in table 5.6. The intercepts at Tungurahua vary from $3.36 \cdot 10^{13} \frac{molec}{cm^2}$ to $4.01 \cdot 10^{13} \frac{molec}{cm^2}$. The variation at Nevado del Ruiz ranges from $4.74 \cdot 10^{13} \frac{molec}{cm^2}$ to $7.21 \cdot 10^{13} \frac{molec}{cm^2}$.
The correlation is as well calculated and ranges from 0.2 for the instrument I2J8546_0 to 0.409 for D2J2200_0.

Table 5.6: The BrO measurement error as a function of the difference of colour index between the reference and the plume is fitted with a first order polynomial for each of the individual instruments at Tungurahua and Nevado del Ruiz. This table shows the fitting parameters slope and intercept. Moreover, the correlation between the BrO error and the absolute colour index difference is shown. In the ΔCI_2 row the colour index difference for which the error doubles compared to a colour index difference of zero is shown.

Instrument	D2J2140_0	I2J8546_0	I2J8548_0	D2J2200_0	D2J2201_0
Slope	$2.30 \cdot 10^4$	$7.92 \cdot 10^{13}$	$1.17 \cdot 10^{14}$	$5.42 \cdot 10^{14}$	$1.91 \cdot 10^{14}$
Correlation	0.267	0.200	0.319	0.409	0.359
Intercept	$4.01 \cdot 10^{13}$	$3.36 \cdot 10^{13}$	$3.47 \cdot 10^{13}$	$7.21 \cdot 10^{13}$	$4.74 \cdot 10^{13}$
ΔCI_2	0.174	0.424	0.297	0.133	0.248

Table 5.7: This table shows the absolute amount and the ratio (to table 5.1) of remaining references if restricting the colour index difference to the mean ΔCI_2 over all instruments ($Mean(\Delta CI_2) = 0.2553$). Here in the "Mean" and "Std" row for each instrument the average restriction is shown with the corresponding standard deviation. The "Min" and "Max" rows show the extend of restriction in the extreme cases (minimum and maximum amount of available references / restriction ratio).

Instrument	D2J2140_0	I2J8546_0	I2J8548_0	D2J2200_0	D2J2201_0
Mean	84.6 ($\widehat{=}\,100\%$)	163.7 ($\widehat{=}\,100\%$)	215.6 ($\widehat{=}\,99.3\%$)	275.4 ($\widehat{=}\,97.0\%$)	219.4 ($\widehat{=}\,97.3\%$)
Std	35.8 ($\widehat{=}\,100\%$)	29.9 ($\widehat{=}\,100\%$)	65.4 ($\widehat{=}\,101\%$)	67.8 ($\widehat{=}\,97.6\%$)	49.86 ($\widehat{=}\,121\%$)
Min	8 ($\widehat{=}\,100\%$)	113 ($\widehat{=}\,100\%$)	97 ($\widehat{=}\,100\%$)	61 ($\widehat{=}\,95.3\%$)	28 ($\widehat{=}\,44.4\%$)
Max	169 ($\widehat{=}\,100\%$)	214 ($\widehat{=}\,100\%$)	399 ($\widehat{=}\,100\%$)	421 ($\widehat{=}\,97.2\%$)	297 ($\widehat{=}\,100\%$)

The $\Delta(CI_2)$ vary from 0.174 to 0.424 at Tungurahua and from 0.133 to 0.248 at Nevado del Ruiz, the the mean can be calculated as: $Mean(\Delta CI_2) = 0.255$. Exclusion of all references with a higher difference in the colour index than 0.255 does not chance the amount of references significantly (see table 5.7).

5.1.6 Elevation Angle

Table 5.8: The BrO measurement error as a function of the difference of elevation angle between the reference and the plume is fitted with a first order polynomial for each of the individual instruments at Tungurahua and Nevado del Ruiz. This table shows the fitting parameters slope and intercept. Moreover, the correlation between the BrO error and the absolute elevation angle difference is shown.

Instrument	D2J2140_0	I2J8546_0	I2J8548_0	D2J2200_0	D2J2201_0
Slope	$1.73{\cdot}10^{8}$	$1.55{\cdot}10^{10}$	$-9.00{\cdot}10^{9}$	$2.92{\cdot}10^{11}$	$-3.96{\cdot}10^{10}$
Correlation	0.000	-0.010	0.012	0.065	-0.034
Intercept	$4.77{\cdot}10^{13}$	$4.23{\cdot}10^{13}$	$3.78{\cdot}10^{13}$	$8.37{\cdot}10^{13}$	$6.44{\cdot}10^{13}$

The elevation angle describes the angle between the viewing direction and the zenith. When using the plume spectrum and the reference spectrum of the same time, the difference in elevation angle cannot be zero, since the location of the plume does not coincidence with the location of the reference.
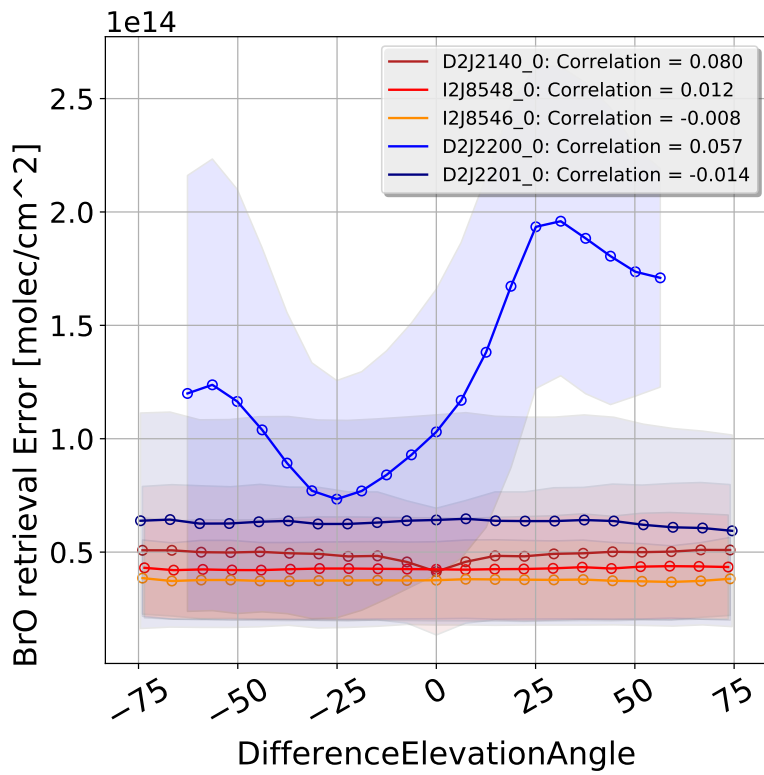
Figure 5.10: The BrO measurement error as a function of the difference of elevation angle between the reference and the plume is shown for each of the individual instruments at Tungurahua and Nevado del Ruiz. To evaluate the plume spectra all reference spectra with a temporal distance of no longer than two weeks are used. The plots do not reveal a symmetry around axis with zero elevation angle difference for all instruments. The D2J2200_0 instrument at Nevado del Ruiz is not symmetric around zero.
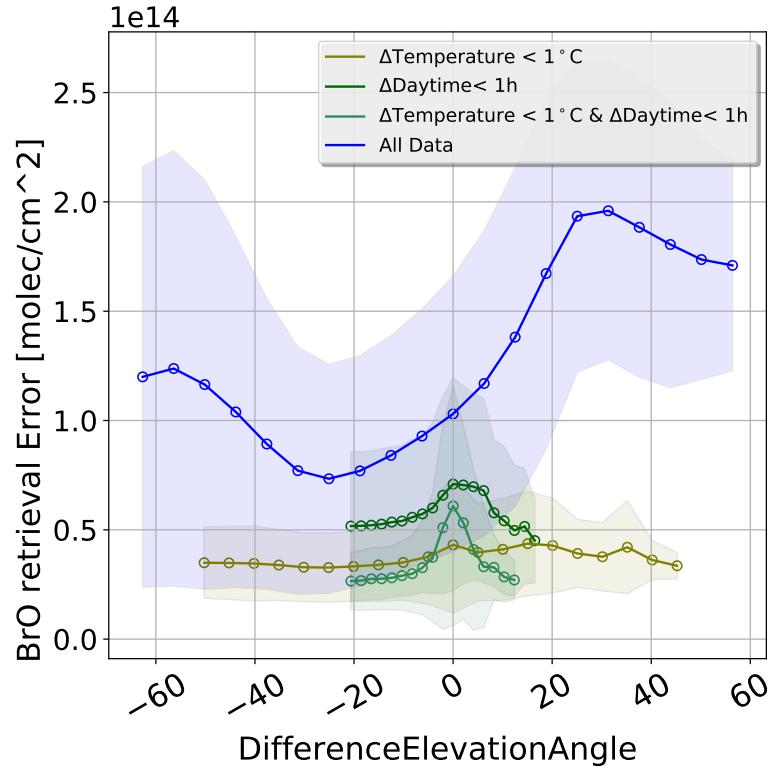
Figure 5.11: The BrO measurement error as a function of the difference of elevation angle between the reference and the plume for the D2J2200_0 instrument. To evaluate the origin of the behavior of the BrO retrieval error of the D2J2200_0 instrument as a function of the difference in elevation angle, the data are analysed on its temperature and daytime dependence. The same dependence is shown with restriction to an difference in temperature (ΔTemperature) of below $1°C$ or restriction on a daytime difference of below 1h ($\Delta Daytime \pm$ 1h). The curves are marked with different green color tones, as it is shown in the legend. The blue line shows the BrO error as function of the elevation angle, when using all data for comprehension.

In fig. 5.10 the BrO error is plotted as a function of the elevation angle. No significant correlation between the two parameters can be identified.

Only the data of the D2J2200_0 instrument significantly vary with the elevation angle. The observable variation of the BrO error with the elevation angle differs from the symmetric dependence of all other external parameter, the minimum BrO error can be found at a difference in elevation angle of -20°. This curve is a result of the solar zenith angle over the day which can be obtained if only using data of the same day time. Such a plot can be seen in fig. 5.11. Figure 5.11 shows the BrO retrieval error as function of the difference elevation angle for the D2J2200_0 instrument at the Nevado del Ruiz volcano. The blue line is equivalent to the results which are shown in fig. 5.10 for comparison. The green lines show data, with a maximal difference in temperature of $1°C$ or maximal difference in daytime of 1h. If restricting the data to just small differences in temperature or/and daytime, the dependence between the BrO retrieval and elevation angle appears to be not significant. Whereas the maximum of the BrO error can be found at an difference in elevation angle of zero.

Because the BrO error does not depend significantly on the elevation angle no restriction on difference of the elevation angle is needed.

5.1.7 Exposure time

The exposure time is the time interval the sensor of the NOVAC instrument is exposed to light. In one scan the exposure time is set constant to the exposure time of the first scan, the pre-reference. The amount of light that reaches the film or image sensor is proportional to the exposure time. The exposure time is adjusted in the way that the maximum intensity does not overly the capacity of the sensor. Thus, the exposure time can be used as a proxy for the degree of sky lightness.

A small dependence of the BrO error on the exposure time can be observed at Tungurahua and Nevado del Ruiz as it is shown in fig. 5.12. The BrO error as a function of the difference in exposure time is also symmetric around zero for all instruments. Thus the absolute difference in the exposure time is sufficient for the evaluation.

The instruments at Tungurahua do not show a significant dependence (correlation coefficient between 0.067 and 0.251) on the exposure time, even though there is always a minimum of the BrO error at a difference of the Exposure Time of 0ms.

Nevado del Ruiz shows a stronger correlation between the BrO error and the exposure time.

Table 5.9 shows the slope, correlation, intercept and the ΔET_2s. The differences in exposure time where the BrO error increases by a factor of two compared to the difference of exposure time of zero. Restrictions of the exposure time to the mean of the ΔET_2s of all instruments which is 632.25 ms leads to an average decrease compared to table 5.1 of data of 98.78%. The results for each instrument can be found in table 5.10.

Table 5.11 shows the amount of possible references if the only data are consid-
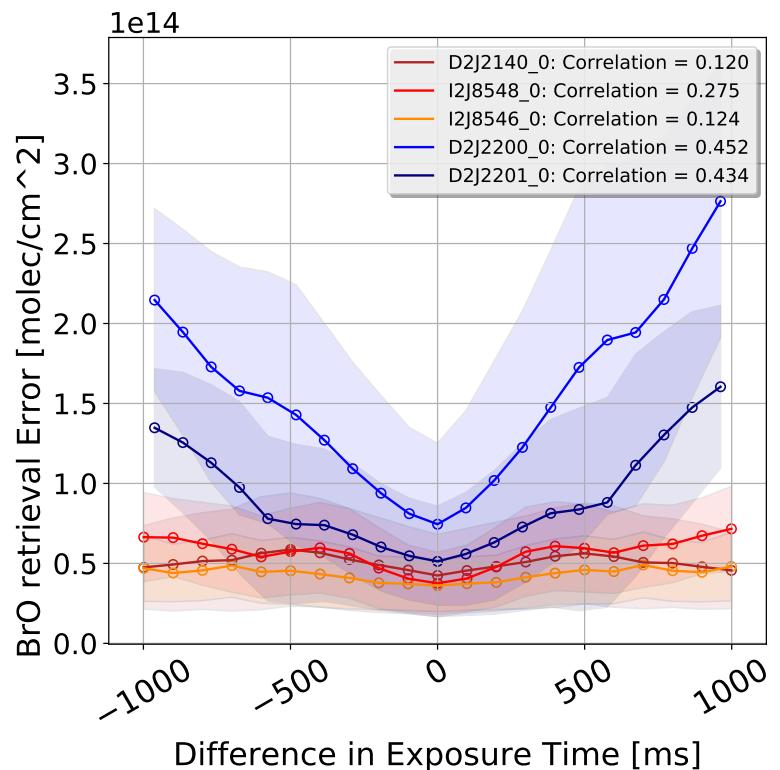
Figure 5.12: The BrO measurement error as a function of the difference of exposure time between measuring the reference and the plume are shown. To evaluate the plume spectra all reference spectra with a temporal distance of no longer than two weeks are used. An increase of the BrO error with the distance in exposure time is observable.

Table 5.9: The BrO measurement error as a function of the difference of exposure time between the reference and the plume is fitted with a first order polynomial for each of the individual instruments at Tungurahua and Nevado del Ruiz. This table shows the fitting parameters slope and intercept. Moreover, the correlation between the BrO error and the absolute exposure time difference is shown.

Instrument	D2J2140_0	I2J8546_0	I2J8548_0	D2J2200_0	D2J2201_0
Slope	$5.54 \cdot 10^9$	$1.54 \cdot 10^{10}$	$3.04 \cdot 10^{10}$	$1.72 \cdot 10^{11}$	$9.37 \cdot 10^{10}$
Correlation	0.067	0.121	0.251	0.452	0.434
Intercept	$4.63 \cdot 10^{13}$	$3.58 \cdot 10^{13}$	$3.87 \cdot 10^{13}$	$6.88 \cdot 10^{13}$	$4.68 \cdot 10^{13}$
ΔT_2	8357	662	1273	95	499

Table 5.10: Amount of possible references when restricting the difference in exposure time between plume and reference to differences below 632.25 ms.

Instrument	D2J2140_0	I2J8546_0	I2J8548_0	D2J2200_0	D2J2201_0
Mean	81.7 ($\widehat{=}96.5\%$)	162.8 ($\widehat{=}99.4\%$)	212.8 ($\widehat{=}98.0\%$)	284.0 ($\widehat{=}100\%$)	225.6 ($\widehat{=}100\%$)
Std	35.3 ($\widehat{=}98.6\%$)	30.1 ($\widehat{=}101\%$)	64.5 ($\widehat{=}99.5\%$)	69.5 ($\widehat{=}100\%$)	41.2 ($\widehat{=}100\%$)
Min	8 ($\widehat{=}100\%$)	113 ($\widehat{=}100\%$)	95 ($\widehat{=}97.9\%$)	64 ($\widehat{=}100\%$)	63 ($\widehat{=}100\%$)
Max	167 ($\widehat{=}98.8\%$)	214 ($\widehat{=}100\%$)	395 ($\widehat{=}99.0\%$)	433 ($\widehat{=}100\%$)	297 ($\widehat{=}100\%$)

ered which do not exceed the thresholds in each external parameter. The average amount of available references per plume decreases to 64%. While the performance is as good as without the restriction, this means the averaged BrO fit error is almost the same (deviations are below 0.1%).

Dependence of external parameters on each other

In all discussions on the impact of the external parameter on the retrieved BrO error the dependency of the external parameter on each other are neglected. It is plausible that the temperature correlates with the cloudiness or the lightness due to sunlight. Therefore the correlation of the exposure time with the BrO error could be a result of the correlation of the temperature with the BrO error. Figure 5.13 shows an example of the dependency of external parameters on each other. The difference in temperature as a function of the difference in exposure time. The BrO error is color-coded.

All correlations between the external parameters are shown in Figure 5.14. Fig-

Table 5.11: Amount of possible references while restricting the difference in colour index between plume and reference to differences above 0.255. maximal Time difference is 3.358°C, maximal daytime difference is 4.75h without Exposure Time between plume and reference to differences below 632.25 ms.

Instrument	D2J2140_0	I2J8546_0	I2J8548_0	D2J2200_0	D2J2201_0
Mean	36.0 ($\hat{=}42.6\%$)	112.9 ($\hat{=}69.0\%$)	148.9 ($\hat{=}68.6\%$)	217.0 ($\hat{=}76.4\%$)	140.4 ($\hat{=}62.2\%$)
Std	22.35 ($\hat{=}62.4\%$)	50.6 ($\hat{=}169.2\%$)	75.9 ($\hat{=}117.1\%$)	82.1 ($\hat{=}118.1\%$)	71.0 ($\hat{=}172.3\%$)
Min	1 ($\hat{=}12.5\%$)	8 ($\hat{=}7.1\%$)	12 ($\hat{=}12.4\%$)	3 ($\hat{=}4.7\%$)	6 ($\hat{=}9.5\%$)
Max	127 ($\hat{=}75.1\%$)	212 ($\hat{=}99.1\%$)	382 ($\hat{=}95.7\%$)	398 ($\hat{=}91.9\%$)	283 ($\hat{=}95.3\%$)

ure 5.14 shows discrete correlation values from 0.3 to 1. Correlations below 0.3 are ignored. Small plus and minus signs indicate whether the correlation is negative or positive. The temperature depends on the daytime, due to the dependence of the temperature on the sun, thus a correlation between the difference in temperature and the difference in daytime (correlation of ≈ 0.5) can be observed. The temperature depends on the intensity of the sun, thus, it also correlates with the difference in exposure time (correlation of ≈ 0.4). The difference in temperature also slightly correlates with the difference in colour index, due to the dependency of temperature on the cloudiness (correlation of ≈ 0.3). The low correlations could appear due to the uniform cloudiness near to the equator. The correlation between the temperature difference to the temporal difference (correlation of ≈ 0.3) probably occurs due to long term changes in temperature. Furthermore the difference in exposure time correlates with the daytime and the colour index (correlation of ≈ 0.4) as a result of the dependency on the sun intensity.

To eliminate the correlation between the external parameters the BrO error dependency on one external parameter where calculated by keeping the differences in the other external parameters constant. Hereby only parameters were kept constant, where the correlation is above 0.3. Thus, when looking at the daytime, only the difference in temperature and exposure time need to be constant, because the daytime difference does not correlate with the other considered external parameter. The results can be seen in fig. 5.15 to fig. 5.16.

Figure 5.15 shows the BrO retrieval error as a function of the temporal difference between the reference and the plume spectrum. All differences in temperature are below one degree. Compared to the correlations, calculated without eliminating the dependence on the temperature, the correlations increase. The dependence of the instruments installed at Tungurahua are still significant higher. From the results can
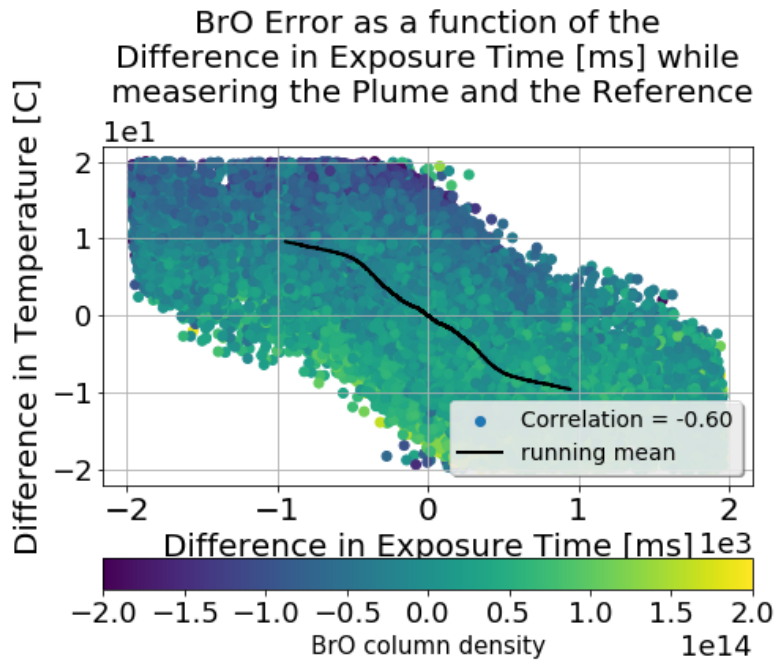
Figure 5.13: An example of the dependency of external parameters on each other. The difference in temperature as a function of the exposure time. Data from Tungurahua.

be interpreted that the temporal difference between the time when measuring the plume and the reference has a impact on the fit quality, but this impact is smaller as the impact of the instrument temperature.

Figure 5.16 shows the BrO retrieval error as a function of the difference in daytime for all considered instruments. As it can be seen in fig. 5.14 the exposure time and the temperature need to be kept constant. The difference in temperature is below 1 degree, the difference in exposure time below 100 ms. A general decrease of the correlations compared to fig. 5.6 is observable.

Figure 5.17 shows the BrO retrieval error as a function of the difference in colour index for all instruments. The temperature and the exposure time shows a dependency on the colour index as it can be seen in fig. 5.14. Both are kept constant, the difference in temperature is below 1 degree and the difference in exposure time is below 100 ms. The correlations decrease compared to fig. 5.9. Especially the correlation of the D2J2201_0 instrument decreases from 0.359 to 0.068.

Figure 5.18 shows the dependency of the BrO retrieval error on the difference in exposure time for all considered instruments. Hereby, only data are used, where the difference in temperature is below 1 degree, the difference in colour index is below 0.05 and the difference in daytime is below one hour. The temporal difference and the difference in elevation angle are not kept constant, because one could not observe a relation between the exposure time and the temporal difference or the elevation angle. The correlations between the BrO fit error and the difference in exposure

time decrease for each instrument if the temperature, daytime and colour index are kept constant. Even though, the correlations at Nevado del Ruiz are still higher as the correlations at Tungurahua.

Restricting the data, to where the temperature difference is kept below one degree, leads to an distortion of the data. Thus the results plotted in fig. 5.15 to fig. 5.16 could also have systematic errors.

When comparing the correlations of the data from fig. 5.15 and fig. 5.18 to the correlations of fig. 5.5 to fig. 5.12 a large reduction of the correlation is obvious. Only the difference in temperature still shows a significant correlation to the BrO error. However, the minimal BrO error coincidence in almost all cases with a difference in external parameters of zero. A dependency of the BrO error on the external parameter can still be seen even tough the correlation is very small.

Excluding of the external parameters due to the rather low correlation leads to a worse quality of the results, because the effects of the single parameter add up to a not negligible amount. However, note that the added impact of all external parameter except for the temperature are less important than the temperature. The BrO fit error of contaminated spectra evaluated with the new method in the following refereed to as decontamination module (See chapter 6) increases by 15% if the other external parameters are excluded. If all external paramter except for the temperature are used the calculated BrO fit error increases by 37%.

For the final evaluation of contaminated data I use the results of fig. 5.7 to fig. 5.9. Because the correlations between the external parameters are considered in the final 4 dimensional fit.

5.2 BrO dependence on external parameters

The external parameters not only influence the fit quality but also the evaluation of the gas amount. A high difference in certain external parameter could distort the calculated BrO column density. Figure 5.19 shows the evaluation of one plume with respect to different references. The temporal difference between the references and the plume do not exceed two weeks. In theory it is expected that the choice of the reference should not make a difference, therefore all BrO column densities resulting from the evaluation should be equivalent. But one can see a high variation if choosing different references. The variability of the BrO column density depends as well on the external parameters, when looking at the temperature dependency a mean decrease of th BrO column density with an increasing temperature can be observed. Figure 5.19 is a result of an exemplary evaluation of one plume. An examination of all several plumes evaluated by different references is shown in fig. 5.20. The plots are equivalent to the plots for BrO fit error (for an example see fig. 5.7). The BrO SCDs vary strongly with the differences in external parameters. It is observable, that the BrO SCDs recorded by the instruments at Nevado del Ruiz vary in a larger

range than for the BrO SCDs recorded by instruments at Tungurahua. This can also be observed for the BrO retrieval errors. The absolute BrO SCDs increase with the difference in external parameters.

Figure 5.20 (a): Temporal difference: For the temporal difference no significant correlation can be observed. Figure 5.20 (b): Difference in daytime: For the instruments at Nevado del Ruiz the BrO SCD correlates strongly with the difference in daytime. This can be a result of the dependence on the temperature, because the correlations are very similiar, only the correlations are a little bit stronger for the difference in temperature. Figure 5.20 (c): Difference in temperature: For the instruments at Nevado del Ruiz the BrO SCD correlates strongly with the difference in temperature. The correlations from the instruments at Tungurahua vary very much from -0.696 (D2J2140_0) to 0.198 (I2J8546). Figure 5.20 (d) Difference in color index: The correlations differ for every instrument even for instruments of the same volcano. The correlations vary from -0.368 to 0.46. Figure 5.20 (e) The strange dependence which can be seen between the BrO fit error and the difference in elevation angle for the D2J2200_0 instrumnt can be seen in this plot as well. The other instruments do not show any correlation between the BrO SCD and the difference in elevation angle. Figure 5.20 (f) The correlations for the difference in exposure time are opposite to the correlations in daytime.
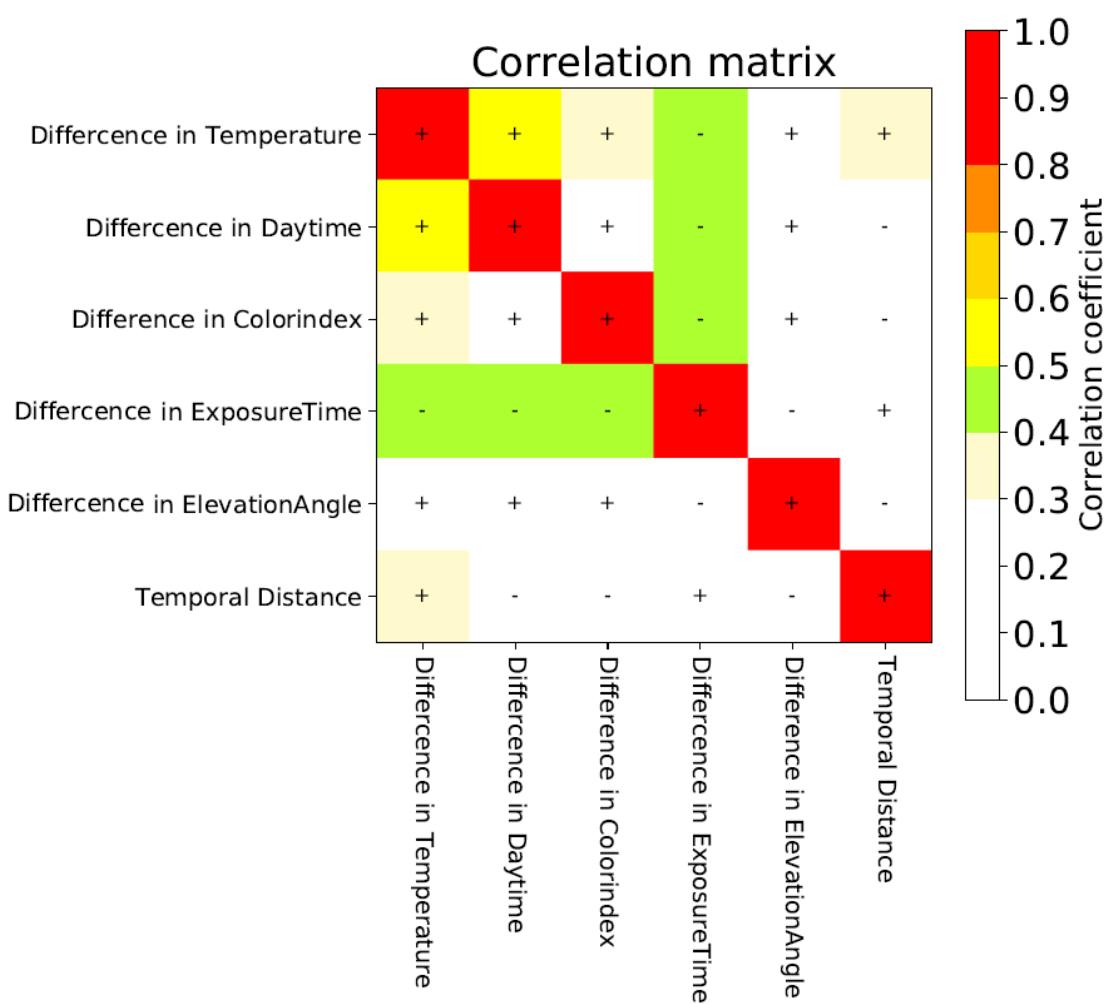
Figure 5.14: Correlation matrix of the external parameters. The correlation is discrete colour coded. Positive correlation is labeled with a plus whereas negative correlation is labeled with a minus. The correlation matrix is calculated using the data from D2J2140_0.
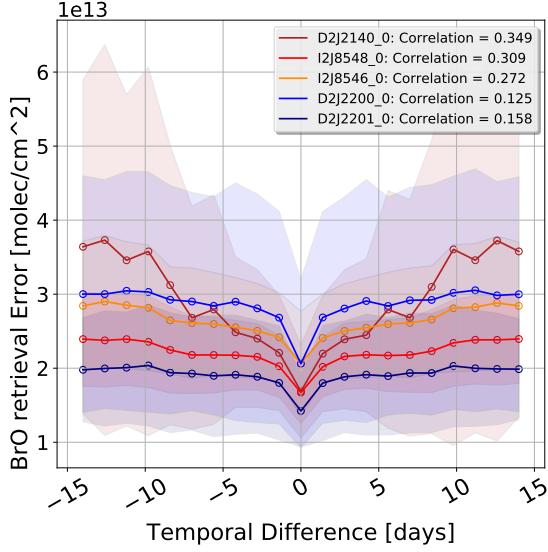
Figure 5.15: The BrO measurement error as a function of the temporal difference between measuring the reference and the plume are shown. Therefore, the reference spectra are restricted such that the maximal temperature difference between reference and plume is 1° C.
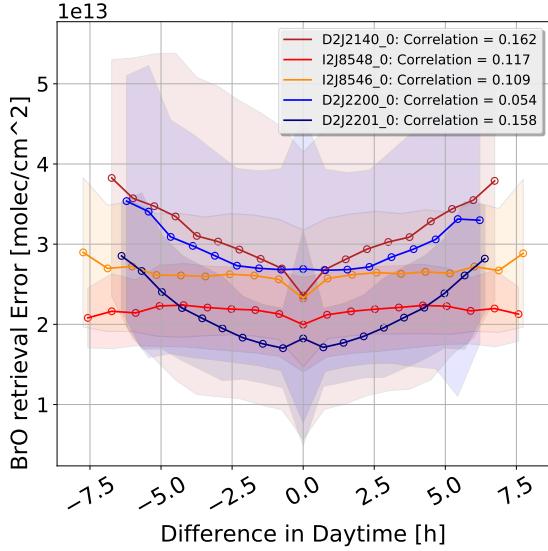
Figure 5.16: The BrO measurement error as a function of the daytime difference between recording the reference and the plume are shown. Therefore, the reference spectra are restricted such that the maximal temperature difference between reference and plume is 1°C. The maximal exposure time difference is 100ms.
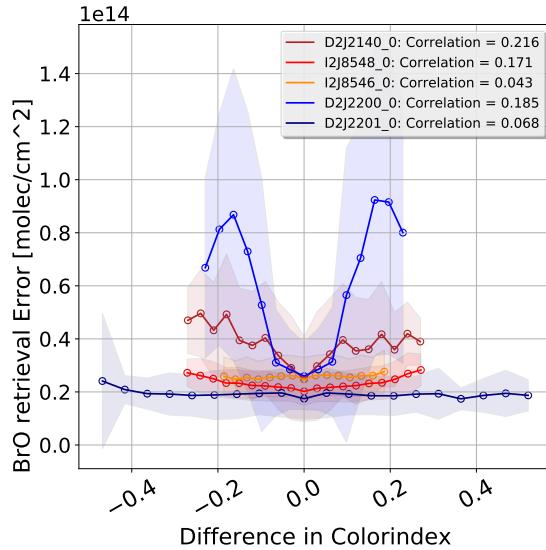
Figure 5.17: The BrO measurement error as a function of the color index difference between recording the reference and the plume are shown. Therefore, the reference spectra are restricted such that the maximal temperature difference between reference and plume is 1°C. The maximal exposure time difference is 100ms.
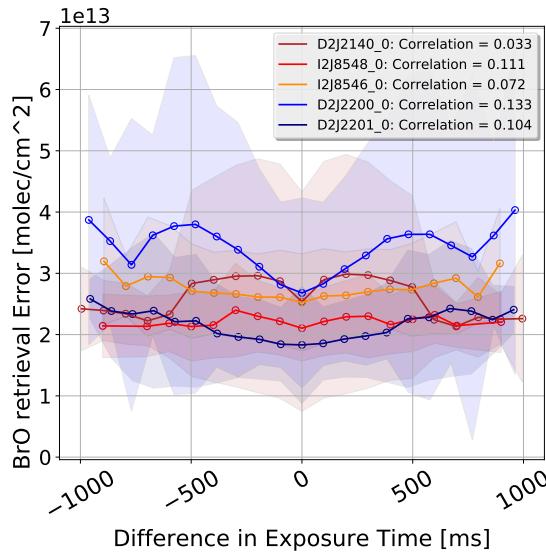
Figure 5.18: The BrO measurement error as a function of the exposure time difference between recording the reference and the plume are shown. Therefore, the reference spectra are restricted such that the maximal color index difference between reference and plume is 0.05. The maximal daytime difference is 1h.

(a)   (b)
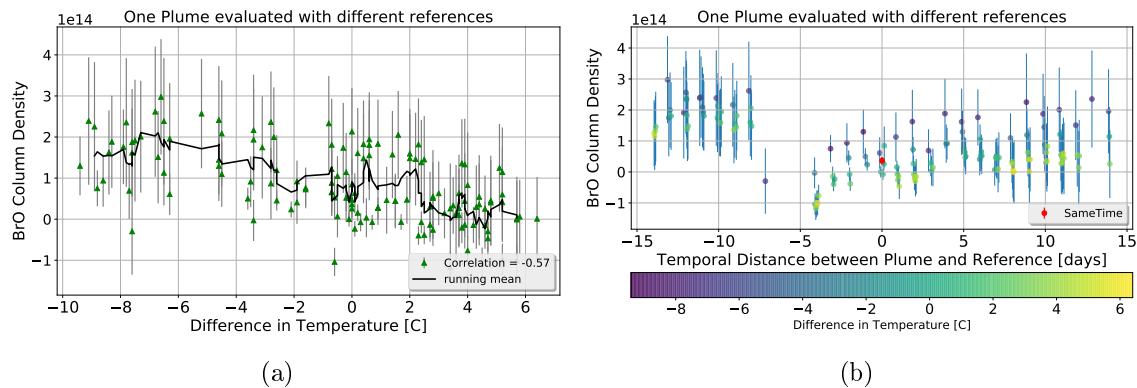
Figure 5.19: One plume is evaluated by using different references. The plume is
recorded at Tungurahua volcano with the D2J2140_0 instrument. The
recording time was the 03.12.2008 at 16:46 o clock. The y axis shows
the BrO column density difference between the NOVAC method and
decontamination module. (a) The difference in BrO is plotted as a
function of the temperature difference between the plume and the ref-
erences. Every data point indicates one reference. (b) The difference
in BrO is plotted as a function of the temporal difference between the
one plume and the different references.

(a)

(b)

(c)

(d)

(e)

(f)
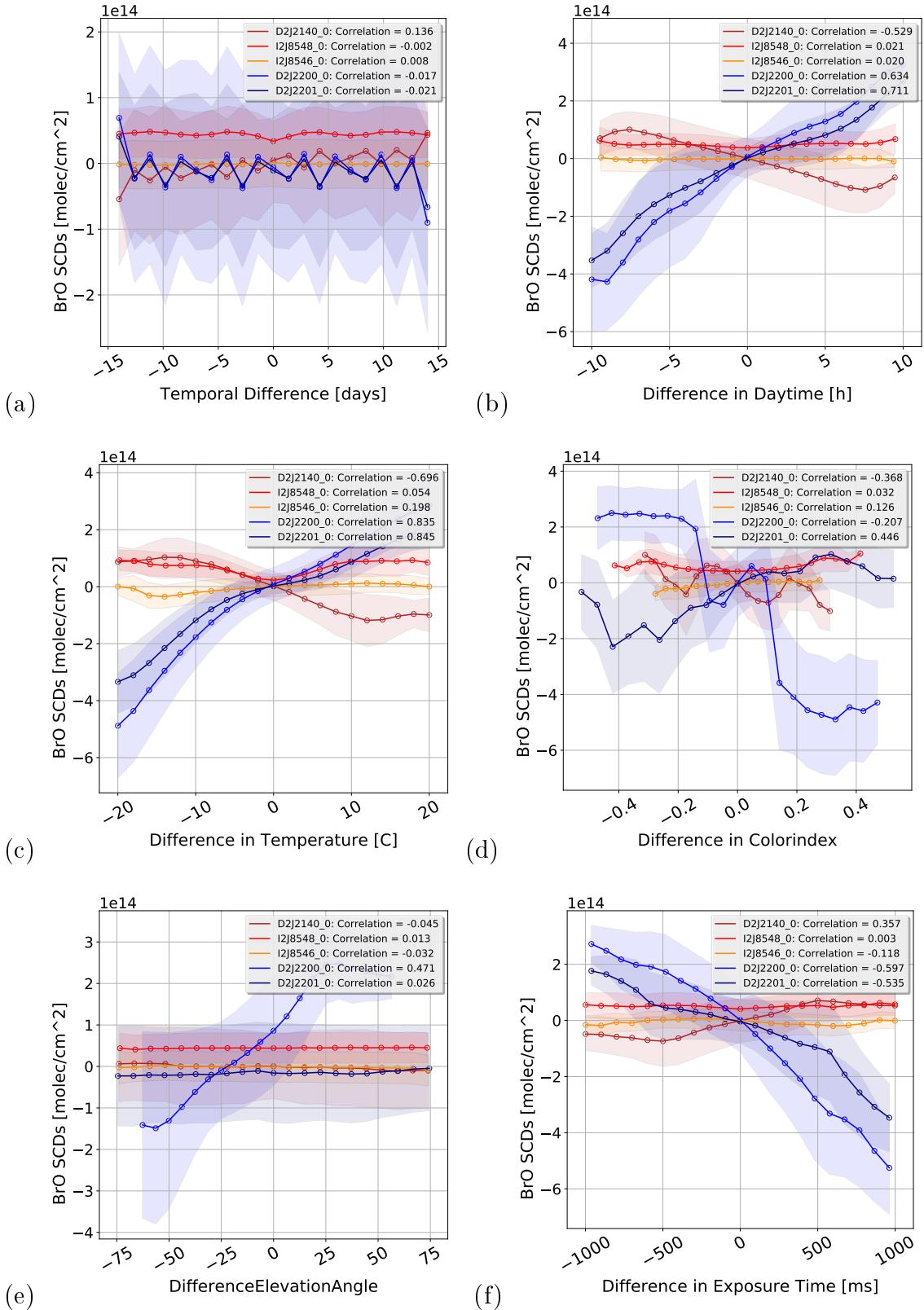
Figure 5.20: The BrO SCD as a function of the difference of the external parameters between measuring the reference and the plume are shown.

Summary

This chapter examines the influence of external on the precision of the BrO evaluation. Hereby the following parameter are considered: temporal difference, temperature, daytime, colour index, elevation angle, exposure time. The findings are based on the data of three instruments installed at the Tungurahua volcano and two instruments at the Nevado del Ruiz volcano. The maximal temporal difference between measuring the plume and the reference is set to 14 days to prevent large uncertainties in the BrO evaluation. Due to the mechanical influence on the instrument line function the temperature for all analysed instruments has the most significant impact on the BrO evaluation for all considered external parameters. The elevation angle does not seem to influence the evaluation for all examined instruments thus the elevation is excluded from the evaluation. The influence of the other external parameter change at every instrument. So a relatively strong impact of the exposure time can be seen at the D2J2201_0 instrument at Nevado del Ruiz, while the exposure time does not seem to significantly influence the evaluation of the data from the I2J8548_0 at Tungurahua.

Part III

Retrieval advances

6 Decontamination module

Based on the findings about the influence of external parameters on the BrO error I propose an algorithm which is able to pick an appropriate volcanic-trace-gas free reference. The algorithm uses the dependencies found in section 5.1 to find a sufficiently good matching reference.

The first step is, to evaluate every reference with solar atlas spectrum, to check for contamination. A reference is classified as contaminated if the fit against the solar atlas spectrum yields an SO_2 SCD above the plume limit $(2 \cdot 10^{17})$.

In the second step for each contaminated reference an alternative gas-free reference spectrum need to be found:

- A list of possible references is created where all references are not contaminated and the temporal distance to the plume date is no longer than 14 days.

- For all possible references the differences in the external parameters are calculated with respect to the corresponding plume spectrum.

- The analysis of external parameters as described in section 5.1 is used to estimate the BrO error of all references

- The reference with the smallest estimated BrO fit error is chosen as new reference

- The plume spectra of the corresponding scan is evaluated with the new reference.

ϵ_0 is the BrO error when evaluate the plume spectrum with the "same-time-reference". The assumption is, that the BrO error ϵ_{BrO} can be described as the sum of ϵ_0 and the deviation of ϵ_{BrO} with respect to all external parameters. It is limited by the precision of the NOVAC-instruments.

$$\epsilon_{BrO} = \epsilon_0 + \frac{d\epsilon}{dt} + \frac{d\epsilon}{d\circ} + \frac{d\epsilon}{dT} + \frac{d\epsilon}{dDt} + \frac{d\epsilon}{dc} + \text{further influences} \qquad (6.1)$$

$$\rightarrow \Delta\epsilon_{BrO} = \epsilon_{BrO} - \epsilon_0 = \frac{d\epsilon}{dt} + \underbrace{\frac{d\epsilon}{d\circ}}_{=0} + \frac{d\epsilon}{dT} + \frac{d\epsilon}{dDt} + \frac{d\epsilon}{dc} + \text{further influences} \quad (6.2)$$

Here the parameter t stands for the time between plume-time and reference-time. The parameter T is the difference in temperature. The parameters Dt and c are the
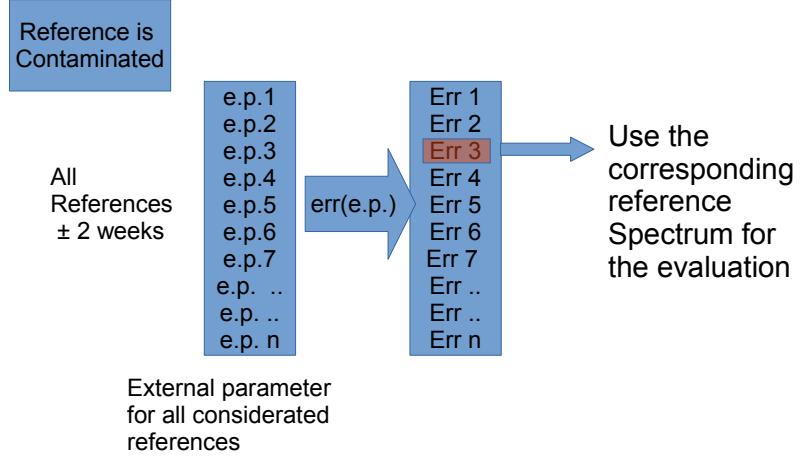
Figure 6.1: Visualization of the decontamination module. A list of possible references is available, where the temporal difference between the plume and the reference is not longer than two weeks. For every possible reference, the estimated BrO fit error is calculated by considering the corresponding difference in important external parameters. The reference with the so calculated minima BrO fit error is used for the evaluation.

differences in the daytime and the colour index. The task occurring at this stage is to find the best representation for the deviations. And then find the reference which minimize $\Delta\epsilon_{BrO}$

The straight-forward way is to just calculate the BrO error of all possible references for every plume by using the DOASIS routine. If this method is used it is possible to choose the reference for which the BrO error is minimal. However this takes to much computation time because the evaluation time would be proportional to the number of possible references because the evaluation needs to be done for $\mathcal{O}(n)$ with n as the number of potential reference spectra. Doing this evaluation for every plume-reference pair makes it impossible to do the evaluation in real, or near real time. Furthermore taking the minimum in all cases is statistically risky because the good results can occur accidental. The interpretation is thus more easy if the algorithm searches for an appropriate reference in a defined parameter range.

In this thesis a novel approach of identifying an ideal reference spectrum, by considering externel parameters, is introduced. This way a much faster estimation with constant complexity $\mathcal{O}(1)$ is reached. But the above described optimal evaluation is used to rate new approach and compare them among each other. The optimal evaluation always choose the reference with the smallest absolute error. We don't use the relative error due to its vulnerability. Using the relative error leads to less precision because the references with the highest BrO column density is preferred. The results of the algorithm which chooses the reference automatically are described relative to an optimal evaluation. To avoid an distortion of the results due to rela-

tively bad match between reference and plume spectra all data with a relative BrO fit error larger than one are excluded from the evaluation.

In the following I examine several methods for choosing the best reference based on the analysis of external parameters.

6.1 Fit with a first order polynomial

The following chapter analyses fitting the data with a first order polynomial. Figure 5.7 to fig. 5.12 show the BrO error as a function of external parameters. Hereby, the curves are symmetric around zero difference in the respective external parameter. Therefore, it is not necessary to distinguish between positive or negative deviations from the equal surrounding conditions. Thus, the absolute differences can be utilized. Using the absolute difference leads to less complex calculations and therefore to a lower calculation time. On the other hand not using the absolute difference leads to no measurable advantages.

A linear approximation of the BrO error as function of the considered external parameters leads to a variation of eq. (6.2) : With linear differentiations of the BrO error with respect to the respective external parameters eq. (6.2) can be written as:

$$\Delta\epsilon_{BrO} = a_t\cdot\Delta t + a_{ET}\cdot\Delta ET + a_T\cdot\Delta T + a_{Dt}\cdot\Delta Dt + a_c\cdot\Delta c + \text{further influences} \quad (6.3)$$

To determine the coefficients a_x (eq. (6.3)) the data visualized in fig. 5.7-5.12 where used. The fitting is done with an ordinary least square linear regression. In particular I used the python function linear regression from the library sklearn (scikit learn.org).

   As it can be seen in section 5.1 the impact of the different external parameters change for every instrument depending on the location and the instrument themselves. While the BrO error does not show any dependence on some external parameters for some instruments, the error has very strong dependence on the same external parameter at an other instrument. An example is the correlation between BrO error and the difference in daytime of 0.6 for D2J2201_0 (Nevado del Ruiz) and a correlation of 0.16 for I2J8546_0 (Tungurahua). To get a more stable algorithm less external parameter are preferable. Thus, it is necessary to distinguish between the stability of the fit, which improves with less external parameters and quality of the fit, which improves with more external parameters. A preferable strategy is, to find a solution which is valid for all instruments. Moreover, utilizing less external parameters saves computation time. One possibility is to use all external parameters where the correlation is above a certain value. Because a selection valid for all instruments is preferred there are two possibilities: The first one is that one decide

by using the mean correlation of all instruments. The second option is to use the highest correlation.

Table 6.1: The correlation coefficients between the BrO measurement error and the different external parameters. As a correlation value both the average and the maximum correlation is given.

	Mean - Correlation	Highest - Correlation
Temperature	0.798	0.92
Colorindex	0.3108	0.409
Exposure time	0.265	0.452
Elevation Angle	0.02	0.067
Daytime	0.395	0.631

To answer this question quantitatively for the fitting routine I evaluated data of Tungurahua and Nevado del Ruiz with different combinations of the external parameter described in section 5.1. Because one could not observe any correlation between the BrO error and the elevation angle the external parameter elevation angle was neglected in this analysis. To rate the results for the single instruments (three at Tungurahua and two at Nevado del Ruiz) the difference to the "NOVAC-evaluation" is used. Hereby the factor X, a quantity which describes the distinction between the NOVAC-Method and the decontamination module, serves as a indicator:

$$X = \frac{1}{n} \sum_{k}^{n} \frac{E_{ContBased,k}}{E_{novac,k}} \qquad (6.4)$$

n is the total amount of contaminated spectra, $Enovac$ is the relative BrO error, in the NOVAC-evaluation, $EContBased$ is the relative BrO error, in the contamination based-evaluation. Figure 6.2 shows the X factor for the Tungurahua and the Nevado del Ruiz volcano. The y-axis shows the factors X averaged over all instrument at the volcanoes.

As it can be seen in fig. 6.2 for both volcanoes the X factor is minimal for the combination of the following external parameters:

For the final algorithm this combination of external parameters is used.

- Temperature
- Daytime
- Colorindex
- Temporal Difference

The coefficients a_x are calculated for each instrument at Nevado del Ruiz and Tungurahua. Furthermore, the coefficients a_x are calculated with the combined data from all instruments installed at one volcano. The results for the Nevado del Ruiz volcano can be found in tab. 6.1 and for the Tungurahua volcano in tab. 6.1.

(a) Nevado del Ruiz

(b) Tungurahua
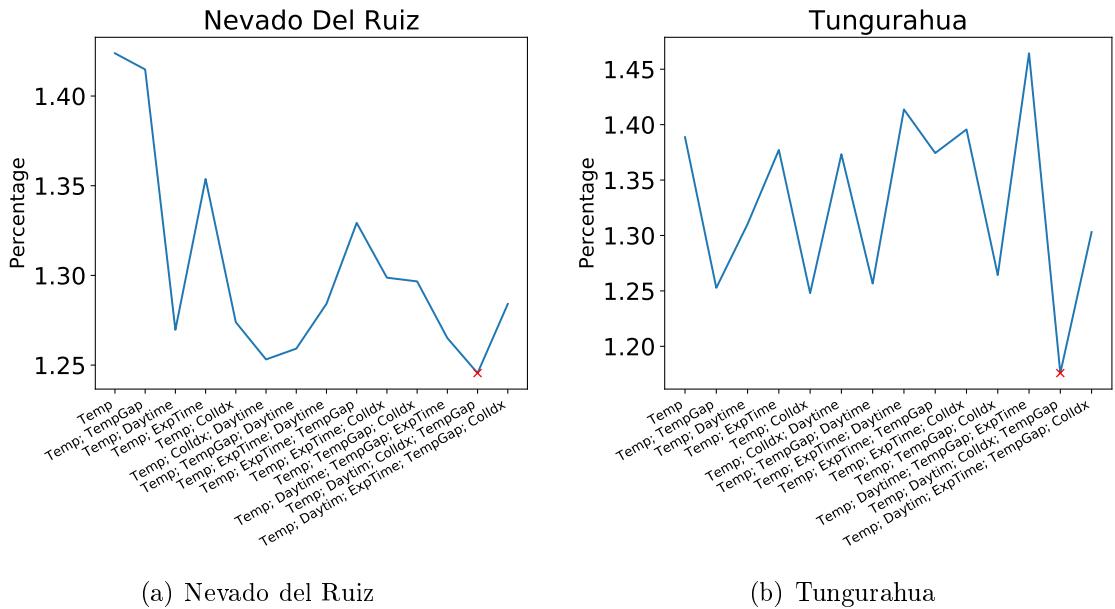
Figure 6.2: Deviation from the NOVAC-evaluation as a function of the selection of differences in external parameters which are used for the evaluation. Here the utilized combination of external parameters are plotted on the x-axis and the deviation on the y-axis. The ideal combination (lowest deviation) is marked with a red cross.

(a) Data of Nevado Del Riz D2J2201_0			(b) Data of Nevado Del Riz D2J2200_0			(c) Data of Nevado Del Both Instruments		
Const	value	import	value	import	value	import
a_T	$7.5 \cdot 10^{12}$	0.866	$1.2 \cdot 10^{13}$	0.925	$1.1 \cdot 10^{13}$	0.973
a_{CI}	$3.5 \cdot 10^{13}$	0.048	$1.0 \cdot 10^{14}$	0.046	$3.5 \cdot 10^{10}$	0.070
a_t	$-3.2 \cdot 10^{09}$	0.0	$-1.6 \cdot 10^{09}$	0.0	$-9.1 \cdot 10^{08}$	0.0
a_{dt}	$1.9 \cdot 10^{12}$	0.095	$1.1 \cdot 10^{12}$	0.033	$1.5 \cdot 10^{11}$	0.006
					$-6.8 \cdot 10^{13}$	-0.047

Table 6.2: The results of the fitting with a first order polynomial. The constants of eq. (6.3) are calculated. The value shows the actual number. The importance, referred to as import, indicates the relative impact on the evaluation and is shown in percent. (a) Data from Nevado del Ruiz from the D2J2201_0 instrument. (b) Data from Nevado del Ruiz from the D2J2200_0 instrument. Data from Nevado del Ruiz from both instrument.

The fitting routine provides a list, where the possible references are sorted by there probable compatibility with the plume spectra. To quantize the influence of the choice of the reference on the BrO SCD, the BrO SCDs, retrieved by using the first 10 spectra of the list provided by the fitting routine are compared. For Tungurahua the mean standard deviation between the different BrO SCDs calculated with the different references is 28.7 % of the mean BrO SCD. For comparison, the mean BrO retrieval error is 43.8% of the BrO SCD. At Nevado del Ruiz the standard deviation of the BrO SCD is 25.4% of the mean BrO SCD. The mean BrO retrieval error is 36.9% of the BrO SCD.

As it is shown in section 5.2, not only the BrO retrieval error depends on the difference in external parameter but also the BrO SCD (see fig. 5.20). Thus I need to assure, that the BrO SCD does not chance significantly due to the usage of a alternative reference. Whether the correlation between the BrO fit error and an considered external parameter affects the results retrieved with the decontamination module can be answered by analysing the correlation between the BrO SCDs resulting from the decontamination module and the external parameter. The maximal correlation is hereby below 0.01. On comparison, the maximal correlation if all references are used is above 0.8. Thus one can conclude, that the BrO SCDs resulting from the fit routine do not depend largely on the differences in external parameter. The restriction of the external parameters to low differences in external

	(a) Data of Tungurahua D2J2140_0		(b) Data of Tungurahua I2J8548_0	
Const	value	import	value	import
a_T	$3.7 \cdot 10^{12}$	0.664	$6.5 \cdot 10^{12}$	0.920
a_{CI}	$7.0 \cdot 10^{13}$	0.078	$2.8 \cdot 10^{13}$	0.066
a_t	$3.5 \cdot 10^{10}$	0.2	$1.2 \cdot 10^{10}$	0.13
a_{dt}	$7.8 \cdot 10^{11}$	0.069	$-6.0 \cdot 10^{11}$	-0.055

(c) Data of Tungurahua I2J8546_0		(d) Data of Tungurahua all instruments	
value	import	value	import
$3.9 \cdot 10^{12}$	0.850	$5.0 \cdot 10^{12}$	0.838
$-1.5 \cdot 10^{13}$	-0.042	$2.5 \cdot 10^{13}$	0.057
$2.0 \cdot 10^{10}$	0.2	$1.8 \cdot 10^{10}$	0.117
$1.2 \cdot 10^{11}$	0.017	$-1.1 \cdot 10^{11}$	-0.012

Table 6.3: The results of the fitting with a first order polynomial. The value shows the actual number. The importance, referred to as import, indicates the relative impact on the evaluation is shown in percent. The constants of eq. (6.3) are calculated. (a) Data from Tungurahua from the instrument D2J2140_0. (b) Data from Tungurahua from the instrument I2J8548_0. (c) Data from Tungurahua from the instrument I2J8546_0. (e) Data from Tungurahua averaged over all instrument.

parameters further ensures that systematic distortion of the BrO SCD are avoided.

6.2 Other approaches

Fitting is not the only possibility of finding the optimal reference out of the list of all possible references.
In the following two additionally possibilities are presented. Both are based on the findings in section 5.1.

6.2.1 Nearest neighbor approach

Beside linear regression also the nearest neighbor approach can be utilized to estimate the BrO fit error for the evaluation with a potential reference spectrum. The nearest neighbor search[*] describes an optimization problem for a given point $m \in \mathbb{R}^n$ and a set $S \subset \mathbb{R}^n$:

$$\bar{s}(m) = \min_{s \in S} d(m, s) \tag{6.5}$$

Here $d(\cdot, \cdot)$ is a distance function that computes the dissimilarity between the two input arguments. Typical distance metrics are the L1 distance $d_{\mathrm{L1}}(m, s) = ||m - s||^2$ or the L2 (also euclidean) distance function $d_{\mathrm{L2}}(m, s) = ||m - s||$.

In many cases not only one nearest neighbor but a set M of k nearest neighbors is of interest. In this case the optimization problem of Eq. 6.5 must be modified to

$$\bar{S}_k(m) = \min_{S_k \subset S} \sum_{s \in S_k, m \in M} d(s, m) \tag{6.6}$$

In many cases the nearest neighbor search is used to estimate a target variable y_m for a feature vector $m \in \mathbb{R}^n$. This method assumes a given set feature vectors S for which the target variables y_S are known. Then the target variable y_m for a given m can be estimated by:

$$y_m = \frac{1}{k} \sum y_S \tag{6.7}$$

Advantages of the nearest neighbour approach

The main advantage of the nearest neighbour method is that there is no need for a pre-assumption of a fitting function. The fitting method assumes that the BrO fit error depends linearly on the external parameter. As it can be seen in fig. 5.7-fig. 5.12 this does not need to be the case. Thus, the nearest neighbour method is able to approximate the BrO fit error without considering an specified function.

Disadvantages of the nearest neighbour approach

Compared to fitting the data, the nearest neighbour is much slower. The reason for this is, the vast amount of compassion operations that is necessary for each computation. Thus, the calculation time increases with the amount of training data.
To normalize the distances d, the normalization function needs to be chosen and

---

[*]python library sklearn, version 0.18.1

therefore pre-assumptions about feature importance are required. The X factor increases by 80%, from 1.24 for the fitting method to 2.24 for the nearest neighbour method. Including the fact, that the results of the nearest neighbor method is worse compared to the fitting method, the disadvantages of the nearest neighbour method outweigh the advantages.

6.2.2 Iterative approach

The idea of the iterative method is, that the importance of the individual external parameters are very different, that means if there is a list of possible references, all references where the temperature difference is minimal are used, to get a new, much smaller list of possible references. From this list all references where the next external parameter for example the daytime is minimal are chosen to again get a new list. I proceed this way with the following external parameters. I experiment with the sequence of the parameters, to increase the success of the method. The final sequence is:

$$Temperature \bullet Daytime \bullet Colorindex \bullet Temporal\ Difference \bullet Exposure\ time$$

Advantages of the iterative approach

The advantages of the iterative approach is the simple calculation and thus the short calculation time. The temperature is by far the external impact with the largest impact on the evaluation, thus it is reasonable to look at first at the temperature, and after that on the other parameters.
Another advantage is, that the external conditions of the resulting references, are in an well-defined framework, similar to the conditions of the plume. Therefore the systematic errors resulting from the effects on the BrO SCDs (see fig. 5.20) can be kept small.

Disadvantages of the iterative approach

The iterative approach leads to an rigid evaluation of the data. References, which have very similar conditions as the plume could be excluded of the evaluation due to an large difference in one external parameter. The decision for the best suited reference is based on one by one parameter. Thus it is impossible to look at all parameters by the same time. This could lead to a less optimal evaluation when looking at the BrO fit error. As a result the iterative method has a worse X factor (X=1.73) compared to the nearest neighbour (X=2.24) and the fitting method (X=1.24).

Summary

In this section three methods of finding the most suitable reference for a plume are presented. Two of the presented method use the differences in external parameter between the plume and the reference to extrapolate to an possible error. At the end the reference with the lowest probable error is taken for the evaluation. One of these, is fitting method: A five dimensional first order polynomial is fitted on the difference of external parameter as a function of the BrO fit error. The other one the nearest neighbor method uses plume reference pairs with similiar differences in external parameters to guess a possible error. The third option uses a iterative approach to find the most suitable reference. The performance of the methods differ not very much. However in calculation time and in the amount of pre-assumptions which need to be made for the the methods are different. The fitting method has the best performance. The nearest neighbor method need the fewest pre-assumptions, while the calculation time and the performance is much worse than for the fitting method and the iterative approach. The iterative approach has the lowest calculation time, but the amount of pre assumptions is the largest. Thus the advantages of the fitting method predominate, therefore I use the fitting method for the evaluation.

7 Results

This chapter discusses the difference of the SO_2, BrO and BrO/SO_2 ratio data when evaluating with the NOVAC-routine, or with the decontamination module. The aim is to discover the systematic differences between the different retrievals and to discuss the reliability of the data.

To obtain the reference leading to an evaluation with minimal expected BrO error, the calculation of eq. (6.3) and the corresponding coefficients from tab. 6.1 (Tungurahua) and tab. 6.1 (Nevado del Ruiz) are used. For the retrieval only "Multi Add" data are used. The maximal temporal difference between measuring the reference and the plume, accepted for the retrieval, is two weeks. The maximal accepted temperature difference is 3.3 °C.

We are interested in the systematic differences when using the contaminated same time references spectrum or a gas free alternative reference. fig. 7.1 shows a comparison of the results of contaminated data when performing the evaluation with the NOVAC-routine and the decontamination module. As expected the SO_2 SCDs are larger for almost every measurement when retrieved with the decontamination module compared to the classical NOVAC-routine. The difference between the SO_2 SCDs retrieved by the conventional NOVAC-routine increases slightly with increasing SO_2 SCD. Fitting of the data results in a slope of 1.22 (Tungurahua) and 1.16 (Nevado del Ruiz). Thus, one can conclude that a higher SO_2 amount leads to a slightly higher contamination (see fig. 7.1). The extent of BrO contamination does not seem to depend on the BrO amount. The slope of the linear fit of the BrO SCDs have a slope which does not differ significantly from one. The slope at Tungurahua is 1.01 and for Nevado del Ruiz is 1.07.

Figure 7.2 shows the difference of the BrO/SO_2 ratio when performing the evaluation with the NOVAC method and the decontamination module (fig. 7.2(b) , 7.2(d)).

Figure 7.2(a) and 7.2(b) show the results of the decontamination module plotted against the results of the NOVAC method. Figure 7.2(c) and 7.2(d) show the actual difference between both methods. The column density calculated with NOVAC is subtracted from the corresponding column density retrieved with the decontamination module. For low BrO/SO_2 ratios ($\approx$below zero), the ratios calculated with the decontamination module are higher than the ratios retrieved with the NOVAC method. For higher BrO/SO_2 ratios ($\approx$above zero) the ratios calculated with the NOVAC method are larger. Due to the increase of the SO_2 column density when performing the evaluation with the decontamination module more SO_2 SCD lies above the plume limit of $7 \cdot 10^{17} \frac{molec}{cm^2}$. This leads to an increase of the amount of

(a) Data of Tungurahua

(b) Data of Nevado Del Riz

(c) Data of Tungurahua

(d) Data of Nevado Del Riz
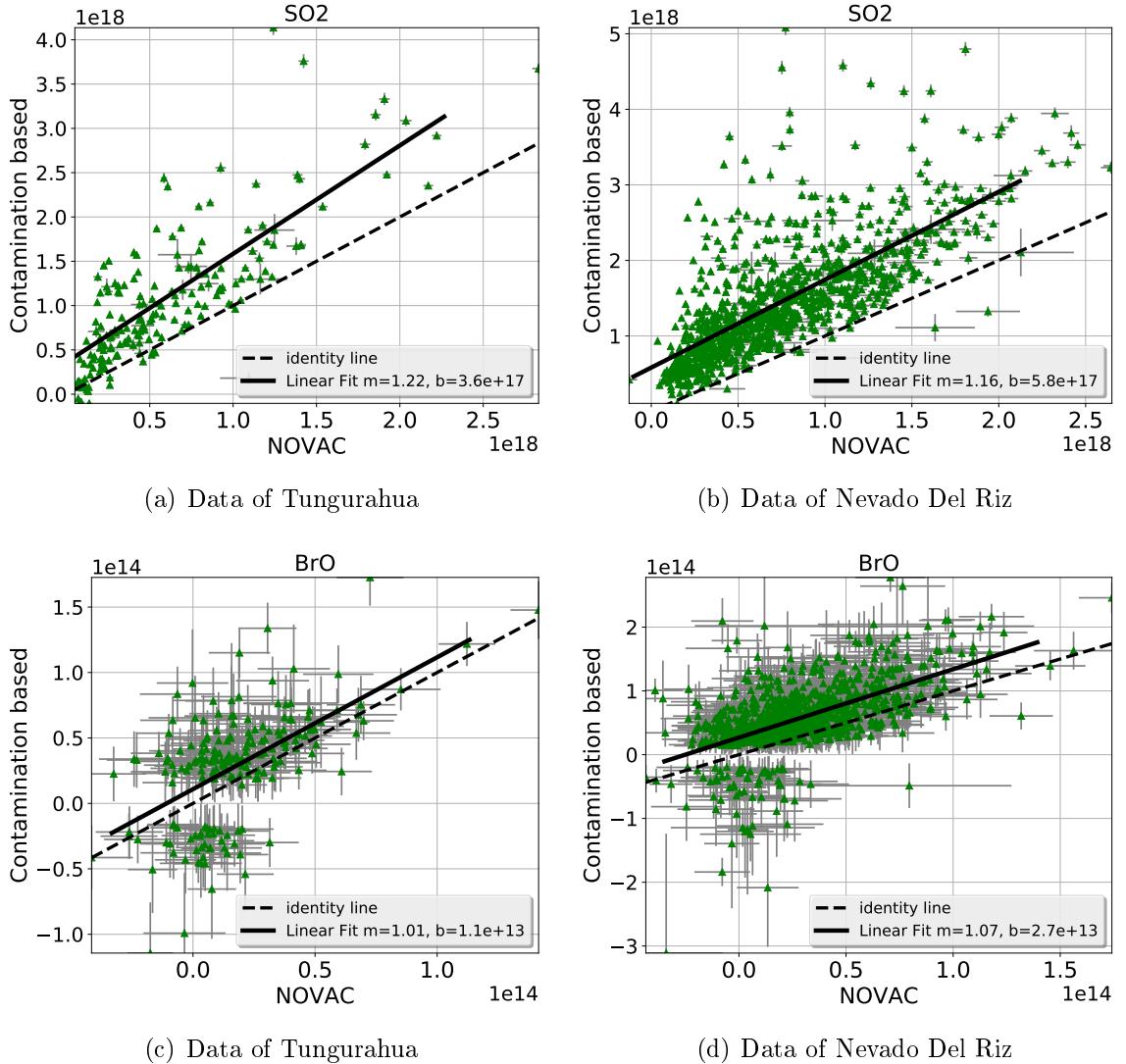
Figure 7.1: Comparison of the results of contaminated data for performing the evaluation with the NOVAC-routine and the decontamination module. The black solid line shows a linear fit of the data (m: slope, b: intercept). For the fit only data are used where the corresponding SO_2 column density (retrieved from the decontamination module) lies above the plume limit of $SO2_{SCD} > 7 \cdot 10^{17} \frac{molec}{cm^2}$. The dotted line indicates the unity line. (a) Results for the SO_2 column densities from Tungurahua; (b) Results for the SO_2 column densities from Nevado del Ruiz; (c) Results for the BrO column densities from Tungurahua; (d) Results for the BrO column densities from Nevado del Ruiz.

data which show a large SO_2 signal.

In the following I discuss the results for the Tungurahua volcano and the Nevado del Ruiz.

		Tungurahua	Nevado del Ruiz
Total amount of scans		6500	14005
NOVAC: SO$_2$ SCDs above plume limit		6.4%	12.1%
NOVAC: SO$_2$ SCDs above plume limit without cont.		5.5%	8.8%
contaminated scans		6%	9.9%
	NOVAC: above plume limit	15.3%	32.8%
	Contbased: above plume limit	29.9%	59.8%
In total: above plume limit		7.3%	14.0%

Table 7.1: Results for Tungurahua and Nevado del Ruiz. The absolute amount of data and the amount of data above the plume limit and the amount of contaminated data are shown. The temporal difference between the measuring times of plume and reference is not longer than $\pm$2week. The maximal temperature difference is smaller then 3.3°C ($\Delta T < 3.3$°C). The maximal relative BrO fit error for the contaminated data is not larger as the corresponding BrO SCD.

7.1 Tungurahua

In the considered time interval from June 2008 to August 2009, 6500 multi add spectra are available.

If contamination is not considered 6.4% of the evaluated volcanic gas plumes contained SO$_2$ above the "plume threshold of $7 \cdot 10^{17} \frac{molec}{cm^2}$. Thus 6.4% of the data can be used for the examination of the volcanic gas emissions in this timespan.

The analysis of the reference with an solar atlas spectrum spectra found 6.0 % of all spectra as contaminated. To prevent a systematic error of the results this spectra need to be excluded from the conventional NOVAC-evaluation if no further calculations are made.

From the remaining data, if the contaminated spectra are excluded, only 5.5 % of the SO$_2$ column densities are above the plume limit (see Table 7.1).

A higher amount of spectra above the SO$_2$ plume limit can be found in the contaminated data even if the contaminated data are evaluated with the NOVAC-routine. Here, the percentage of data in the plume-limit is 0.153%. This means that the contaminated data are 2.381 times more frequently above the plume limit. This leads to the presumption, that the probability of getting contaminated data increases with

the gas amount leaving the volcano.

The following paragraph deals only with the contaminated data: When performing the evaluation of the contaminated data with the decontamination module 29.9% of the resulting SO_2 column densities are in the plume limit. Thus, the reliable amount of contaminated data increase bya factor of two while the total amount of data increase by 1.8 percent points. Thus 7.3% of all data are above plume limit when using the decontamination module.

By using trace gas free references instead of contaminated references about 25.2 % more data are available.

7.2 Nevado del Ruiz

At Nevado del Ruiz a larger time span (from the end of 2009 to the end of 2011) is examined. The resulting amount of "Multi Add" data is 14005. Neglecting contamination and thus evaluate all data using the conventional NOVAC method results in 12.1% of all data above the plume limit. The total amount of contamination data is 1392. This is equivalent to 9.9% of all data. Evaluating the contaminated data with the NOVAC-routine yields in 32.8% of the cases in SO_2 SCDs above the plume limit. As at Tungurahua the occurrence of data above the plume limit within the contaminated data is larger as for not contaminated data (by a factor of 2.7).

The following paragraph only deals with the contaminated data. If using the decontamination module 59.8% of the SO_2 column densities are above the detection limit. Thus, an increase of the number of detected SO_2 SCDs above the plume limit within the contaminated data of 95% is observable. In total the number of SO_2 SCDs above the plume limit increases by 2.7 percent points. As a result 14.8% of all data are above the plume limit.
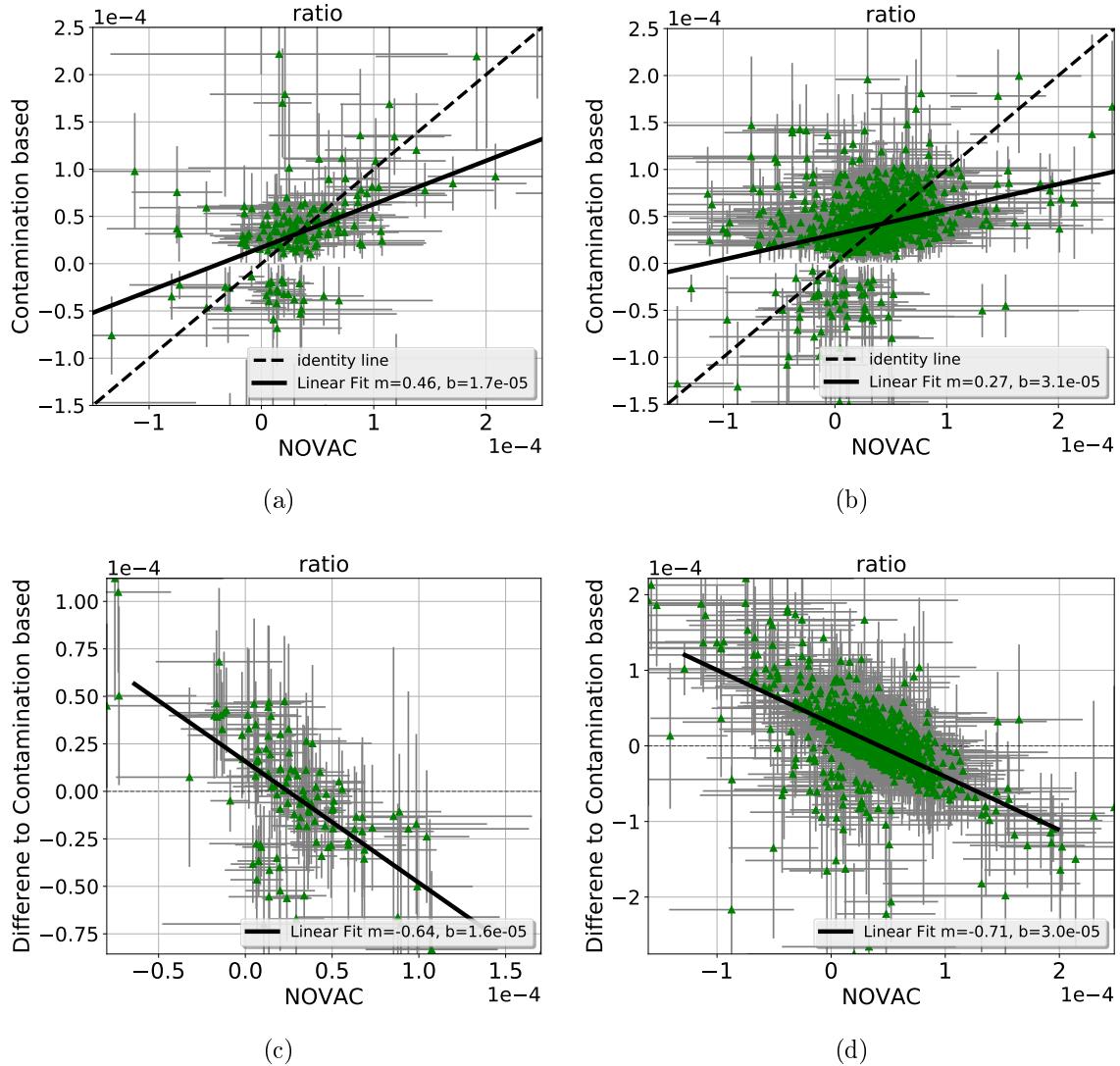
Figure 7.2: Comparison of the results of contaminated data for performing the
evaluation with the NOVAC-routine and the decontamination module.
(a)+(b): The black solid line shows a linear fit of the data (m:slope,
b:intercept). For the fit only data are used where the corresponding
SO_2 column density (retrieved from the decontamination module) lies
above the plume limit of $SO2\_SCD > 7 \cdot 10^{17} \frac{molec}{cm^2}$. The dotted line
indicates the unity line. (a) Results for the BrO /SO_2 column densities
from Tungurahua; (b) Results for the BrO /SO_2 column densities from
Nevado del Ruiz. (c) +(d) The column density calculated with NOVAC
is subtracted from the corresponding column density retrieved with the
decontamination module. The black valid line indicates a linear fit of the
data, the dotted grey line shows where the difference is zero. That means
both evaluations lead to the same ratio. (c) Tungurahua (d) Nevado del
Ruiz.

7.3 BrO/SO$_2$ time series

This section presents the final time series of SO$_2$, BrO and BrO/SO$_2$ for Tungurahua and Nevado del Ruiz.

Contaminated data either need to be excluded from the evaluation or to corrected due to using a not contaminated reference. If the contaminated data are excluded from the evaluation, the amount of data where the corresponding SO$_2$ amount is above the plume limit is significantly smaller. The additionally data retrieved by using the decontamination module can be seen in fig. 7.3 for Tungurahua (visualized with red circles) respectively for Nevado del Ruiz in fig. 7.4. The time series of Tungurahua and Nevado del Ruiz show, that contamination occurs rather frequently at high SO$_2$ and BrO column densities. The share of contaminated data above a SO$_2$ SCD of $2e18\frac{molec}{cm^2}$ is significantly higher as below (see fig. 7.4 for Nevado del Ruiz and fig. 7.3 for the Tungurahua volcano). High BrO SCDs (above $1e14\frac{molec}{cm^2}$) are as well above average contaminated data.
While the SO$_2$ SCDs and BrO SCDs increase on average due to using the contaminated data the average BrO/SO$_2$ ratio does not chance significantly compared to the average ratio when only using not contaminated data, as can be seen in fig. 7.3 for Tungurahua (the plot at the bottom) or in fig. 7.4 for Nevado del Ruiz.

Daily Means

Due to the very small amount of volcanic gas plumes with BrO column densities above the detection limit often the daily mean of the BrO/SO$_2$ ratios is used. Hereby at least four "Multi Adds" per day above the plume limit are considered in order to avoid outliers. Thus, performing the evaluation of contaminated data with the decontamination module leads to more data.

At Tungurahua 30.8% more daily mean data can be retrieved when using the decontamination module compared to exclude the contaminated data. The amount of daily means increases less than the total amount of data, this effect can be explained due to a higher occurrence of contamination if the SO$_2$ column densities are high, thus more data are retrieved for days with a high SO$_2$ amount. In the considered time period there are data on 365 days. If I exclude the contaminated data from the evaluation I get at 36 days daily means (more than 4 valid data points per day). If the contamination problem is neglected at 43 days daily means are retrieved. At 52 days the daily means can be calculated if the decontamination module is used, this is equivalent to 14.% of all data.

At Nevado del Ruiz the amount of daily means increases by 27.9%. if the contaminated data are used compared to the scenario where the contaminated data are excluded. In total there are data at 688 days. Without the contaminated data daily
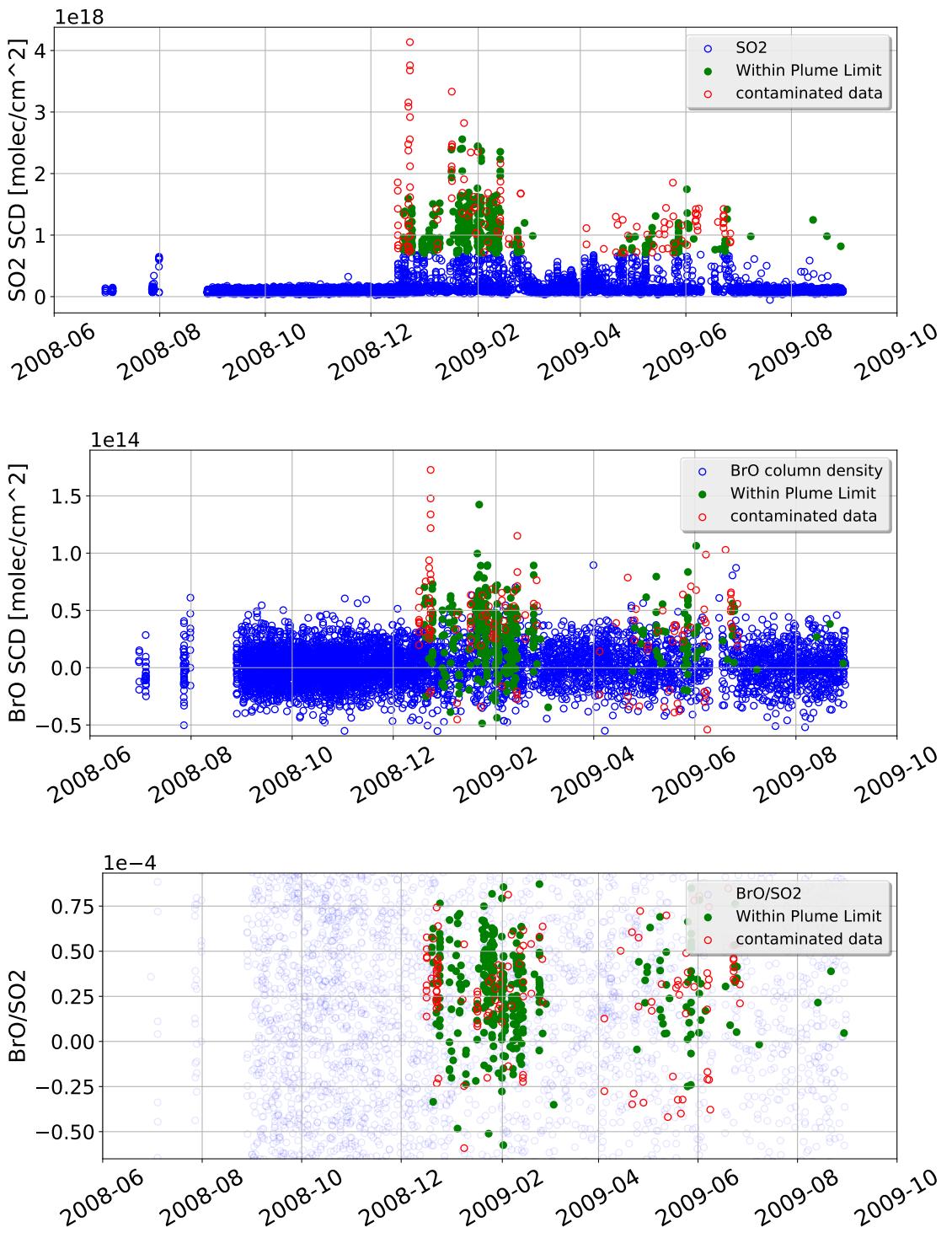
Figure 7.3: Time series of the BrO/SO$_2$ ratios for Tungurahua. The contaminated data are evaluated by using the decontamination module. Blue data points are below the detection limit, green data points are not contaminated, valid SO$_2$ SCDs. Red data points are contaminated data, evaluated with the decontamination module.
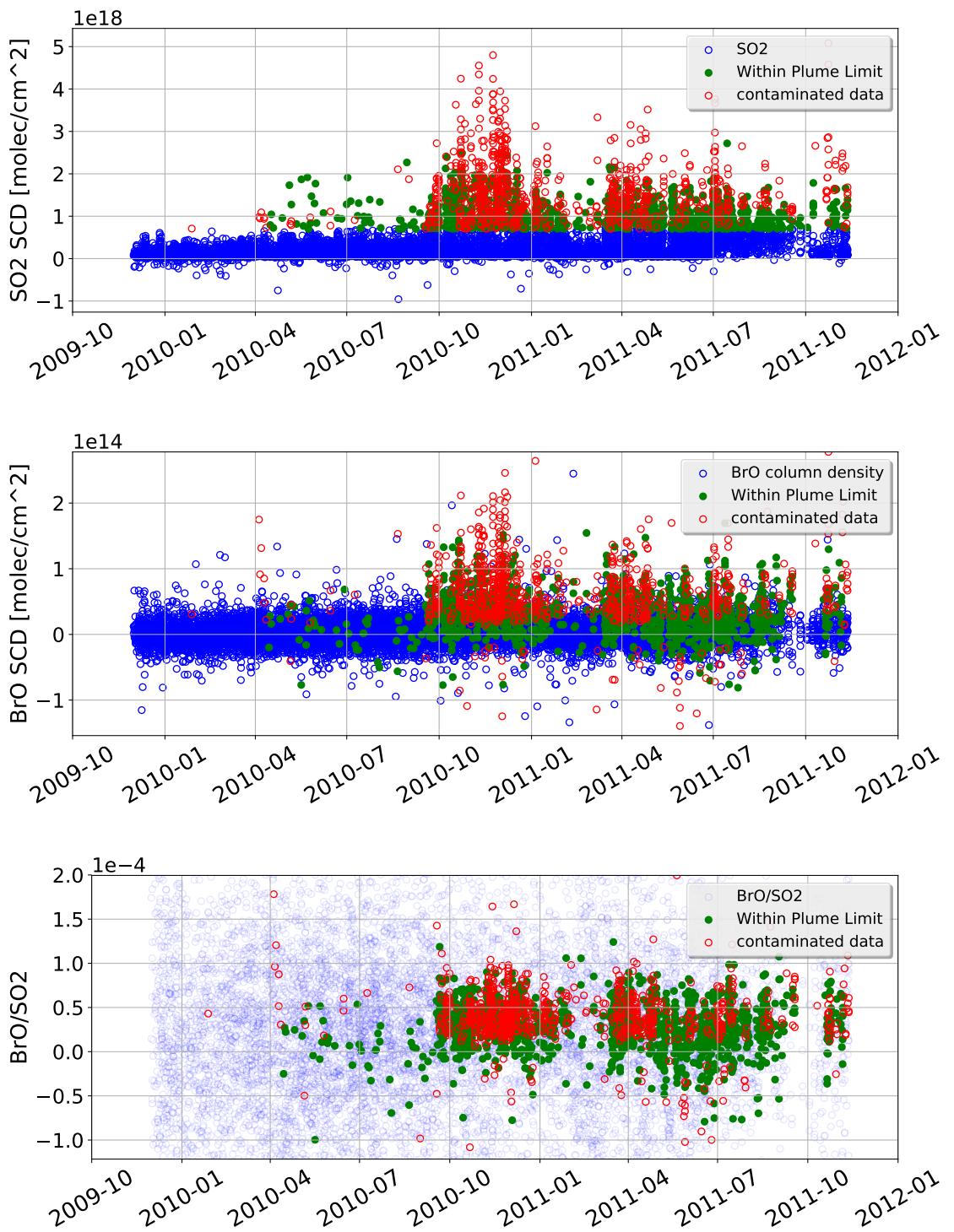
Figure 7.4: Time series of BrO, SO$_2$ and the BrO/SO$_2$ ratios for Nevado del Ruiz . The contaminated data are evaluated by using the decontamination module. Blue data points are below the detection limit, green data points are not contaminated, valid SO$_2$ SCDs. Red data points are contaminated data, evaluated with the decontamination module. The contaminated data points are only marked in red, if the SO$_2$ SCD is above the plume limit. Contaminated data below the detection limit are not particularly marked.
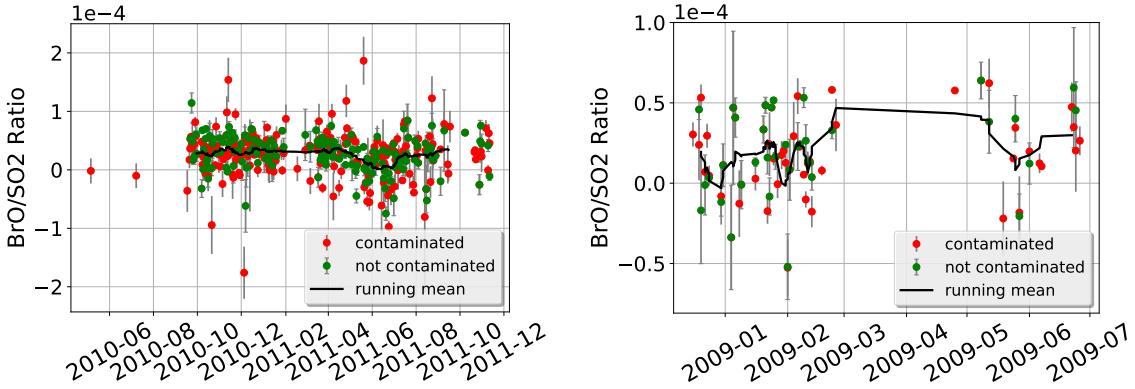
Figure 7.5: BrO/SO$_2$ ratio daily mean time series for Nevado del Ruiz (left) and Tungurahua (right). SO$_2$ SCDs used for this plot are above the plume limit of 7·10^{17}. The minimum amount of data per day are four. Days where less than four valid ratios are recorded are not considered in this plot. As a result of using the contaminated data as well more daily means are available, because more days have an amount of valid data's above four. Those dates are marked with red. The other data are colored in green.

	Tungurahua	Nevado del Ruiz
Decrease of the mean daily mean error	22.5%	39.2%

means can be retrieved at 165 days. If the contamination problem is neglected the total amount of daily means in the evaluated time period is 198. If the decontamination module is used for the contaminated data there are in total an amount of 229 daily means. This is equivalent to 33% of all data. Thus the amount of daily means at means at Nevado del Ruiz is twice as high compared to the amount of daily means at Tungurahua.

More data leads to a smaller error of the daily mean data, because the standard derivation decreases if the amount of data increases (Standard derivation is proportional to $\frac{1}{\sqrt{n}}$). The mean error of the daily means excluding the contaminated data is $1.49 \cdot 10^{-5}$ (Tungurahua) and $1.7 \cdot 10^{-5}$ (Nevado del Ruiz). If the contaminated data are decontaminated and considered for the daily mean calculation the mean error decreases to: $1.16 \cdot 10^{-5}$ (Tungurahua) and $1.036 \cdot 10^{-5}$ (Nevado del Ruiz). Figure 7.5 shows a time series of Daily means of the BrO/SO$_2$ ratio. The minimum amount of valid data point within one day is above 4. Days where 3 or less valid data where recorded are not considered in this figure. Thus all considered ratios have an SO$_2$ SCD above the plume limit. The red marked ratios shows daily means which includes at least one contaminated spectra.
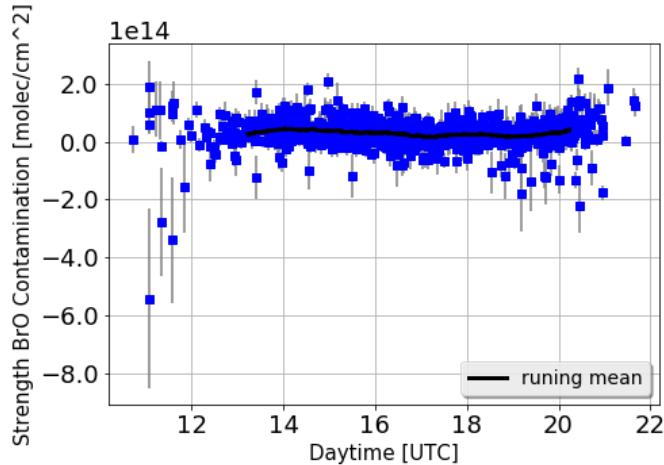
Figure 7.6: Strength of BrO contamination as a function of the daytime. The strength of BrO contamination is calculated as the difference in the BrO SCD when using the contaminated same time reference and the not contaminated reference provided by the decontamination module.

7.4 Discussion of the BrO contamination

The evaluation with a gas free reference show higher SO_2 SCDs as well as higher BrO SCDs. Thus one can conclude that the reference region is contaminated in both, SO_2 and BrO. A result which can not be retrieved by using a solar atlas spectrum as alternative gas free reference.

The SO_2 lifetime [*] is estimated from 4h to several days dependent on the conditions. SO_2 is filtered by aerosols and in the end washed out of the atmosphere. This processes limits the SO_2 lifetime. The BrO lifetime is rather hard to define due to continues reformation (see fig. 2.2). There a several interpretations for the BrO contamination.

Taking scenario described in fig. 4.9 as basis: Contamination is in this case a result of an old plume. The age of the plume is here in the order of hours to days. Thus I can make the assumption, that the BrO lifetime is in the same order. BrO lifetimes below this would make BrO contaminations in the scenario of fig. 4.9 rather unlikely. In this case contamination is rather a result of the scenarios described in fig. 4.10. This would lead to the result, that the problem of plume contamination is also rather unlikely. An dependency of the strength of contamination on the daytime cannot be observed (see fig. 7.6), because the BrO formation depends on the sunlight this might be unexpected, but the scattered light even before the sunset is sufficient for Br_2 photolysis. (The three data point with a BrO contamination strength below -2·10^{14} are a result of the low quality of the scans which can be concluded from the very large errors.)

---

[*]meaning the time until the amount decreased to $\frac{1}{e}$ of the initial amount

94

Another possibility for the BrO contamination would be, that the DOASIS fit routine does not evaluate BrO and SO_2 independently, thus, if the fit routine finds more SO_2 due to a not contaminated reference the calculation systematically overestimates the BrO SCD. A higher SO_2 emission usually coincidence with increased emission of all other volcanic trace gases, therefore this possibility also needs to be considered.

8 Conclusion

The Network for Observation of Volcanic and Atmospheric Change provides a very large amount of longtime timeseries. This treasure of data contains a huge amount of informations about volcanoes, which give an interesting insight of the physical foundations on volcanic activity.

The evaluation of the volcanoes is in particular based on the assumption that the atmospheric background of the volcanic trace gases SO_2 and BrO is negligible. This is important to assure because the DOAS method only captures the difference in gas amount between the background, the reference and the signal, the plume spectra.

By the usage of a solar atlas spectrum as reference, ? found that the reference provided by the NOVAC-Instrument is not always gas free. But is sometimes (ca 10% of the data) contaminated with volcanic trace gases. If that is the case the contaminated spectra either needs to be excluded from the evaluation or the contaminated reference needs to be replaced by a gas free reference. If the contaminated data should not be excluded of the evaluation an appropriate gas free reference need to be found. A solar atlas spectrum can not be used for the BrO evaluation due to the low amount of BrO and the increase of the BrO fit error if using a solar atlas spectrum. Thus, a gas free reference recorded by the same instrument is a possible choice. As the instruments are recording continuously, there are multiple potential gas free reference spectra available for each plume spectrum. Due to the low accuracy of the BrO retrieval it is reasonably to choose the reference with respect to the BrO fit error. An analysis of the dependency of the BrO fit error on several external parameters is presented. Hereby I focus on the temporal difference and the differences in temperature, colour index, exposure time, elevation angle and daytime between the plume and the reference spectra. These external parameters are found crucial for the retrieved BrO fit error. The dependence of the BrO column density on external parameters was discussed as well.

SO_2 contamination

The analysis of the occurrence of contamination as a function of the daytime showed, that contamination mostly occur after 11:00 am. In the morning contamination occur only rarely, thus a result of this thesis is, that the emission of the day before plays at most only a subordinated role in order of SO_2 contamination.

Influence of external parameter

The result of this analysis is, that in general the retrieved BrO fit error is minimal, if the considered parameter are similar for the plume spectrum and the reference

spectrum. From the estimated external parameter only the elevation angle does not seem to influence the retrieval. From the considered parameter the temperature has the most significant impact of 60% up to 97% compared to the other parameters. Based on this findings an algorithm is introduced to automatically find an alternative reference spectrum if the "same time reference" is contaminated.

Fitting the data with a four dimensional first order polynomial turned out to give the best estimation of the expected error on the trace gas measurement.

Increase of data amount

A further advantage of the new calculation is, that due to the higher amount of the SO_2 SCDs the amount of data above the plume limit increases. Using the decontamination module leads to an total increase of data of 36.4% (Tungurahua) and 59.1% (Nevado del Ruiz) compared to the amount of data which is retrieved by using the conventional NOVAC-routine. When only considering the amount of daily means an increase of the data amount of 30.8% (Tungurahua) and 27.9% (Nevado del Ruiz) is reached. The mean error of the daily means decreases by 22.5% (Tungurahua) and 39.2% (Nevado del Ruiz) due to more data retrieved by the decontamination module compared to the conventional NOVAC-routine.

Evaluation by using the decontamination module

The evaluation of the contaminated data with the here proposed algorithm shows that BrO as well as SO_2 was underestimated by ignoring the contamination problem. We shows that the decontamination module leads to an in average higher value of the BrO column density. The BrO SCD increases $1.7 \cdot 10^{13} \frac{molec}{cm^2}$ at Tungurahua and $2.9 \cdot 10^{13} \frac{molec}{cm^2}$ at Nevado del Ruiz. The SO_2 SCD increases as well by an amount of $6.3 \cdot 10^{17} \frac{molec}{cm^2}$ at Tungurahua and $7.6 \cdot 10^{17} \frac{molec}{cm^2}$ at Nevado del Ruiz. The results for the BrO/SO_2 ratio calculated with the decontamination module changed compared to the conventional method in the way, that low ratios increases, while high ratios decreased.

On average contaminated data have rather large BrO and SO_2 SCDs. Thus looking at all data, including the not contaminated data, using the decontamination model leads to an increased mean SO_2 respectively BrO SCDs as I showed in this thesis. However the mean BrO/SO_2 ratio, including the not contaminated scans, does not change significantly.

The method proposed in this thesis improves the evaluation of the spectra provided by NOVAC and eliminates the systematic error occurring due to contamination. As a result the amount of usable data increases. This is a important step fo a better understanding of volcanoes.

Part IV

Appendix

Dependence external parameters on each other

In addition to **??** here the parameter of a linear fit[*] between the external parameters. Significant correlations can be found in **??**.

Difference of Temperature on Difference of exposure time

$$\Delta T = -26.32 \cdot \Delta ExpTime + 2 \cdot 10^{-15} \tag{.1}$$

Difference of Temperature on Difference of colour index

$$\Delta T = 0.0022 \cdot \Delta ColIdX + 2 \cdot 10^{-19} \tag{.2}$$

Difference of Temperature on Difference of Day time

$$\Delta T = 0.262 \cdot \Delta daytime - 4 \cdot 10^{-17} \tag{.3}$$

Difference of Temperature on Difference of Elevation angle

$$\Delta T = 1.08 \cdot \Delta ElevAngle - 1 \cdot 10^{-16} \tag{.4}$$

Difference of Exposure on Difference of Col Idx

$$\Delta Exposure = -6.22 \cdot 10^{-5} \Delta ColIdx + 1 \cdot 10^{-18} \tag{.5}$$

Difference of Exposure on Difference of Day time

$$\Delta Exposure = -0.004 \cdot \Delta daytime - 1 \cdot 10^{-17} \tag{.6}$$

Difference of Exposure on Difference ofElevation angle

$$\Delta Exposure = -0.047 \cdot \Delta ElevAngle + 3 \cdot 10^{-16} \tag{.7}$$

Difference of Colorindex on Difference of Day time

$$\Delta ColIdX = 4.51 \cdot \Delta daytime - 1.2 \cdot 10^{-15} \tag{.8}$$

Difference of Colorindex on Difference of Elevation angle

$$\Delta ColIdX = -52 \cdot \Delta ElevAngle + 1.45 \cdot 10^{-14} \tag{.9}$$

Difference of Colorindex on Difference of Elevation angle

$$\Delta ColIdX = 3.5 \cdot \Delta ElevAngle - 6 \cdot 10^{-16} \tag{.10}$$

---

[*]calculated by python using the numpy library (version) based on least square method

A Lists

A.1 List of Figures

A.2 List of Tables

104

B Bibliography

Steffen Beirle, Christoph Hörmann, M Penning de Vries, Stefan Dörner, Christoph Kern, and Thomas Wagner. Estimating the volcanic emission rate and atmospheric lifetime of so 2 from space: a case study for kīlauea volcano, hawaii. *Atmospheric Chemistry and Physics*, 14(16):8309–8322, 2014.

Nicole Bobrowski and G Giuffrida. Bromine monoxide/sulphur dioxide ratios in relation to volcanological observations at mt. *Etna*, 2009:433–445, 2006.

Nicole Bobrowski and U Platt. So2/bro ratios studied in five volcanic plumes. *Journal of Volcanology and Geothermal Research*, 166(3-4):147–160, 2007.

Nicole Bobrowski, G Hönninger, B Galle, and U Platt. Detection of bromine monoxide in a volcanic plume. *Nature*, 423(6937):273, 2003.

Nicole Bobrowski, R Von Glasow, A Aiuppa, S Inguaggiato, I Louban, OW Ibrahim, and U Platt. Reactive halogen chemistry in volcanic plumes. *Journal of Geophysical Research: Atmospheres*, 112(D6), 2007.

JP Burrows, A Richter, A Dehn, B Deters, S Himmelmann, S Voigt, and J Orphal. Atmospheric remote-sensing reference data from gome—2. temperature-dependent absorption cross sections of o3 in the 231–794 nm range. *Journal of quantitative spectroscopy and radiative transfer*, 61(4):509–517, 1999.

Mike Burton, Patrick Allard, Filippo Muré, and Alessandro La Spina. Magmatic gas composition reveals the source depth of slug-driven strombolian explosive activity. *Science*, 317(5835):227–230, 2007.

Markus Bussemer. Der ring-effekt: Ursachen und einfluß auf die spektroskopische messung stratosphärischer spurenstoffe. *Diplomathesis, University of Heidelberg*, 1993.

K Chance and RL Kurucz. An improved high-resolution solar reference spectrum for earth's atmosphere measurements in the ultraviolet, visible, and near infrared. *Journal of quantitative spectroscopy and radiative transfer*, 111(9):1289–1295, 2010.

Oliver C Fleischmann, Matthias Hartmann, John P Burrows, and Johannes Orphal. New ultraviolet absorption cross-sections of bro at atmospheric temperatures measured by time-windowing fourier transform spectroscopy. *Journal of Photochemistry and Photobiology A: Chemistry*, 168(1-2):117–132, 2004.

Bo Galle, Mattias Johansson, Claudia Rivera, Yan Zhang, Manne Kihlman, Christoph Kern, Thomas Lehmann, Ulrich Platt, Santiago Arellano, and Silvana Hidalgo. Network for observation of volcanic and atmospheric change (novac)—a global network for volcanic gas monitoring: Network layout and instrument description. *Journal of Geophysical Research: Atmospheres*, 115(D5), 2010.

TM Gerlach. Volcanic sources of tropospheric ozone-depleting trace gases. *Geochemistry, Geophysics, Geosystems*, 5(9), 2004.

Hans-F Graf, Johann Feichter, and Bärbel Langmann. Volcanic sulfur emissions: Estimates of source strength and its contribution to the global sulfate distribution. *Journal of Geophysical Research: Atmospheres*, 102(D9):10727–10738, 1997.

Minard L Hall, Claude Robin, Bernardo Beate, Patricia Mothes, and Michel Monzier. Tungurahua volcano, ecuador: structure, eruptive history and hazards. *Journal of Volcanology and Geothermal Research*, 91(1):1–21, 1999.

Martina M Halmer, H-U Schmincke, and H-F Graf. The annual volcanic gas input into the atmosphere, in particular into the stratosphere: a global data set for the past 100 years. *Journal of Volcanology and Geothermal Research*, 115(3-4): 511–528, 2002.

C Hermans, AC Vandaele, S Fally, M Carleer, R Colin, B Coquart, A Jenouvrier, and M-F Merienne. Absorption cross-section of the collision-induced bands of oxygen from the uv to the nir. In *Weakly interacting molecular pairs: unconventional absorbers of radiation in the atmosphere*, pages 193–202. Springer, 2003.

Silvana Hidalgo, Jean Battaglia, Santiago Arellano, Alexander Steele, Benjamin Bernard, Julie Bourquin, Bo Galle, Santiago Arrais, and Freddy Vásconez. So2 degassing at tungurahua volcano (ecuador) between 2007 and 2013: Transition from continuous to episodic activity. *Journal of Volcanology and Geothermal Research*, 298:1–14, 2015.

C Hörmann, H Sihler, Nicole Bobrowski, S Beirle, M Penning De Vries, U Platt, and T Wagner. Systematic investigation of bromine monoxide in volcanic plumes from space by using the gome-2 instrument. *Atmospheric Chemistry and Physics*, 13(9):4749, 2013.

IPCC. *Summary for Policymakers*, book section SPM, page 1–30. Cambridge University Press, Cambridge, United Kingdom and New York, NY, USA, 2013. ISBN ISBN 978-1-107-66182-0. doi: 10.1017/CBO9781107415324.004. URL www.climatechange2013.org.

Christoph Kern. *Spectroscopic measurements of volcanic gas emissions in the ultraviolet wavelength region*. PhD thesis, 2009.

Stefan Kraus. *DOASIS: A framework design for DOAS*. Shaker, 2006.

T Lehmann. *Improving the sensitivity of spectroscopic measurements of atmospheric trace gases by modern signal processing algorithms.* PhD thesis, Ph. D. thesis, IUP, University Heidelberg, in preparation, 2011.

Peter Lübcke. *Optical remote sensing measurements of bromine and sulphur emissions: Investigating their potential as tracers of volcanic activity.* PhD thesis, 2014.

Peter Lübcke, Nicole Bobrowski, S Arellano, Bo Galle, G Garzón, Leif Vogel, and U Platt. Bro/so 2 molar ratios from scanning doas measurements in the novac network. *Solid Earth*, 5(1):409, 2014.

Richard Meller and Geert K Moortgat. Temperature dependence of the absorption cross sections of formaldehyde between 223 and 323 k in the wavelength range 225–375 nm. *Journal of Geophysical Research: Atmospheres*, 105(D6):7089–7101, 2000.

nevado-del-ruiz colombia: Windrose.

Kimio Noguchi and Hiroshi Kamiya. Prediction of volcanic eruption by measuring the chemical composition and amounts of gases. *Bulletin Volcanologique*, 26(1): 367–378, 1963.

NOVAC-website. Novac-project. http://www.novac-project.eu/. Accessed: 2018-01-29.

Clive Oppenheimer, David M Pyle, and Jenni Barclay. Volcanic degassing. Geological Society of London, 2003.

Maddalena Pennisi and Marie-Françoise Le Cloarec. Variations of cl, f, and s in mount etna's plume, italy, between 1992 and 1995. *Journal of Geophysical Research: Solid Earth*, 103(B3):5061–5066, 1998.

D Perner and U Platt. Detection of nitrous acid in the atmosphere by differential optical absorption. *Geophysical Research Letters*, 6(12):917–920, 1979.

G Pinardi, MV Roozendael, and C Fayt. The influence of spectrometer temperature variability on the data retrieval of so2. *NOVAC second annual activity report, NOVAC consortium*, 44:48, 2007.

U Platt and N Bobrowski. Quantification of volcanic reactive halogen emissions. *Volcanism and Global Change, eds A. Schmidt, K. Fristad, L. Elkins-Tanton, Cambridge University Press, Cambridge, UK, ISBN*, 1466525386, 2015.

U Platt, D Perner, GW Harris, AM Winer, and JN Pitts Jr. Observations of nitrous acid in an urban atmosphere by differential optical absorption. *Nature*, 285(5763): 312, 1980.

Ulrich Platt and Jochen Stutz. Differential absorption spectroscopy. *Differential Optical Absorption Spectroscopy*, pages 135–174, 2008.

Smithsonian Institution Global Volcanism Program. https://volcano.si.edu/. Accessed: 2018-03-20.

Alan Robock. Volcanic eruptions and climate. *Reviews of Geophysics*, 38(2):191–219, 2000.

GG Salerno, MR Burton, C Oppenheimer, T Caltabiano, VI Tsanev, and N Bruno. Novel retrieval of volcanic so2 abundance from ultraviolet spectra. *Journal of Volcanology and Geothermal Research*, 181(1-2):141–153, 2009.

Pablo Samaniego, Jean-Philippe Eissen, Jean-Luc Le Pennec, M Hall, Michel Monzier, P Mothes, P Ramón, Claude Robin, J Egred, I Molina, et al. Los peligros volcánicos asociados con el tungurahua. 2003.

A Schmidt and A Robock. Volcanism, the atmosphere and climate through time. *Volcanism Glob. Environ. Chang*, pages 195–207, 2015.

Anja Schmidt, Kirsten Fristad, and Linda T Elkins-Tanton. Volcanism and global environmental change, 2015.

Hans-Ulrich Schmincke. *Vulkanismus*. Wissenschaftliche Buchgesellschaft, 3 edition, 2000.

Python scikit learn.org. http://scikit-learn.org/stable/modules/generated/sklearn.linear_model.LinearRegression.html. Accessed: 2018-01-19.

John H Seinfeld and Spyros N Pandis. *Atmospheric chemistry and physics: from air pollution to climate change*. John Wiley & Sons, 2016.

S Solomon, RW Portmann, RR Garcia, W Randel, F Wu, R Nagatani, J Gleason, L Thomason, LR Poole, and MP McCormick. Ozone depletion at mid-latitudes: Coupling of volcanic aerosols and temperature variability to anthropogenic chlorine. *Geophysical research letters*, 25(11):1871–1874, 1998.

Susan Solomon, Arthur L Schmeltekopf, and Ryan W Sanders. On the interpretation of zenith sky absorption measurements. *Journal of Geophysical Research: Atmospheres*, 92(D7):8311–8319, 1987.

Jochen Stutz and Ulrich Platt. Numerical analysis and estimation of the statistical error of differential optical absorption spectroscopy measurements with least-squares methods. *Appl. Opt.*, 35(30):6041–6053, Oct 1996. doi: 10.1364/AO.35.006041. URL http://ao.osa.org/abstract.cfm?URI=ao-35-30-6041.

Christiane Textor, Hans-F Graf, Claudia Timmreck, and Alan Robock. Emissions from volcanoes. In *Emissions of Atmospheric Trace Compounds*, pages 269–303. Springer, 2004.

Thorvaldur Thordarson and Stephen Self. Atmospheric and environmental effects of the 1783–1784 laki eruption: A review and reassessment. *Journal of Geophysical Research: Atmospheres*, 108(D1), 2003.

S Twomey. Pollution and the planetary albedo. *Atmospheric Environment (1967)*, 8(12):1251–1256, 1974.

Ann Carine Vandaele, Christian Hermans, Paul C Simon, Michel Carleer, Réginald Colin, Sophie Fally, Marie-France Merienne, Alain Jenouvrier, and Bernard Coquart. Measurements of the no2 absorption cross-section from 42 000 cm- 1 to 10 000 cm- 1 (238–1000 nm) at 220 k and 294 k. *Journal of Quantitative Spectroscopy and Radiative Transfer*, 59(3-5):171–184, 1998.

Ann Carine Vandaele, Christian Hermans, and Sophie Fally. Fourier transform measurements of so2 absorption cross sections: Ii.: Temperature dependence in the 29 000–44 000 cm- 1 (227–345 nm) region. *Journal of Quantitative Spectroscopy and Radiative Transfer*, 110(18):2115–2126, 2009.

Leif Vogel. *Volcanic plumes: Evaluation of spectroscopic measurements, early detection, and bromine chemistry*. PhD thesis, 2011.

T Wagner, S Beirle, and T Deutschmann. Three-dimensional simulation of the ring effect in observations of scattered sun light using monte carlo radiative transfer models. *Atmospheric Measurement Techniques*, 2(1):113–124, 2009.

T Wagner, A Apituley, S Beirle, S Dörner, U Friess, J Remmers, and R Shaiganfar. Cloud detection and classification based on max-doas observations. *Atmospheric Measurement Techniques*, 7(5):1289–1320, 2014.

Simon Warnach. Improvements of bro and so2 retrievals of novac data - tungurahua volcano as a case study. Master's thesis, 2015.

Erklärung:

Ich versichere, dass ich diese Arbeit selbstständig verfasst habe und keine anderen als die angegebenen Quellen und Hilfsmittel benutzt habe.

Heidelberg, den (Datum)   ....